VIBRATION MEASUREMENTS ON THE WIDELY EXPOSED GERBIL EARDRUM

Zinan He

Department of Biomedical Engineering
McGill University
Montréal, Québec

February 2012

A thesis submitted to the Faculty of Graduate Studies and Research
in partial fulfilment of the requirements of the degree of

Master of Engineering

Abstract

Hearing loss is one of the most common birth defects. Early identification of hearing loss is very important because even a mild hearing loss can seriously delay language development and compromise communication, educational and social capabilities. Tympanometry is a promising tool to identify conductive hearing loss through examining the eardrum responses. However, current clinical results are unsatisfactory due to our inadequate knowledge of the complex mechanics of the middle ear. The vibration pattern of the eardrum is a critical factor for understanding tympanometry and the underlying sound transmission in the middle ear. However, very few experimental studies have investigated the vibration patterns of the eardrum.

This study involves *in vivo* measurements of gerbil eardrum vibrations using laser Doppler vibrometry. An experimental approach to widely expose the eardrum has been developed. This wider exposure allows measurements to be taken on a larger area so as to better characterize the vibration pattern across the eardrum.

Résumé

Les troubles de l'audition sont un des plus communs défauts de naissance. Il est très important d'identifier rapidement les troubles de l'audition car même un trouble léger peut retarder de façon sérieuse le développement du langage et compromettre la communication ainsi que les capacités éducatives et sociales. La tympanométrie est un outil prometteur pour identifier la surdité de transmission. Cependant, les résultats cliniques actuels ne sont pas satisfaisants en raison de notre connaissance inadéquate du mécanisme complexe de l'oreille moyenne. La caracterisation des vibrations du tympan est un facteur critique dans la compréhension de la tympanométrie et de la transmission sous-jacente des sons dans l'oreille moyenne. Cependant, peu d'études expérimentales ont investigué les vibrations du tympan.

Cette étude implique la mesure *in vivo* des vibrations du tympan de la gerbille à l'aide d'un vibromètre à laser Doppler. Une approche expérimentale visant à largement exposer le tympan a été développée. Cette large exposition permet de prendre les mesures sur une plus grande surface dans le but de mieux caractériser les vibrations du tympan.

Acknowledgements

I would like to express my sincerest gratitude to my supervisor, Dr. W. Robert J. Funnell for the inspiration of this project and for his valuable guidance throughout the years of my graduate education. I am deeply appreciative of his enthusiastic insight in research, suggestions and teachings, for they have greatly improved my work. I would also like to acknowledge his patience in reviewing many drafts of this manuscript. Foremost, his professionalism, passion for research, perseverance, integrity and ethics have had a positive impact on me both intellectually and personally.

I would also like to thank my co-supervisor Dr. Sam J. Daniel, for his support in the experimental and clinical aspects of this research and for his invitations to multiple seminars in related medical fields.

I am also thankful for all my friends and colleagues in the lab, especially Dan, Nima, Sophia and Victoria who have always provided me with generosity during experiments.

Above all, I am forever grateful for the unconditional support of my beloved parents Ji Qiang and Li Zhen to whom all my work is dedicated. Without their love, understanding and encouragement, this thesis would not have been fulfilled.

This work was funded by the Canadian Institutes of Health Research, the Fonds de recherche en santé du Québec, the Natural Sciences and Engineering Research Council Canada, the Montréal Children's Hospital Research Institute and the McGill University Health Centre Research Institute.

Table of Contents

Chapter 1
Introduction

1.1 Motivation

Hearing is one of the five senses; it is the ability to perceive acoustical stimulation. Hence, hearing loss refers to a complete or partial inability to perceive sound in one or both ears. According to the World Health Organization (WHO), 278 million people were estimated to have moderate to profound hearing loss in 2006; a quarter of those cases began during childhood and half of them were preventable (WHO, 2011). In North America, hearing loss is one of the most common birth defects: approximately 6 in 1000 babies are born with some level of hearing loss (Marazita et al., 1993). Early diagnosis is extremely important because even a mild hearing loss can seriously delay language development and thus compromise the child's communication and social capabilities (NIDCD, 1993; ASHA, 1994).

The middle ear plays an essential role in sound perception: it conducts air-borne sound energy from the external environment into liquid waves inside the inner ear via ossicular vibrations. However, the middle ear is often the site of infections, congenital disorders and other pathologies, which can lead to conductive hearing loss. Furthermore, transient middle-ear problems due to the effects of residual vernix, mesenchyme and liquid in the middle ear are common in newborns. This transient issue greatly alters the results of newborn screening tests because none of those tests can effectively distinguish between conductive and sensorineural hearing loss. Hence, there is an increasing demand for a fast and effective method to identify conductive loss.

Tympanometry is a promising tool for evaluating middle-ear function by measuring eardrum mobility. It involves a tone introduced to the ear canal in the presence of a range of static pressures, and measurement of the acoustical input admittance. The functional status of the middle ear will be reflected in the admittance measurement, which is

dominated by the eardrum. Therefore, a better understanding of the behaviour of the eardrum has important clinical implications.

1.2 Background

Numerous studies of middle-ear sound transmission and of the mechanical properties of middle-ear components have been performed around the world over many decades. Many groups have experimentally investigated ossicle and eardrum motions in response to both sound pressure and quasi-static pressure, and with both normal and experimentally impaired ears. These studies have involved animal models, human cadavers and living human subjects.

In order to achieve a more complete and quantitative understanding of middle-ear mechanics, various numerical models have been developed to interpret experimental data. In the first era of quantitative middle-ear modelling, lumped-parameter models were used extensively. However, those models contain parameters that are not directly related to middle-ear anatomy and structure, and cannot effectively simulate the complex three-dimensional motions of the middle-ear system, which consists of asymmetrical, irregular and interconnected components. To overcome this deficiency, Funnell first introduced finite-element models into middle-ear research in 1975. They are constructed based on real anatomical shapes, material properties, boundary conditions and loading conditions. Since then, more and more groups have used finite-element models to analyze middle-ear responses in humans and in other animals.

In spite of the number of middle-ear studies published to date, many gaps still remain in our knowledge, especially with respect to eardrum vibration patterns. Most of the previous experimental studies of eardrum vibrations were conducted in *post mortem* animals. Although a few measurements have been made in living animals, most of them were limited to a fairly small part of the eardrum due to the obstruction of bony structures. In order to achieve a better understanding of the middle ear, a more complete

characterization of spatial vibration patterns of the eardrum is required.

1.3 Research objectives

The goal of this study was to further explore eardrum vibrations by acquiring *in vivo* vibration displacement measurements across a wide region of the eardrum, in response to sound-pressure stimuli. Accordingly, there were three specific aims:

1) to gain more experience with long-lasting anaesthesia, so that the quality and repeatability of *in vivo* measurements could be improved;
2) to develop a technique to widely expose the eardrum, so that vibration patterns in previously hidden regions would be revealed; and
3) to address some experimental concerns by using a finite-element model.

An animal model is used in this research because it allows various experimental approaches that are not possible with living human subjects. In particular, the Mongolian gerbil was chosen because of its relatively large middle-ear structures and easy eardrum accessibility. Most importantly, it has recently become a popular species for middle-ear experimental research worldwide.

1.4 Thesis outline

After concisely reviewing middle-ear anatomy and its contributions to sound transmission in Chapter 2, I outline some previous studies related to our research in Chapter 3. The experimental approach and the equipment used for this study, as well as the modelling techniques, are then described in Chapter 4. Experimental measurements and simulated results are presented in Chapter 5 and Chapter 6 respectively. Final conclusions are presented in Chapter 7, where potential future research directions are highlighted as well.

Chapter 2
Middle-ear anatomy and function

This chapter provides an overview of middle-ear anatomy, followed by a brief discussion of middle-ear mechanics. In Section 2.1, both gross and microscopic anatomy of the human middle ear is reviewed, with sub-sections describing the eardrum, the ossicles, the middle-ear muscles and ligaments, the bony middle-ear cavity and the Eustachian tube. In Section 2.2, structural differences between the human and gerbil middle ears are explained since the gerbil was chosen for this study. Finally, important issues in middle-ear mechanics and pressure regulation are discussed in Sections 2.3 and 2.4 respectively.

2.1 Human middle ear

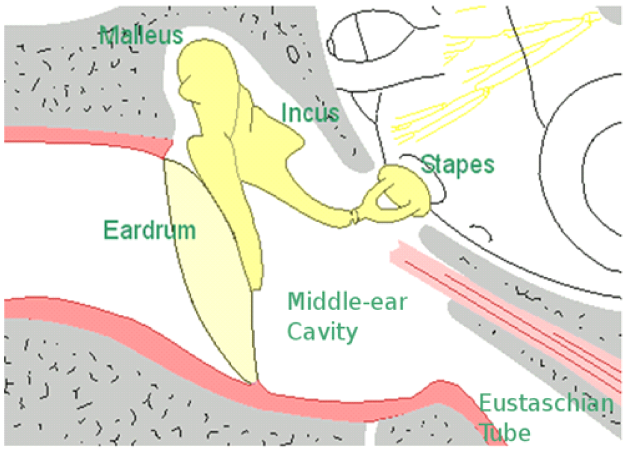

Figure 2.1: Human middle ear. (After Funnell, 2011)

The human middle ear consists mainly of the eardrum, three interconnected ossicles, ligaments, muscle tendons, an air-filled bony cavity and the Eustachian tube, as shown in Figure 2.1. These middle-ear structures together transmit acoustic energy from the external environment to the inner ear. The following descriptions of individual components of the middle ear are based primarily on two human-physiology textbooks (Stanfield & Germann, 2007; Young et al., 2010), and details regarding eardrum morphology and function are based primarily on a comprehensive review by Funnell and Laszlo (1982).

2.1.1 Tympanic membrane

The tympanic membrane (TM), also called the eardrum, is conical with the apex pointing towards the inner ear. The diameter of the human TM is around 8–10 mm and varies slightly according to body size. Using confocal microscopy, Kuypers et al. (2006) measured the nonuniform thickness distribution of the human TM, with the maxima located near the annulus and manubrium, and the minima in the regions between them, as shown in Figure 2.2. The thickness of the human TM displays a large inter-subject variation. For example, Kuypers et al. (2006) reported mean TM thicknesses of 40, 50, and 120 μm in three human TM's.

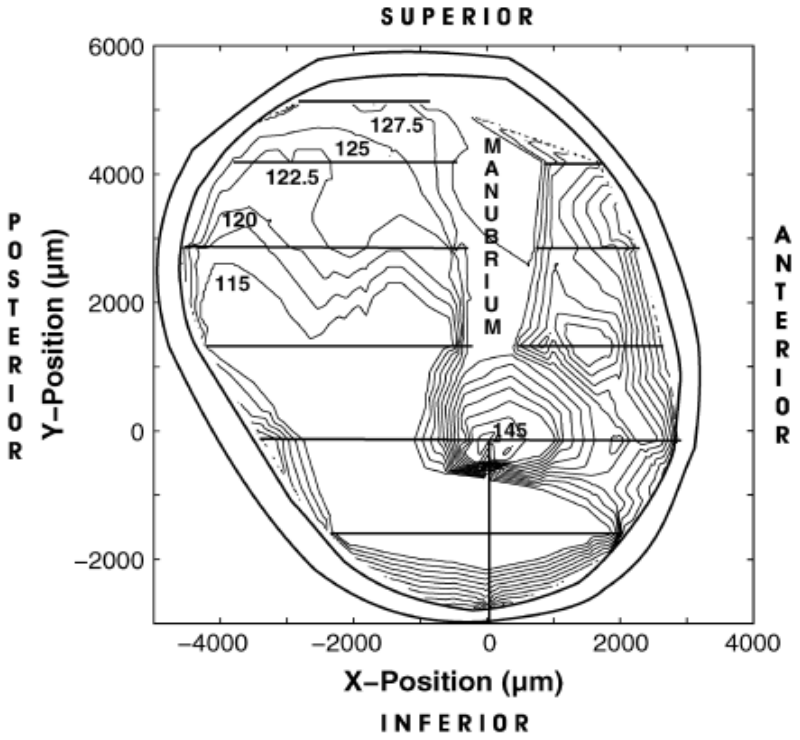

Figure 2.2: Contour plot of a fresh human TM thickness distribution, measured using confocal microscopy. (Kuypers et al., 2006)

The TM is composed of the pars tensa (PT) and the pars flaccida (PF). The PT includes most of the TM, and the PF is the remaining small portion of the TM located superior to the PT, as shown in Figure 2.3. The deepest part of the conical TM is called the umbo and is often used as a landmark for TM vibration measurements. The rim of the TM is firmly attached to the bony wall of the ear canal by the fibrocartilaginous ring.

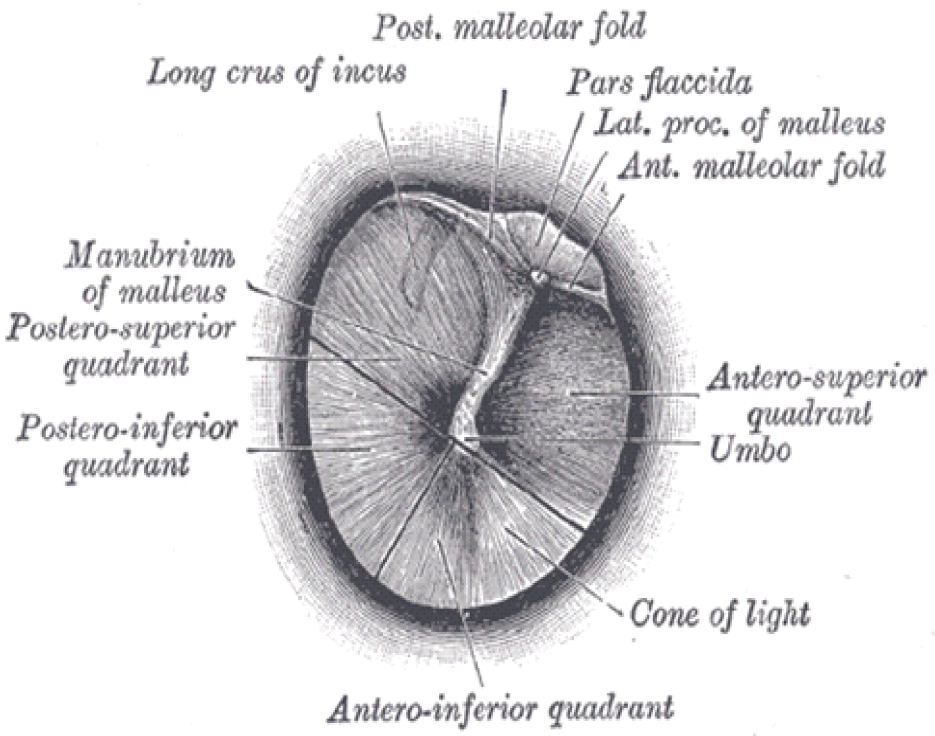

Figure 2.3: Anatomical details of human TM, medial view. (Gray, 1918)

The TM itself consists of three layers: the outer epidermal layer on the lateral side, which is continuous with the epidermis of the external ear; the intermediate layer, or lamina propria; and the inner mucosal layer on the medial side, which is continuous with the mucous lining inside the middle ear. When new epithelial cells grow on the TM, the epithelium migrates outwards from the centre of the TM and peels off as it reaches the external ear canal. This phenomenon provides the human ear with a self-cleaning ability.

In the PT, the lamina propria consists of four sub-layers, as shown in Figure 2.4: two layers of loose connective tissue located next to the epidermis and mucosa respectively; and two intermediate layers containing collagen fibres which are oriented circularly around the manubrium in one layer and radially between the manubrium and the annulus in the other layer. The circular-fibre layer is very thin or even absent around the centre of the TM and becomes thicker towards the annulus. On the other hand, the radial fibres are more densely packed near the centre of TM as the fibres converge towards the manubrium. The anatomical anisotropy due to the fibres may affect the mechanical

properties of the TM. With a numerical model, Funnell and Laszlo (1978) showed that higher stiffness in the radial direction than in the circumferential direction could enhance the coupling between the TM and the manubrium. In any case, the two fibrous layers are believed to dominate the mechanical behaviour of the PT.

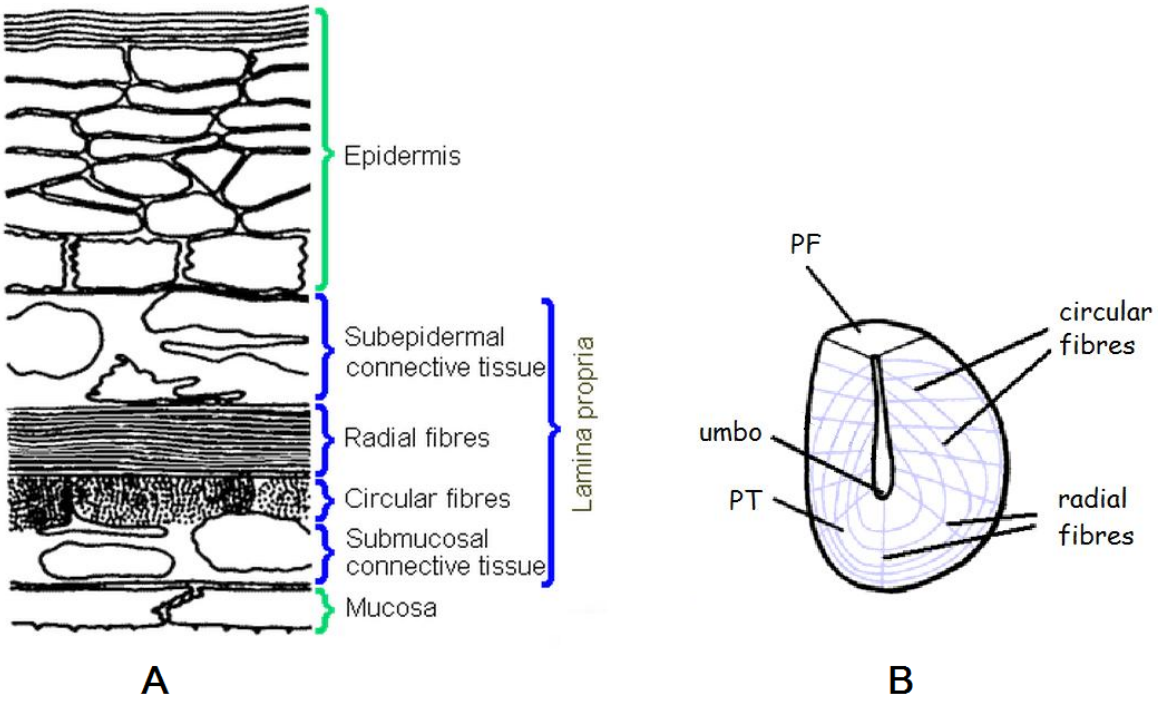

Figure 2.4: (A) Microscopic structure of human PT; (B) schematic illustration of the fibre layers. (After Funnell, 1972)

In the PF, the lamina propria also contains the subepidermal and submucosal layers, but it lacks the layers of highly organized collagen fibres and hence the PF is more flaccid than the PT.

2.1.2 Middle-ear cavity

All middle-ear structures are located within an air-filled bony cavity of the temporal bone. In the human, this cavity has convex medial and lateral walls, as shown in Figure 2.5; it can be further divided into three compartments: the tympanic cavity proper, the epitympanic recess and the mastoid antrum (Moore, 1992).

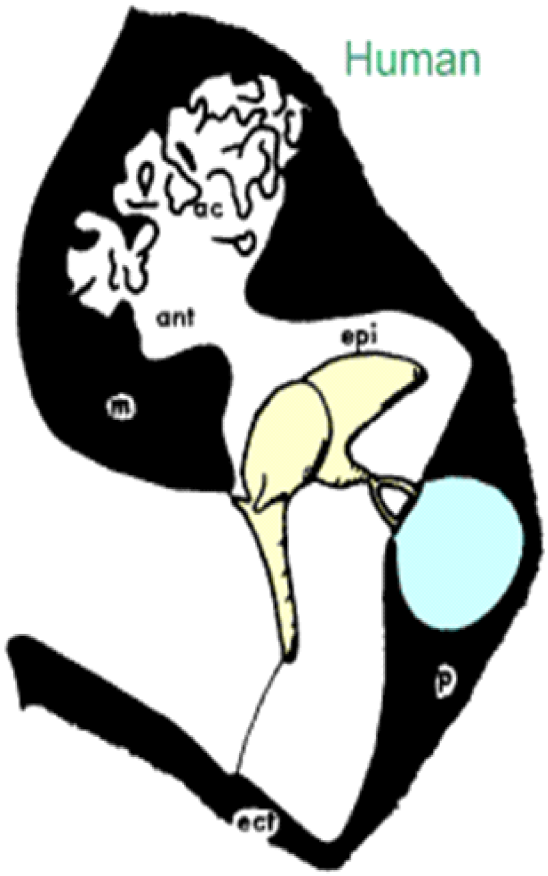

Figure 2.5: Human middle-ear cavity, the anterior view of a section through the right ear (ac = mastoid air cell; ant = antrum; epi = epitympanic recess; m = mastoid bone; p = petrosal bone; ect = ectotympanic bone / tympanic bone). (After Funnell, 1972)

The tympanic cavity proper is the space directly medial to the TM. Its lateral wall contains the TM and surrounding tympanic bone; its medial wall is formed by the dense petrosal bone where the cochlea and vestibular system are encased. Those walls then converge to a narrow anterior wall in which the tensor tympani and the Eustachian tube are located. On the posterior wall, the origin of the stapedius can be found: a tiny bone projection called the pyramidal eminence.

The epitympanic recess is the space directly superior to the tympanic cavity proper, where the head of the malleus and the body of the incus are housed. This cavity is bounded mainly by the mastoid bone which cannot be clearly distinguished from the petrosal bone.

The mastoid antrum is located in the postero-superior part of the epitympanic recess, and leads to the mastoid air cells. Those cells are formed by cancellous mastoid bone and are mostly filled with air. The volume of air added to the middle ear due to those cells varies greatly across individuals, ranging from 0 to about 30 cm^3 (Flisberg & Zsigmond, 1965).

The interior surface of the middle-ear cavity (MEC) is covered by a thin mucus layer excreted by ciliated cells lying on the cavity wall. This mucociliary system is essential for keeping the MEC clean as it transports foreign particles through the Eustachian tube toward the nasopharynx by means of cilia motions. The gas concentration in the MEC is a mixture of that in the ambient air and that in the venous blood. Gas exchange occurs between the cavity and the surrounding venous blood flow via the mucus layer; this exchange mechanism is believed to be one of the essential factors in maintaining the gas composition and pressure inside the middle ear in a physiological steady state (Sadé et al., 1975; Sadé & Ar, 1997).

2.1.3 Ossicles

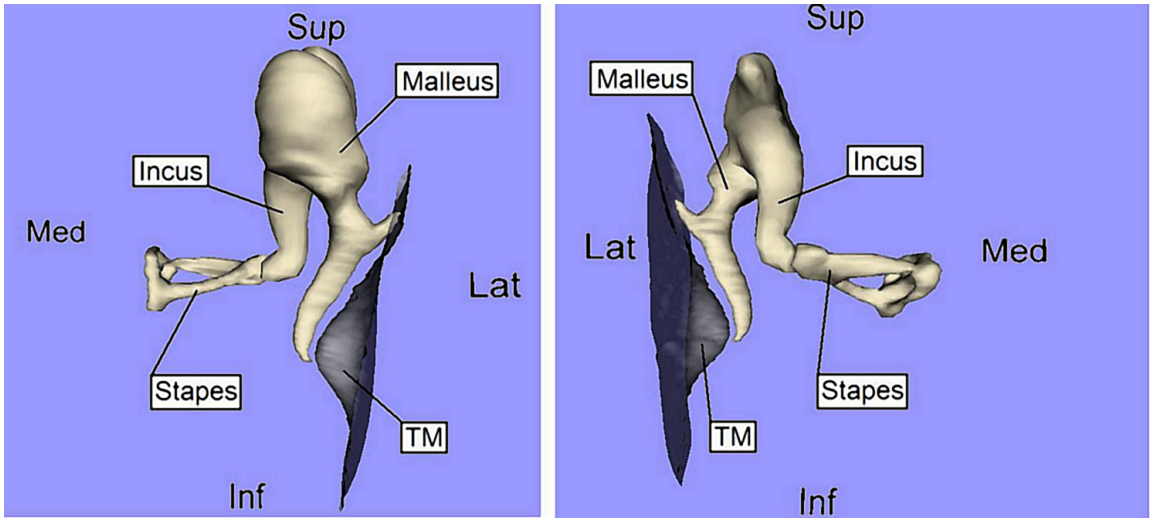

Figure 2.6: Anterior view (left) and posterior view (right) of human middle-ear ossicles (Sup: superior; Inf: inferior; Med: medial; Lat: lateral; TM: tympanic membrane). (After Funnell et al., n.d.)

The middle-ear ossicles are three extremely small bones, namely the malleus, incus and stapes, as shown in Figure 2.6. They are interconnected to form a bony chain with one

end attached to the TM and the other end to the oval window of the inner ear, thereby transmitting sound energy through the middle ear mechanically.

2.1.3.1 Malleus

The malleus (the Latin word for "hammer") is the outermost of the three middle-ear ossicles. It has three processes, as shown in Figure 2.7: the anterior process, the lateral process, and the manubrium which is firmly attached to the medial side of the TM. The inferior tip of the manubrium corresponds to the location of the umbo and is slightly curved and flattened. The head of the malleus is superior to those processes and articulates with the second ossicle, the incus. The small region between the head of the malleus and the manubrium is called the malleus neck.

2.1.3.2 Incus

The incus (the Latin word for "anvil") has three main components, as illustrated in Figure 2.7: the head which articulates with the malleus head by means of a synovial joint; the short process (labelled as "crus" in the figure), which attaches the incus to the cavity wall by ligaments, so as to constrain the motion of the incus; and the long process, of which the tip, called the lenticular process, articulates with the third ossicle, the stapes. As the middle ossicle, the incus transmits sound-induced vibrations from the malleus to the stapes by both rotational and translational motions.

2.1.3.3 Stapes

The stapes, so named for its stirrup-like shape, is the innermost middle-ear ossicle. It is the smallest and lightest bone in the human body and consists of five parts, as shown in Figure 2.7: the head, which forms a synovial joint with the lenticular process; the neck; the anterior and posterior crura; and the footplate (labelled as "base" in the figure) which is roughly flat and is connected to the oval window of the inner ear. In the early stages of embryonic development, the stapedial artery penetrates the stapes and provides the main

blood supply to the embryonic head; towards the end of embryonic development, the carotid artery develops and the stapedial artery disappears in the human ear, leaving a hole between the crura of the stapes (Romer & Parsons, 1977).

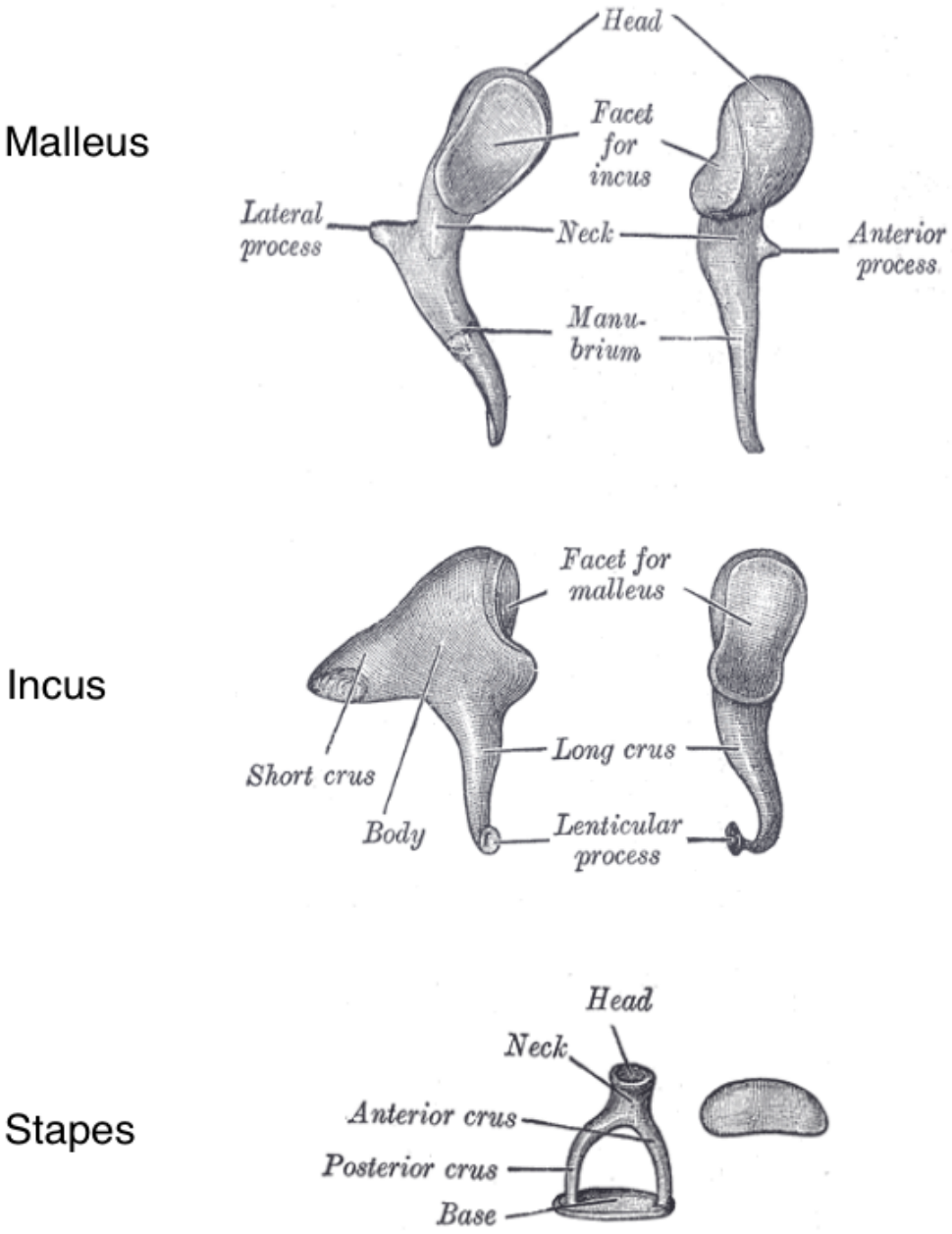

Figure 2.7: Malleus, incus, stapes of the human middle ear. (After Gray, 1918)

2.1.4 Ligaments and muscles

2.1.4.1 Ligaments

Middle-ear ligaments play an essential role in structural support in the middle ear. The malleoincudal joint capsule, the incudostapedial joint capsule and the stapedial annular ligament are made of elastic fibres which stabilize the joints and ensure proper articulations between the ossicles, so that sound energy can be effectively transferred to the inner ear.

The malleoincudal complex is suspended by several ligaments, of which the posterior incudal ligament (PIL) and the anterior mallear ligament (AML) fix the complex to two points on the MEC walls and tend to define an axis of rotation.

2.1.4.2 Muscles

There are two muscles in the middle ear, as shown in Figure 2.8: the stapedius and the tensor tympani. The stapedius is the smallest skeletal muscle in the human body; it is embedded in the posterior wall of the MEC and is connected to the neck of the stapes. This muscle is innervated by the facial nerve, and displaces the head of the stapes in the posterior direction upon contraction.

The tensor tympani is connected to the neck of the malleus, with the body of the muscle embedded in the bony wall of the air cavity. This muscle is innervated by the mandibular nerve and contraction of this muscle generates tension in the TM.

In addition, smooth-muscle fibres have been found in the fibrocartilaginous ring surrounding the TM (e.g., Yang & Henson, 2002). Their function is unknown.

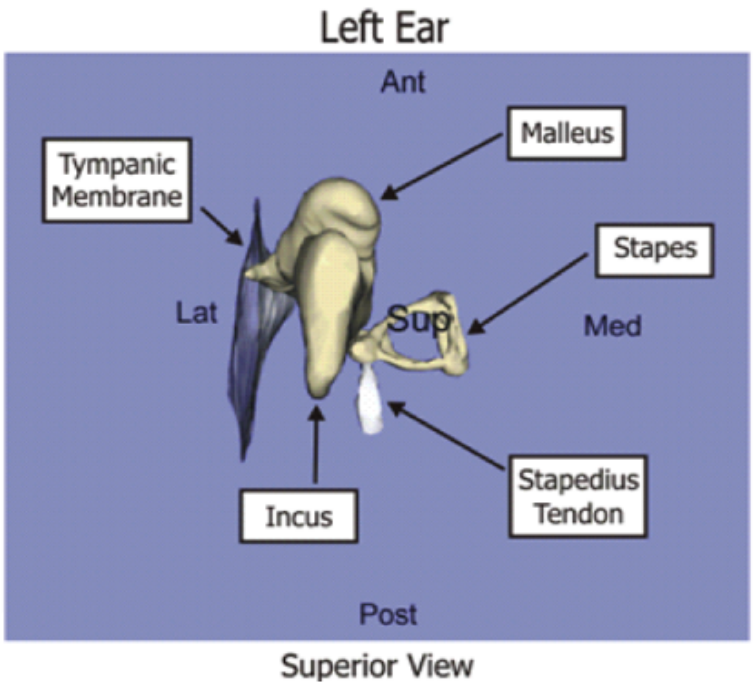

Figure 2.8: Muscles in the middle ear: stapedius and tensor tympani. (After Funnell et al., n.d.)

2.1.5 Eustachian tube

The Eustachian tube (ET) is a canal, roughly 3 cm long, connecting the anterior portion of the MEC to the nasopharynx, as shown in Figure 2.9. Similar to the MEC, the ET surface is covered by a mucociliary system which can continuously remove debris from the MEC to the nasopharynx. Thus, it is believed to be another factor essential for the well-being of the middle ear (Sadé & Ar, 1997).

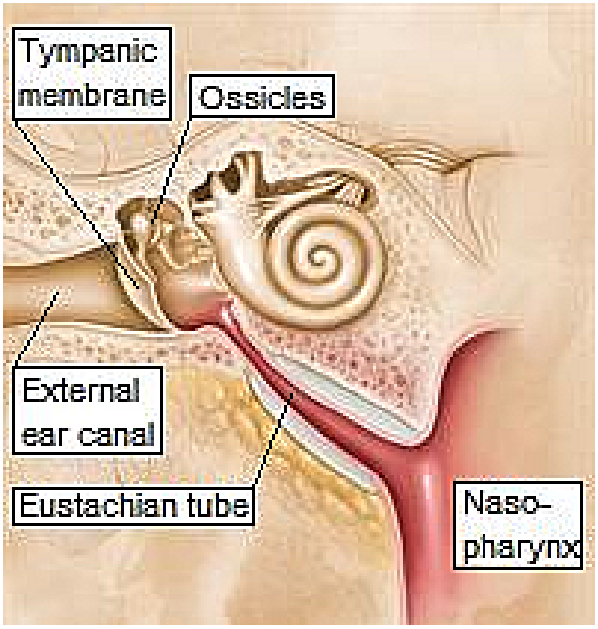

Figure 2.9: Human Eustachian tube. (Lisano Valentino, 2009)

The ET plays an important role in middle-ear pressure regulation. A slight change in the middle-ear pressure can reduce sound transmission into the middle ear, thereby affecting the ability to hear. A large pressure variation in the middle ear, for example during middle-ear infection or under conditions like flying and diving, causes an uncomfortable feeling at best and may damage the TM. In order to equalize the middle-ear pressure to the ambient pressure (in the pharynx), the ET normally opens for about 0.2 second once every 1 to 2 minutes due to muscle contractions during mandible movements such as swallowing and yawning (Sadé & Ar, 1997). Hence, the TM is protected from pressure disturbances under normal circumstances.

2.2 Gerbil middle ear

The Mongolian gerbil was chosen for our experiments. Hence, the morphology of the gerbil middle ear is compared with that of the human in this section.

2.2.1 Bulla

In gerbils, the inflated (hypertrophied) ectotympanic bone forms a large MEC, called the bulla, in which most middle-ear components (ossicles, muscles, ligaments, etc.) except the TM are encased. However, in the human middle ear, the ectotympanic bone is not inflated and thus there is no bulla. As shown in Figure 2.10, the MEC volume encapsulated by the gerbil's bulla is almost as large as that of its brain case (Lay, 1972). The large volume is thought to enhance the gerbil's hearing sensitivity at low frequencies, allowing the gerbil to detect approaching predators faster (Rosowski et al., 1997).

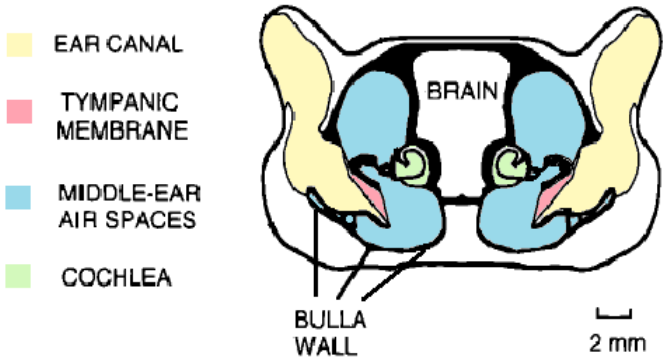

Figure 2.10: A schematic coronal section of the gerbil head. (After Ravicz et al., 1992)

As shown in Figure 2.11, a part of the bulla inferior to the canal entrance overlaps with a portion of the bony external ear canal lateral to the TM, together largely obstructing the view of the PT. It is therefore very difficult to measure PT vibrations in gerbils.

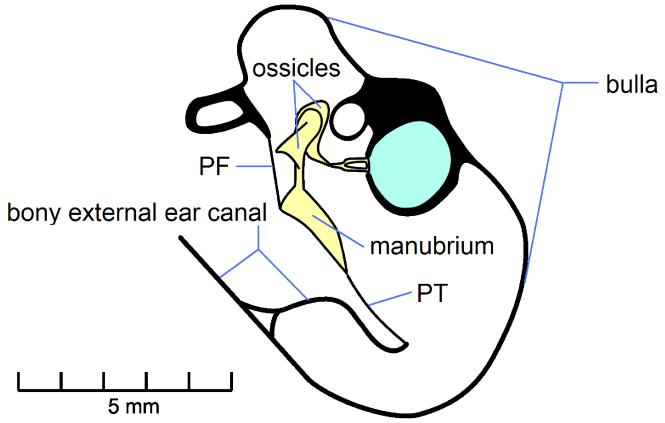

Figure 2.11: Gerbil middle-ear cavity: anterior view of a section through the right ear. (http://audilab.bme.mcgill.ca/AudiLab/teach/me_saf/me_saf.html, Funnell, 2011)

2.2.2 Pars flaccida

The PF in the gerbil is roughly circular and is relatively large, with its surface area being 10-20% of the total TM surface area (Dirckx et al., 1998), as shown in Figure 2.12. On the other hand, the human PF is triangular and relatively small with a surface area of only 2-3% of the TM surface area (Dirckx et al., 1998).

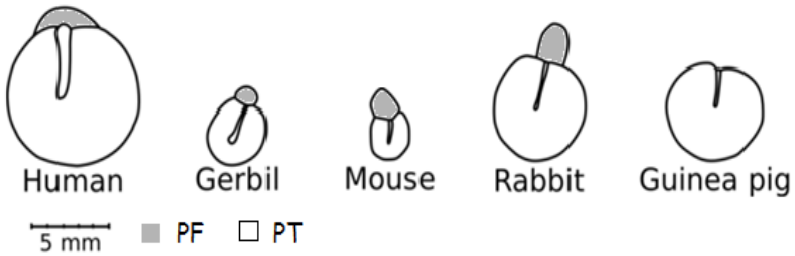

Figure 2.12: Human TM compared with TM of other species. (After Funnell, 2011)

The TM in gerbil is also relatively large compared with its body size, which is believed to improve the low-frequency hearing sensitivity (Rosowski et al., 1997). The plane of the PF is inclined about 30° with respect to the TM annulus plane, resulting in a fold at the boundary between the PF and the PT. This boundary is reinforced by the attachment of the lateral process of the malleus, and is believed to be a functional border of the inferior PF as it does not move, or barely moves, with the whole PF in the presence of middle-ear

pressure gradients (Dirckx et al., 1997). The PF is also bounded inferiorly by a border formed by the anterior and posterior tympanic striae (Gea et al., 2010). The anterior, superior and posterior rim of the PF is firmly attached to a thin bony ledge.

2.2.3 Connection between tympanic membrane and manubrium

The manubrium in the gerbil has a T-beam cross-section with the flat top surface tightly attached to the TM. In the guinea-pig, Uno (2000) found that the radial bundles "were continuous with" the manubrium, and that the collagen fibrils "contacted the bone surface". The attachment appears to be similar in the gerbil (Gea et al., 2010).

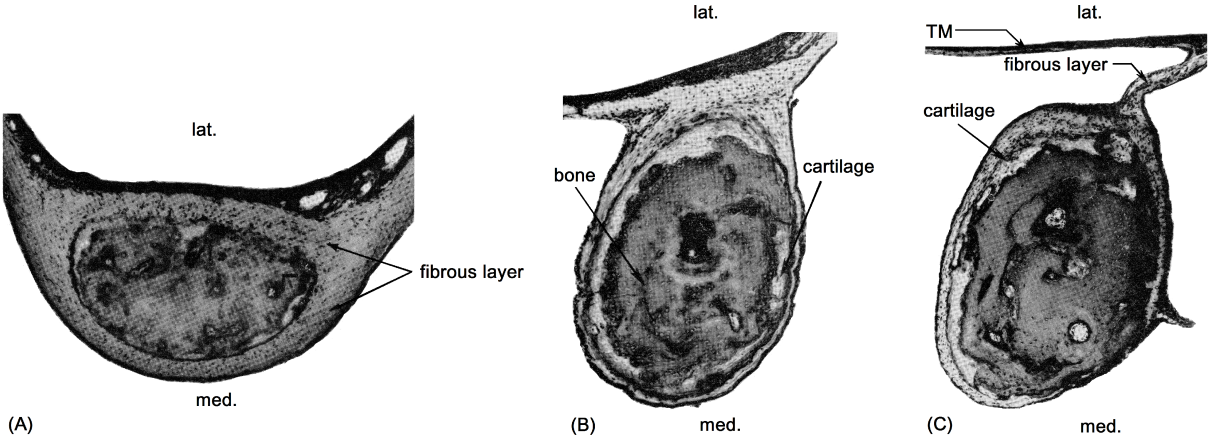

Figure 2.13: Cross-section view of three regions along the human manubrium (med.: medial, lat.: lateral): (A) the umbo region where fibres are equally distributed on both lateral and medial sides; (B) the mid-manubrium region where fewer fibres are found on the medial side; (C) the superior one-third of manubrium where the the connection to the TM is very thin. (After Graham et al., 1978)

On the other hand, the human manubrium has an approximately elliptical cross-section, with its long axis parallel to the TM at the umbo then gradually becoming perpendicular to the TM towards the lateral process. Both the superior and inferior regions of the manubrium are tightly connected to the TM, being firmly wrapped by fibres in the lamina propria layer of the TM. In between those regions, however, the connection is much looser, with a very thin layer of lamina propria fibres extending from the medial side of TM and making contact with the lateral side of the manubrium perichondrium (Graham et al., 1978; Gea et al., 2010), as shown in Figure 2.13C.

2.2.4 Anterior mallear process

In gerbils, a bony connection was found by Rosowski et al. (1999) between the temporal bone of the MEC and the anterior process of the malleus. Elkhouri et al. (2006) considered this connection to be composed of soft tissue rather than bone, based on histological and X-ray micro-CT evidence, but recent access to new histological material (e.g., Figure 2.14) provided by C. Northrop (Temporal Bone Foundation, Boston, MA) has made it clear that Rosowski's description was correct.

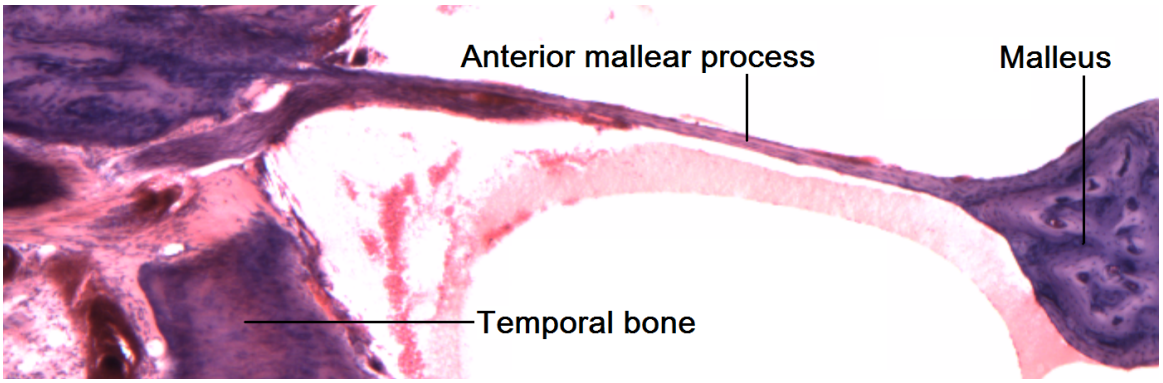

Figure 2.14: A histological section of the anterior mallear process of the right ear in a gerbil; a bony connection can be seen between the temporal bone and the process.

2.3 Middle-ear mechanics

As mentioned earlier, airborne sound waves are transmitted into the liquid-filled inner ear via the middle ear. In order to minimize the loss of acoustic energy transmitted from the low-impedance air medium to the high-impedance liquid medium, the middle ear acts as a mechanical transformer which efficiently transmits the input sound signal. This transmission mechanism is often thought of as being achieved by three anatomical features of the middle ear: the surface-area ratio of the TM and the stapes footplate, the lever ratio of the ossicular chain, and the curvature of the TM.

2.3.1 Surface-area ratio

Pressure is defined as perpendicular force per unit area: $P = F / A$. If a given force is applied to a smaller surface, a greater pressure will be generated. Assuming no energy loss in the ossicular chain, the amount of force exerted on the TM (F_{tm}) must be the same as that exerted by the stapes footplate (F_{fp}), in other words, $P_{tm} A_{tm} = P_{fp} A_{fp}$. Therefore, the sound pressure striking the TM will be multiplied by the TM/footplate surface-area ratio: $P_{fp} = P_{tm} * (A_{tm} / A_{fp})$. Since the surface area of the TM is much larger than that of the footplate, the pressure at the footplate becomes much larger than that at the TM. This greatly enhances sound transmission into the cochlea. This ratio was estimated to be between 15 and 26 in human (Wever & Lawrence, 1954; Békésy, 1960) and about 28 in gerbil (Lay, 1972).

2.3.2 Ossicular lever ratio

The interconnected ossicles form a bony chain which allows sound to travel mechanically from the TM to the oval window. Dahmann (1930) (as cited by Nambiar, 2009) proposed that the malleus and incus act as a mechanical lever system rotating about a fixed axis joining the AML and PIL, as illustrated in Figure 2.15. Two lever arms are formed orthogonal to this axis: the force arm extending from the axis to the umbo, and the

resistance arm running from the axis to the lenticular process of the incus (LPI). The ratio between the force and resistance arms was estimated to be 1.3 in human (Wever & Lawrence, 1954) and about 3.3 in gerbils (Lay, 1972). Hence, this lever ratio would result in greater forces at the stapes, which would then generate greater pressures in the cochlea.

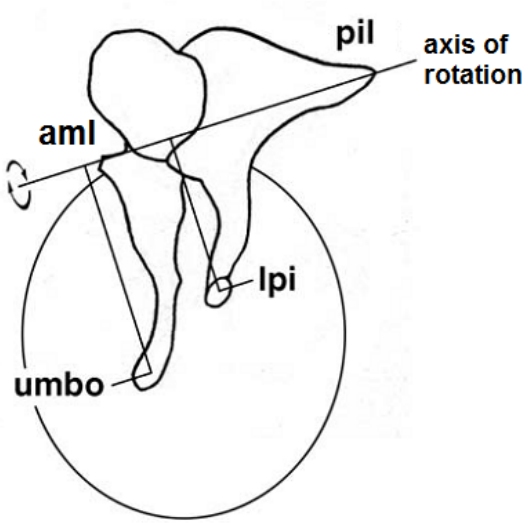

Figure 2.15: Schematic of the lever arm system proposed by Dahmann (aml: anterior mallear ligament; pil: posterior incudal ligament; lpi: lenticular process of the incus). (Willi, 2003)

Ossicular motions become more complicated at high frequencies due to mass effects. Examples of those complications are relative motions between malleus and incus, changes in the axis of rotation, flexing of the manubrium and so on (Gyo et al., 1987; Decraemer et al., 1991, 1994).

2.3.3 Tympanic-membrane curvature

The interaction between the forces along the circular fibres and those along the radial fibres may result in a curvature-related sound transmission mechanism. Helmholtz (1869) suggested that the outward convexity of the TM provides a lever mechanism for the incoming sound pressure. As illustrated in Figure 2.16, a slight variation in sound pressure can change the TM curvature and generate a compression force in the radial fibres; straightening of those fibres results in a relatively large force at the umbo. A study

by Khanna and Tonndorf (1972) supported this theory. Moreover, Funnell (1996) found in simulation results that some regions of the TM were more effective than they would be without this curvature.

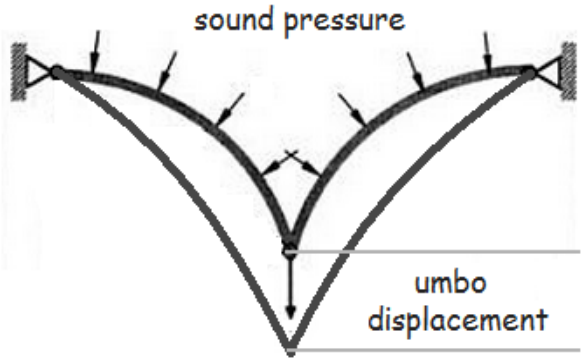

Figure 2.16: Schematic of the sound-pressure multiplication mechanism proposed by Helmholtz. (After Nambiar, 2009)

2.3.4 Overview of transformer mechanism

All of these mechanisms, the TM-footplate area ratio, the ossicular lever ratio and the TM curvature transformation ratio, are tied together in determining the characteristics of the acoustic-signal-to-mechanical-force transformation in the middle ear. They are interrelated and it is thus impossible to cleanly separate the transformation behaviour into distinct mechanisms (Funnell, 1996). Factors such as the geometry of the TM and ossicles, the articulations of the ossicular chain, and the ligaments holding the ossicles, are all involved in these mechanisms and therefore can influence the effectiveness of middle-ear sound transmission.

2.4 Middle-ear pressure regulation

Middle-ear pressure (MEP) is maintained at the physiological steady state by both passive and active gas exchange. The former occurs at the mucosal layer of the MEC wall and the latter involves functions of the ET.

Partial pressures of gases dissolved in the venous blood surrounding the MEC normally display very low O_2, slightly low N_2 and high CO_2 compared with the air at sea level (e.g., in the ear canal), as illustrated in Figure 2.17. Since the partial pressures of gases inside the MEC are initially very similar to that of a mixture of the ambient air and the gas inside the nasopharynx, the resulting pressure gradients trigger gas diffusion across the mucosa so as to equilibrate gas concentrations of the MEC to those of the venous blood.

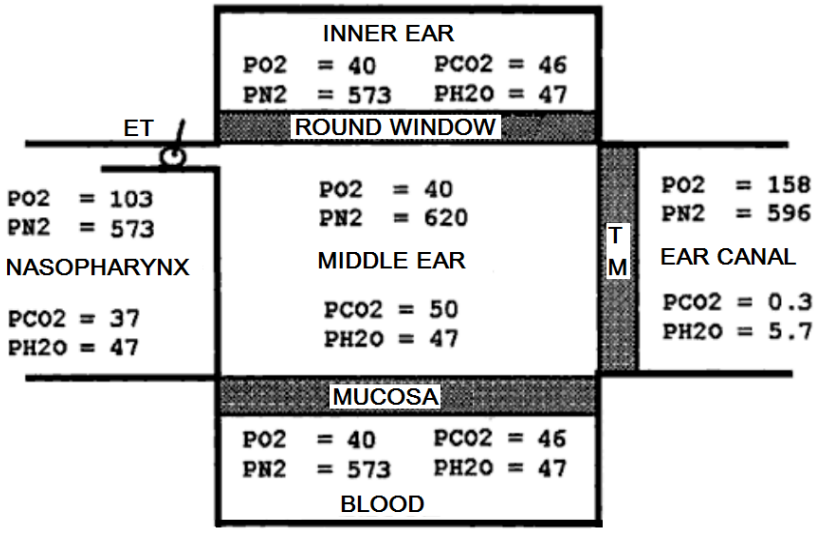

Figure 2.17: Schematic illustration of the middle-ear gas exchange with four compartments. The partial pressures of all gases were measured with closed ET. Gas exchange across the ET is active and muscle assisted; that across the other compartments is passive and diffusive, with the exchange rate through mucosa being the fastest. (After Doyle et al., 2000)

Under normal circumstances, the reactive gases (O_2 and CO_2) exchange much faster than the inert gas (N_2) and therefore can reach equilibrium state with the venous blood quickly. Accordingly, the slow exchange rate of N_2 results in an N_2 partial pressure approximately

50mmHg higher in the MEC than in the venous blood (Felding et al., 1987). In that regard, the exchange rate of N_2 is believed to be a determining factor for the rate of negative pressure development in a closed MEC (Doyle et al., 2000).

This slowly accumulated negative middle-ear pressure, if not released by subsequent openings of the ET, may retract the TM, increase the permeability of the mucosal vasculature to fluid, and pull mucosal fluid from the blood and extracellular spaces into the middle ear. This last process may lead to middle-ear diseases such as secretory otitis media and, in severe cases, mucosal inflammation (Doyle et al., 2000). Moreover, Doyle et al. (1995) have demonstrated that the exchange rate of N_2 increases with increasing blood flow surrounding the middle ear. Hence, under pathological conditions associated with inflammation, the higher N_2 exchange rate can result in a faster accumulation of negative pressure in the middle ear. Such a feedback mechanism may deplete the lamina propria fibres of the TM, and ultimately cause irreversible changes such as the development of retraction pockets and cholesteatoma (Tos et al., 1984; Gaihede et al., 2010).

On the other hand, the MEC can become over-pressurized sometimes. The partial pressure of CO_2 in blood increases during sleep due to respiratory drive suppression (Bylander et al., 1985), which then triggers more CO_2 diffusion from blood into the MEC. Moreover, the ET does not open effectively during sleep, and hence the MEP increases significantly.

Neither positive nor negative MEP is desirable because it increases the acoustical middle-ear impedance and hence compromises the ability to hear. The ET helps to regulate the MEP as it opens periodically and provides direct communication between the MEC and the environment (Doyle et al., 2000). Elner (1976) has estimated that, under physiological steady state, around 1 to 2 ml of gas enters the MEC via the ET per day, which is roughly the same as the amount of net gas loss through trans-mucosa diffusion from the MEC to the venous blood flow.

Chapter 3
Previous Studies

Numbers of *in vivo* and *post mortem* experimental approaches, as well as numerical models, have been used to study middle-ear mechanics in various species. This chapter presents a review of previous studies relevant to our research. In Section 3.1, several human and other non-gerbil studies are discussed briefly. Section 3.2 presents both experimental and numerical studies that have been conducted on the Mongolian gerbil, with a focus on TM vibrations. Finally, Section 3.3 highlights some important issues from previous studies.

3.1 Non-gerbil studies

Various experimental techniques have been used to investigate middle-ear vibrations and deformations, such as capacitive probes, high-speed cinematography, stroboscopic techniques and interferometric methods (laser holography, speckle pattern interferometry, moiré topography and scanning laser interferometry). In particular, laser Doppler vibrometry (LDV) has become a popular method to study the vibration patterns of the TM (Buunen & Vlaming, 1981; Doan et al., 1996; Bigelow et al., 1996, 1998; Akache et al., 2007; Ellaham, 2007; Nambiar, 2009) and the motions of the ossicles (Schön & Müller, 1999; Nakajima et al., 2005); it has also been shown to be helpful in clinical applications for the diagnosis of middle-ear pathologies (Goode et al., 1996; Huber et al., 2001; Rosowski et al., 2003, 2008). In this study, LDV was chosen to measure the vibration patterns of the gerbil TM; further discussions of this technique can be found in Chapter 4.

3.1.1 Tympanic-membrane response

Funnell and Laszlo (1982) presented a comprehensive review of early experimental observations of TM shape and vibrations dating as far back as 1874.

3.1.1.1 Static deformations

The full-field shape deformations of the human TM in response to large static pressures were measured by Dirckx and Decraemer (1991), using phase-shift moiré topography. The authors observed two displacement maxima: one in the posterior region of the PT and a larger one in the anterior region. However, measurements were made only in a single specimen and they speculated that the anterior maximum was unusual due to "a weak spot with reduced elastic modulus". They also reported a strong asymmetry between the lateral and medial movements of the TM, and further concluded that the manubrium was not rotating around a fixed axis under large static pressures. These TM deformations were recorded some time after the application of the large static pressures, so the viscoelastic characteristics of the TM (creep and stress relaxation) must be taken into account. In this and other studies using moiré topography, the deformations are quasi-static, large and non-linear, unlike the dynamic, small and linear deformations in vibration measurements that use frequencies and sound pressures in the normal range for hearing.

3.1.1.2 Sound-induced vibration patterns

The first complete picture of human TM vibrations in response to sound stimuli was obtained by Tonndorf and Khanna (1972), using time-averaged laser holography over the frequency range of 0.4 to 6 kHz. As shown in Figure 3.1, the holographic interference results in dark and bright fringes representing the iso-amplitude contours of vibration. At low frequencies, their results indicate a maximum in the posterior region and another maximum of lower magnitude in the anterior region. As the frequency increases, the vibration patterns become more complex and start to break up into sectional vibrations at about 3 to 4 kHz. Similar results were reported in cats (Khanna & Tonndorf, 1972), in which the transition from simple to complex vibration patterns occurred at around the same frequencies as in human ears.

Figure 3.1: Time-averaged holograms measured at six frequencies between 0.5 to 5 kHz. TM of left human-cadaver ear. Orientation: right = posterior, left = anterior. (Tonndorf and Khanna, 1972)

Laser Doppler vibrometer measurements at multiple points on the rat TM and manubrium for a frequency range of 1 to 10 kHz have been reported by our group (Akache et al., 2007). In that study, the vibration patterns appeared simple up to approximately 6 kHz for most rats. As shown in Figure 3.2, the displacements are smallest at the manubrium and largest in the posterior region.

Recently, Rosowski et al. (2009) used opto-electronic holography to measure TM vibration patterns over the frequency range of 0.5 to 20 kHz in different species: live chinchilla and cadaveric chinchilla, cat and human. Time-averaged holograms of all specimens displayed simple, complex or ordered fringe patterns depending on the frequency. The authors concluded that the surface waves of the TM varied with frequency

and species, and estimated that the wave speeds were from 20 to 65 m/s. Based on the holographic images, they also inferred the presence of standing waves (standing wave ratio > 4) and suggested that at least 36% of the energy in any surface waves was reflected at the boundaries.

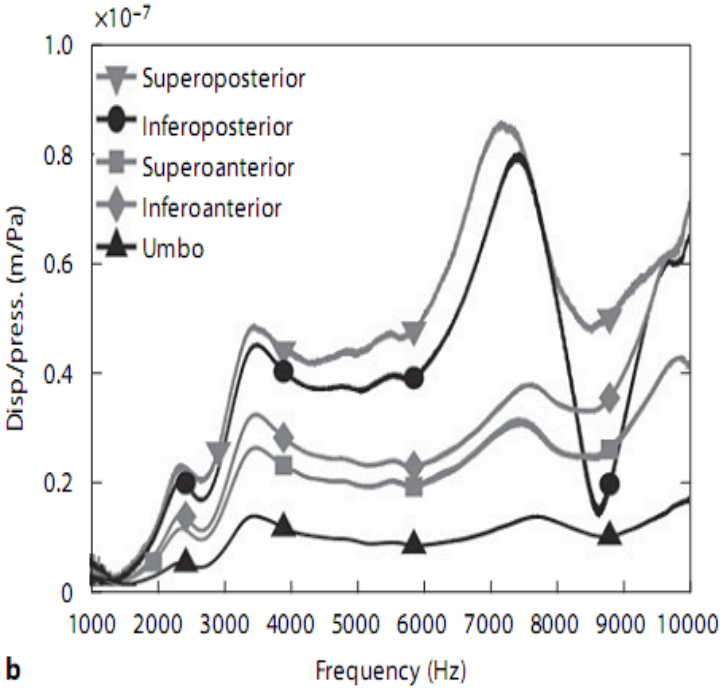

Figure 3.2: Tympanic membrane displacements of a rat specimen. Disp./press. = displacement normalized by input sound pressure. (Akache et al., 2007)

3.1.2 Ossicular motion

The incudo-mallear complex was traditionally thought of as a rigid body rotating around a fixed axis (Békésy, 1949, 1960; Wever & Lawrence, 1954; Tonndorf & Khanna, 1972). Gundersen and Høgmoen (1976) used time-averaged holography to measure the movement of the ossicular chain and observed that the malleus and incus moved like a lever system rotating around a frequency-dependent axis of rotation. Using a video measuring system with a stroboscopic illumination technique, Gyo et al. (1987) noted an increase in the ossicular lever ratio with frequency, which they attributed to a shifting of the incudo-mallear rotational axis. Decraemer et al. (1991) used heterodyne laser

interferometry to study the malleus motion in anaesthetized cats. Using micro-beads to enhance the signal reflectivity, they measured the frequency responses at four points along the manubrium, as illustrated in Figure 3.3. They concluded that the malleus underwent purely translational motions at some frequencies, rotational motions at others and mixed at most frequencies, and that the axis of rotation shifted with frequency. Moreover, they suggested a possible bending at the malleus tip at high frequencies. Incorporating realistic values of manubrial thickness from serial histological sections into a finite-element model of the cat TM, Funnell et al. (1992) provided numerical evidence that such manubrial bending might be expected, and suggested that it might also occur at low frequencies.

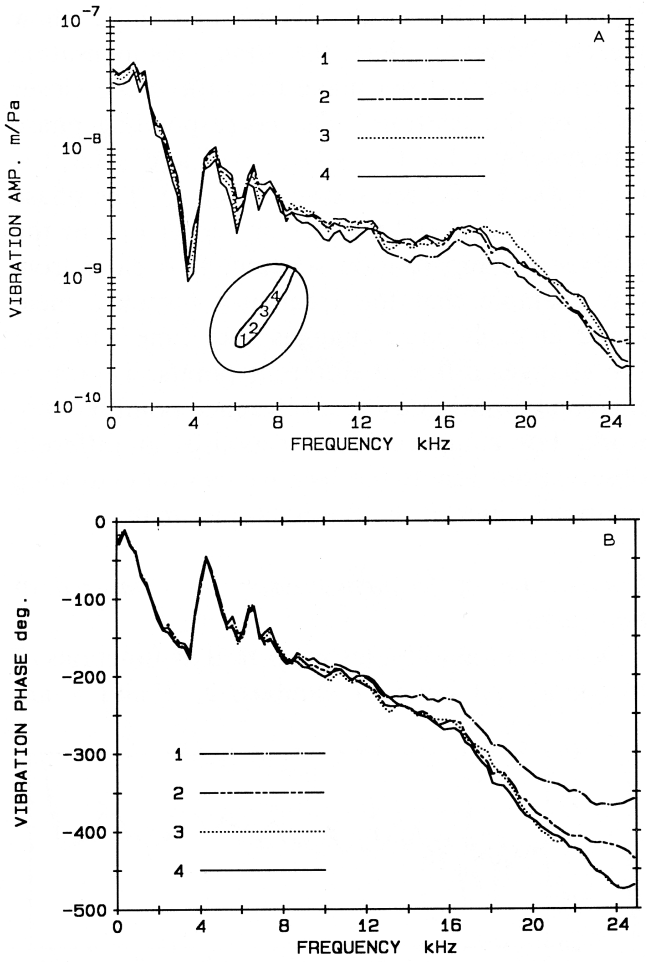

Figure 3.3: Amplitude and phase of the normalized displacements measured at four points along the manubrium. (Decraemer et al., 1991)

Combining an improved heterodyne interferometer which could provide good signal reflectivity without the micro-beads, and a two-axis goniometer with its rotational axes positioned at the focal plane of the interferometer, Decraemer et al. (1994b) obtained three-dimensional vibration measurements at a single point of the cat umbo. They reported that the vibrations at the umbo did not follow a straight line but rather an elliptical path, and that the shape and the orientation of this ellipse varied with frequency, both indicating a shift in the rotational axis. With the same experimental set-up, they later performed one-dimensional vibration measurements along the cat manubrium and concluded that the malleus motion was a frequency-dependent combination of translations and rotations (Decraemer & Khanna, 1994). With further investigations of the bending motion of the cat manubrium, they confirmed that the bending was moderate near the tip at low frequencies, and became quite strong up to the middle of the manubrium at higher frequencies (Decraemer et al., 1994a). Their study of cat malleus vibrations was further extended to three-dimensional measurements at multiple points along the manubrium, providing more experimental evidence against the classical description of a pure rotation about a fixed axis (Decraemer & Khanna, 1996, 1997). More recently, Decraemer et al. (2001) reported three-dimensional vibration measurements of each ossicle in the human ear, confirming the presence of complex motions. Their results also revealed a significant amount of slippage between malleus and incus at low frequencies.

3.2 Gerbil studies

Early gerbil studies focused mainly on auditory sensitivity rather than the vibration motions of middle-ear components. By recording the cochlear microphonic response at the round window, Finck and Sofonglu (1966) estimated that the gerbil's auditory response fell within the range of 0.2 to 32 kHz, with the maximum sensitivity being between 3 and 5 kHz. Similar results were also found by Lay (1972). Ryan (1976) found that the gerbil can respond to acoustic stimuli within the range of 0.1 to 60 kHz, and reported that the auditory thresholds were lowest between 1 and 16 kHz, and decreased with a slope of 12 dB/octave between 0.1 and 1 kHz. Consistent with these findings, Henry et al. (1980) observed a broad mid-frequency profile and elevated high-frequency thresholds from their study of age-related hearing loss in gerbil.

3.2.1 Middle-ear cavity

The morphology of the middle-ear air cavities is an influential factor in determining auditory thresholds. In particular, some small rodents such as kangaroo rats and gerbils show large hypertrophied MEC's which contribute to their low-frequency hearing sensitivity (Webster, 1962; Lay, 1972; Webster & Webster, 1972; Ravicz & Rosowski, 1997).

The first experimental evidence revealing the functional significance of the hypertrophied MEC was presented by Webster (1962). He reduced the MEC cavity volume in kangaroo rats and discovered that the enlarged MEC indeed increased transmission of the middle-ear system by decreasing the stiffness of the air cushion behind the TM, which improved the hearing sensitivity as measured with cochlear microphonics. Later, Webster and Webster (1972) reported a threshold elevation of approximately 10 dB for frequencies below 2 kHz with a 75% volume reduction in the kangaroo rat's MEC. At about the same time, Lay (1972) tested thirteen species of the Gerbillinae and concluded that ears with inflated MEC could result in greater auditory sensitivity and "enhance the ability of these

rodents to survive in open desert situations by detecting and evading predators".

More recently, the group of Rosowski presented a collection of studies on the effects of MEC in gerbils, using middle-ear input impedance measurements and mathematical models (Ravicz et al., 1992, 1996; Ravicz & Rosowski, 1997). They estimated that "below 1 kHz … the middle-ear air spaces contribute about 70% of the acoustic stiffness of the auditory periphery" and that "a reduction in MEC volume to 1/4 its normal value is predicted to cause a frequency-selective elevation in auditory threshold of as much as 12 dB, with the largest elevation occurring in the 1–2 kHz range". Finally, they concluded that the large middle-ear cavities in gerbils and in some other small rodents (kangaroo rats, hamsters and rats) "improve hearing sensitivity below 3 kHz and thereby improve the animal's chances for survival".

3.2.2 Static deformations

Using a real-time differential moiré interferometer, von Unge et al. (1993) recorded the displacement patterns of the gerbil TM in response to static (or quasi-static) pressure differences between the ear canal and the middle ear. From their measurements in eighteen specimens, they found two local displacement maxima whose locations did not vary with pressure: one in the anterior region of the PT, and the other one with greater displacement magnitudes in the posterior region. As shown in Figure 3.4, these maxima are located closer to the manubrium of the malleus than to the annulus; both are at approximately the same level, slightly superior to the umbo.

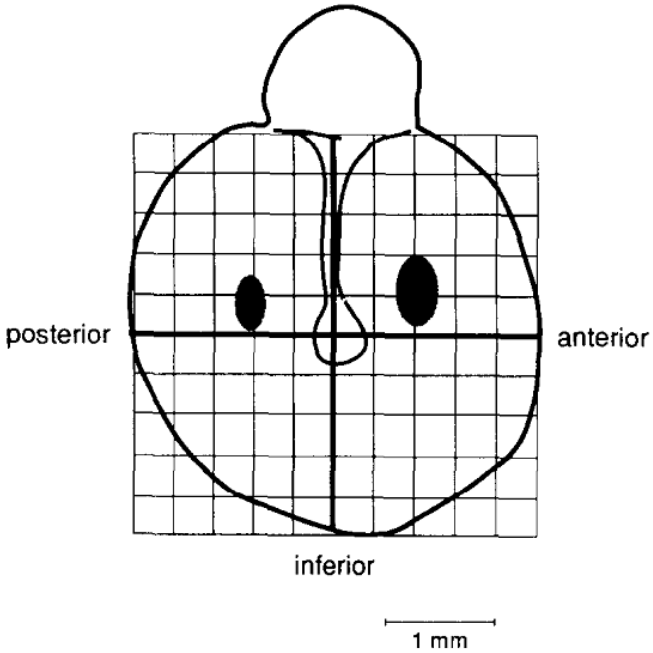

Figure 3.4: A schematic presentation of the gerbil TM showing the two displacement maxima occurred in normal ears under positive pressures up to +20 cm H_2O in the extremal meatus. (von Unge et al., 1993)

Dirckx et al. (1998) used an opto-electronic moiré interferometer to perform *in vitro* measurements of PF volume displacements in gerbils. The specimens were subjected to sequential cycles of both positive and negative pressure difference between the ear canal and the middle ear while measurements were taken at short intervals. They found that both the PF and PT responded non-linearly to the large static pressure differences across the TM. They also observed that the first and last measurements between pressure cycles were significantly different, indicating the dependence on stress-strain history, the effects of hysteresis, and the need for preconditioning.

With a higher-resolution moiré interferometer, Dirckx & Decraemer (2001) obtained full-field gerbil TM deformations at quasi-static pressures after serially removing middle-ear components. For the baseline response, they presented a deformation curve along a line perpendicular to the manubrium and slightly inferior to the umbo. As shown in Figure 3.5B, this curve confirms the existence of two displacement maxima located in the anterior and posterior regions, close to the manubrium. Furthermore, they concluded that

removing cochlea, stapes and tensor tympani had no effect on the static TM deformations. Exposing the incudo-mallear joint increased the TM displacements, possibly because of damage to the posterior incudal ligament, and cutting the anterior mallear bony connection affected the shape of the TM in the rest position.

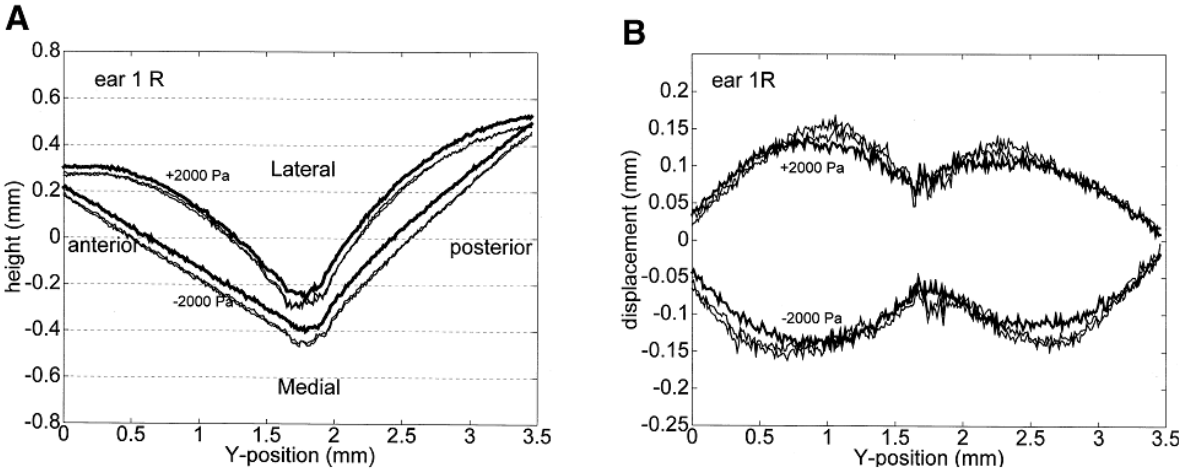

Figure 3.5: Deformation curves along a line perpendicular to the manubrium and slightly inferior to the umbo. All recorded under +2 kPa and -2 kPa, with the thin lines representing two subsequent measurements and the thick line obtained after waiting 45 min. A) Shape profiles; B) deformation profiles. (Dirckx & Decraemer, 2001)

A more recent study by Didyk et al. (2007) using laser Doppler interferometry investigated the PF response under atmospheric-pressure fluctuations. They observed that the PF displacements could follow pressure oscillations within a few Pascals, and that the hysteresis was more pronounced during larger pressure oscillations, indicating visco-elastic effects in the PF. They suggested an important role for the PF as a very sensitive middle-ear pressure regulator in the range of natural atmospheric pressure fluctuations.

3.2.3 Vibration measurements

Various groups have performed vibration measurements on the middle-ear components in gerbils to investigate middle-ear mechanics. Ravicz et al. (1992) and Ravicz & Rosowski (1997) measured the middle-ear input impedance and presented a series of studies on sound-power collection by the auditory periphery. Using interferometric methods, many

groups have measured the ossicular motions, especially the stapes velocity transfer function, over a broad range of frequencies (e.g., Rosowski et al., 1999; Overstreet & Ruggero, 2002; Decraemer et al., 2007; Ravicz et al., 2008; de La Rochefoucauld et al., 2008; Decraemer et al., 2011). However, these studies did not explore the vibration patterns of the TM. From among the many studies of TM vibrations in gerbils, the following studies are discussed in detail: Cohen et al. (1993), measuring umbo velocities in different age groups; Rosowski et al. (1997), comparing umbo and PF velocities, with both open and closed MEC, and with normal, stiffened and removed PF; de La Rochefoucauld and Olson (2007, 2010), presenting velocity measurements at multiple points along the manubrium and along a line on the PT, and at a single point on the stapes; and recent studies from our group (Ellaham, 2007; Nambiar, 2009; Maftoon et al., 2011).

Cohen et al. (1993) studied the development of middle-ear function in live gerbils from eight age groups: 10, 15, 20, 25, 30, 35, 42 days after birth, and adults between 77 and 91 days old. Using a heterodyne laser interferometer, they obtained velocity measurements at the umbo in response to a 100 dB SPL sound stimulus over the range of 0.2 to 40 kHz. Comparing the results of different age groups, the authors observed a 10 dB improvement in the umbo velocity at low frequencies from the 15-to-20-day-old gerbils, whereas the responses at mid and high frequencies remained relatively stable for gerbils up to 42 days old, as shown in Figure 3.6 (left). They attributed the increasing low-frequency sensitivity to an increasing middle-ear admittance due to the expanding MEC with age (0.07 mL at 15 days old to 0.15 mL at 42 days old). On the other hand, the adult responses appeared significantly different from those of the 42-day-old gerbils, with a steeper low-frequency (< 1 kHz) slop and a considerable decrease in high-frequency (> 6 kHz) sensitivity, as shown in Figure 3.6 (right). They proposed that such changes could be a result of the inertial effect due to the increased ossicular mass. However, drilling a hole in the adult bulla in order to allow umbo measurements opened the bulla cavity, thereby affecting the sound transmission in the adult middle ear.

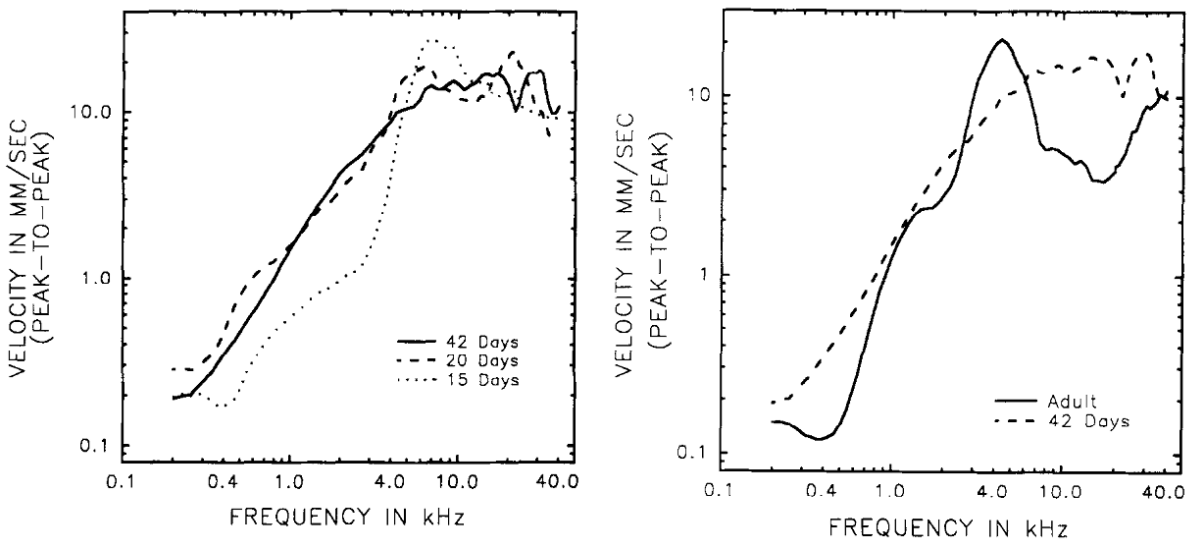

Figure 3.6: Comparisons of umbo velocity measured between gerbils at 15, 20 and 42 days after birth (left), and between 42-day-old and adult gerbils (right). (Cohen et al., 1993)

Rosowski et al. (1997) measured the TM motion at the umbo and on the PF in live gerbils using a vibrometer. Velocity measurements with normal, stiffened and removed PF were reported and compared in both open and closed middle-ear configurations. In the case of open MEC, a 1-mm hole was drilled on the bulla. Figure 3.7 shows the umbo responses measured with normal PF in both open and closed configurations. The authors observed that, for the open MEC, the umbo response was stiffness-dominated at low frequencies, followed by a broad peak at around 1.2 kHz, then dropped with a slope of −6 dB/octave (labelled as a slope of −1 in Figure 3.7) at high frequencies as it became more mass-controlled. An anti-resonance at 3 kHz produced by the interaction of the bulla hole and the middle-ear air space was found in both umbo and PF responses. Closing the bulla hole removed the effect of this anti-resonance; it also shifted the broad peak to around 2.1 kHz and decreased the response at frequencies below this peak resonance. Furthermore, the authors concluded that the PF was a resonant structure with a peak frequency near 400 Hz, compliance-dominated at low frequencies and roughly mass-dominated at high frequencies. In the case of a stiffened PF, this resonance peak decreased greatly in magnitude and shifted to higher frequencies. Based on both the experimental measurements and the results of a circuit model, the authors concluded that, with a closed

MEC, the PF only affects the middle-ear input admittance below 600 Hz, and is responsible for the decreased umbo response below 450 Hz (indicated by the arrow in Figure 3.7).

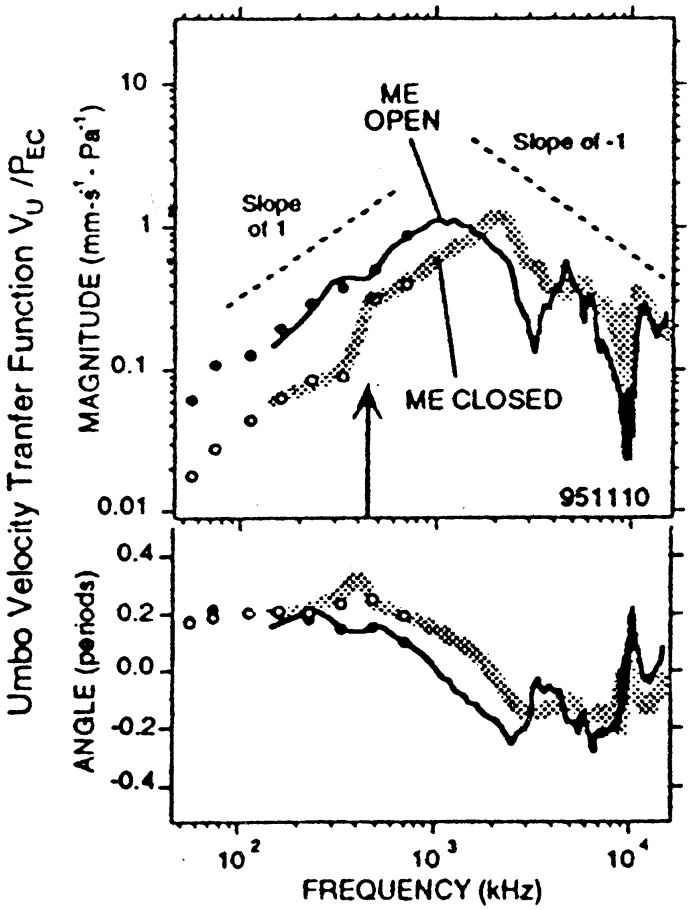

Figure 3.7: Normalized magnitude and phase of the umbo velocity measured with open (black thin line) and closed (thick grey line) MEC. (Rosowski et al., 1997)

De La Rochefoucauld and Olson (de La Rochefoucauld & Olson, 2007, 2010) used a combined confocal microscope and heterodyne laser interferometer to measure velocities at multiple locations along the sound transmission path from the TM to the stapes, for a broad frequency range up to 50 kHz. Their measurements at points along a line in the anterior PT region (extending over approximately one third of the TM radius) indicated that a slow travelling wave was superimposed on the in-and-out motion of the TM, as shown in Figure 3.8; the authors estimated a wave speed of about 11 m/s. Consistent with

some earlier findings, the manubrium appeared to move as a rigid body up to 13.5 kHz, with slight bending at higher frequencies. Based on measurements on the PT and the stapes, they further explored the middle-ear delays and sound transmission in both *post mortem* and live gerbils. However, their measurements were performed under open-field sound stimulation and the results were normalized by the sound pressure recorded at the entrance of the ear canal. Moreover, a part of the PF was removed to allow visual access to the ossicles. In order to compare their results with the others discussed in this section or with our measurements, the acoustic resonance in the ear canal, as well as the effects of removing the PF, would have to be measured and corrected for.

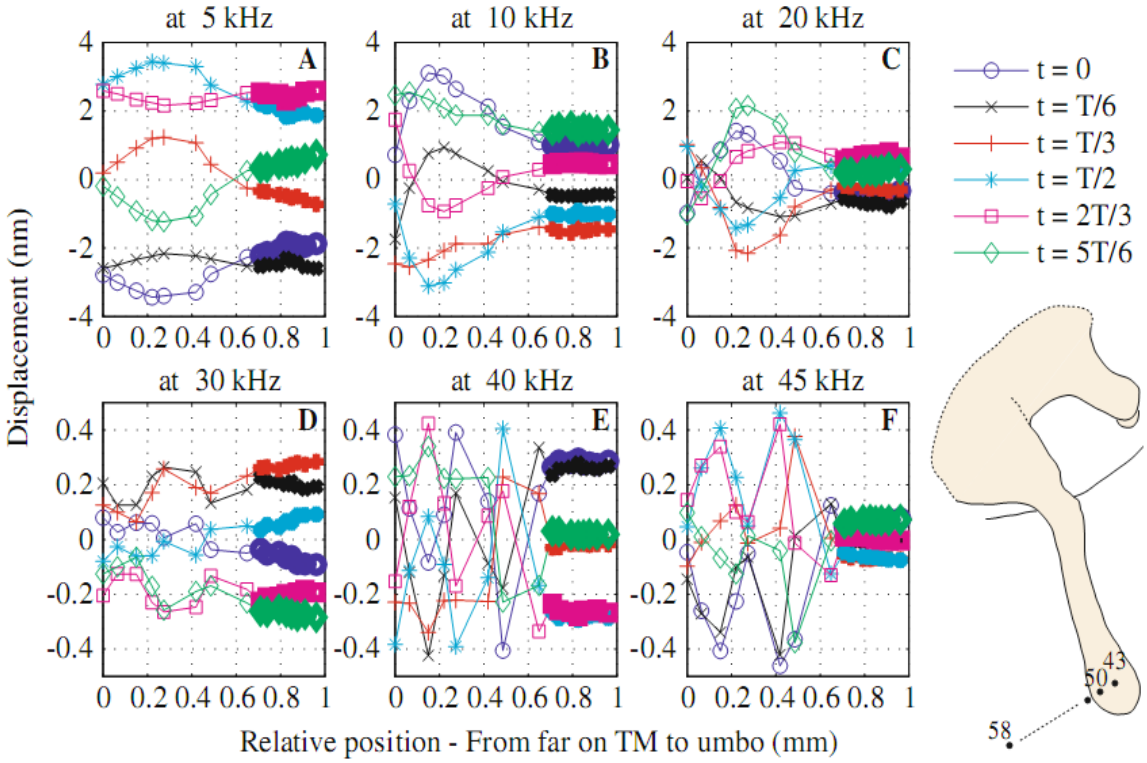

Figure 3.8: Displacement as a function of position as six times (as indicated in the top right corner). Thin lines correspond to positions on the PT for a distance up to 650 micron from the umbo (position 0 = measurement point 58). Thick lines represent the responses measured at the umbo area (position 1 = measurement point 43). Each panel shows the response measured at one frequency. (De La Rochefoucauld & Olson, 2010)

Vibration patterns at multiple points on the gerbil TM were first reported by our group (Ellaham, 2007), and Nambiar (2009) extended that study with measurements in twelve

post mortem gerbils. Using a single-point laser Doppler vibrometer with glass-coated micro-beads placed on the TM to improve the signal reflectivity, Nambiar measured displacements at the umbo, on the PF, and at multiple points on the PT and along the manubrium in response to sound stimuli over the range of 0.2 to 10 kHz. The effects of the size of the bulla opening were also evaluated by measuring the umbo responses while the bulla hole was gradually widened. Results of the umbo, PF and manubrium measurements with both open and closed MEC were generally in agreement with the *in vivo* measurements reported by Rosowski et al. (1997), except for some reductions in the displacement magnitudes and frequency shifts in some TM responses, presumably because of *post mortem* temporal effects due to dehydration of the middle ear. The PT displacements were measured at several points on both the anterior and posterior sides, close to the manubrium. It was observed that, at low frequencies, the PT responses had similar shapes but larger magnitudes compared with the manubrial responses; above 3 kHz, the PT responses became irregular and complex, and broke into sectional and frequency-dependent vibration modes, as shown in Figure 3.9. Similar results were obtained by Maftoon et al. (2011) from *in vivo* gerbil experiments.

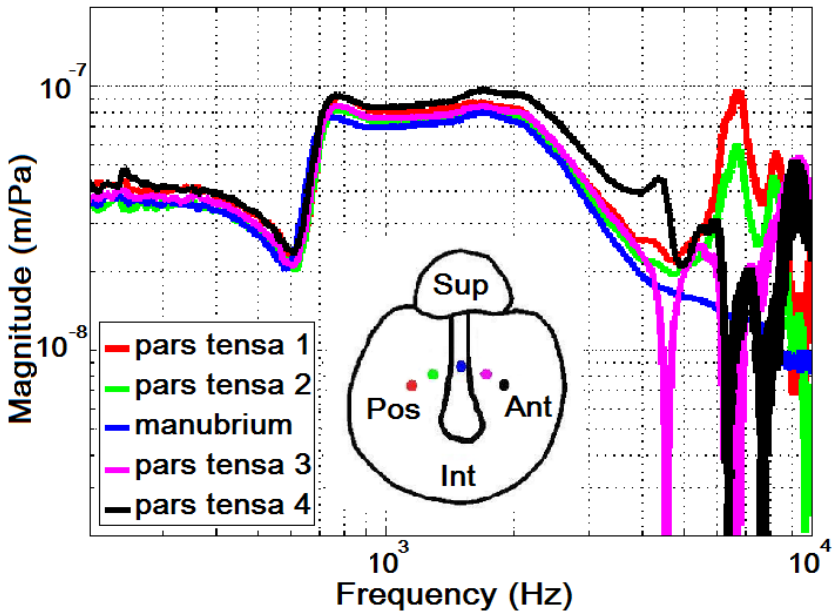

Figure 3.9: Normalized displacements measured on the PT in a gerbil; measurement points across the PT are indicated in the schematic of the gerbil TM. (After Nambiar, 2009)

3.2.4 Finite-element models

Finite-element modelling was first introduced to study TM vibrations by Funnell (1978). The middle-ear system beyond the TM was modelled as "a rigid hinged rod in the vibrating surface", with the effects of reactive forces on the manubrium and of the middle-ear cavities included in the system stiffness matrix. Since then finite-element models have become a popular tool to investigate middle-ear mechanics in humans (e.g., Wada et al., 1992; Beer et al., 1999; Bornitz et al., 1999; Prendergast et al., 1999; Koike et al., 2002; Sun et al., 2002; Qi et al., 2008; Gariepy, 2011; Volandri et al., 2011; Gentil et al., 2011) and in cats (e.g., Funnell & Laszlo, 1978; Funnell et al., 1987, 2005; Tuck-Lee et al., 2008). A finite-element model of the gerbil middle ear has been developed in our lab and is discussed in the following paragraphs.

The gerbil model was first developed by Funnell et al. (1999, 2000), using realistic geometry data for the gerbil TM based on phase-shift moiré topography in collaboration with Decraemer's group. The ossicle geometry was constructed based primarily on magnetic-resonance microscopy (MRM) data, and was further refined based on details from serial histological images. Figure 3.10 shows the simulated vibration patterns of the TM and ossicles at low frequencies for which the inertial and damping effects are negligible. For the parameters employed in this model, the PF showed much greater displacements than the rest of the TM. Besides, this model revealed two local displacement maxima on the PT, one in the anterior region and a more pronounced one in the posterior region. Both maxima were closer to the manubrium than to the annulus, as in the experimental observations of gerbil TM static deformations presented in Section 3.2.1 (von Unge et al., 1993; Dirckx & Decraemer, 2001). The simulated low-frequency ossicular motions had their maximum displacement at the umbo and gradually decreased toward an axis of rotation consistent with the classical notion of a fixed axis joining the tip of the anterior mallear process and the posterior incudal ligament (PIL).

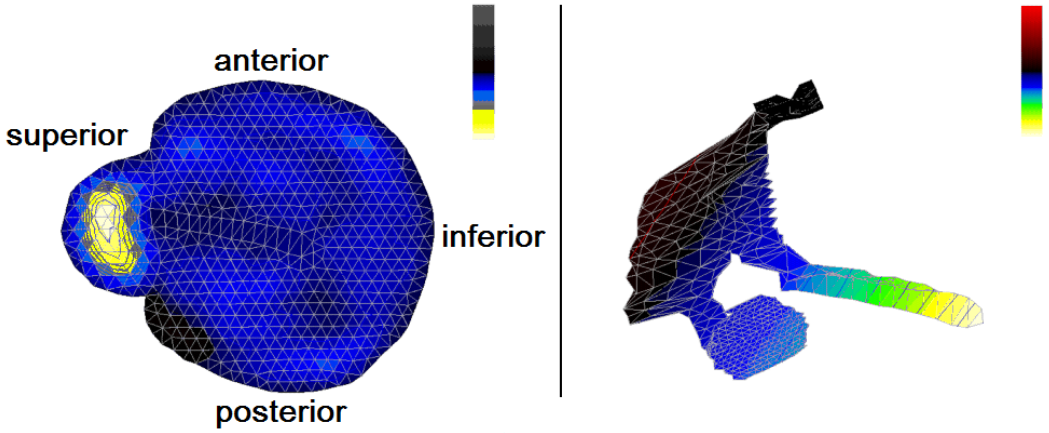

Figure 3.10: Simulated low-frequency vibration patterns of the gerbil TM (left) and the ossicles (right). (After Funnell et al., 2000)

Elkhouri et al. (2006) further improved this model by adding data from X-ray micro-CT images with a voxel size of 5.5 µm, resulting in a more precise three-dimensional reconstruction of the stapedial annular ligament and the tiny pedicle of the incus. The improved model was used to study not only the TM vibration patterns and the ossicular motions at low frequencies, but also the influence of the ossicular suspension on the axis of rotation. Figure 3.11 shows the low-frequency simulation results for the TM and the ossicles. The PT and ossicular vibration patterns, including the locations of displacement maxima, were consistent with the results reported by Funnell et al. (2000). However, displacements of the PF in this model were much smaller than those of the PT.

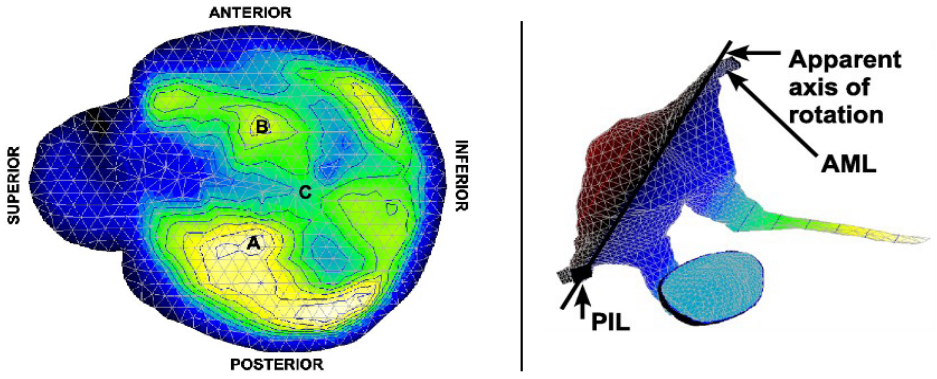

Figure 3.11: Simulated low-frequency vibration patterns of the gerbil TM (left) and the ossicles (right). (After Elkhouri et al., 2006)

More recently, this model was extended to high frequencies (up to 10 kHz) by Maftoon et

al. (2011). Pre-processing work, from the image data to the final mesh, is done using software developed in our lab. The TM is modelled as a thin shell with variable thickness according to the confocal microscopy measurements reported by Kuypers et al. (2005). All middle-ear components are modelled as linear elastic materials with Rayleigh damping. Figure 3.12 shows the simulated frequency responses of multiple points along a line on the TM. Their simulated responses are generally in agreement with the experimental results with an open MEC. The major differences between their experimental and numerical results include the following: (1) the broad peak at 1 to 2 kHz in the experimental results is sharper and at a somewhat higher frequency (~2.5 kHz) in the simulated results; (2) the magnitudes of low-frequency responses are slightly lower in the simulated results; and (3) the simulated TM responses fall off sharply above 5 to 6 kHz and above this frequency are smoother than the experimental results, indicating that the model exhibits too much damping at higher frequencies. Details of the complex high-frequency resonance structures in the PT response are difficult to compare because those details vary so greatly from location to location, from frequency to frequency and from ear to ear.

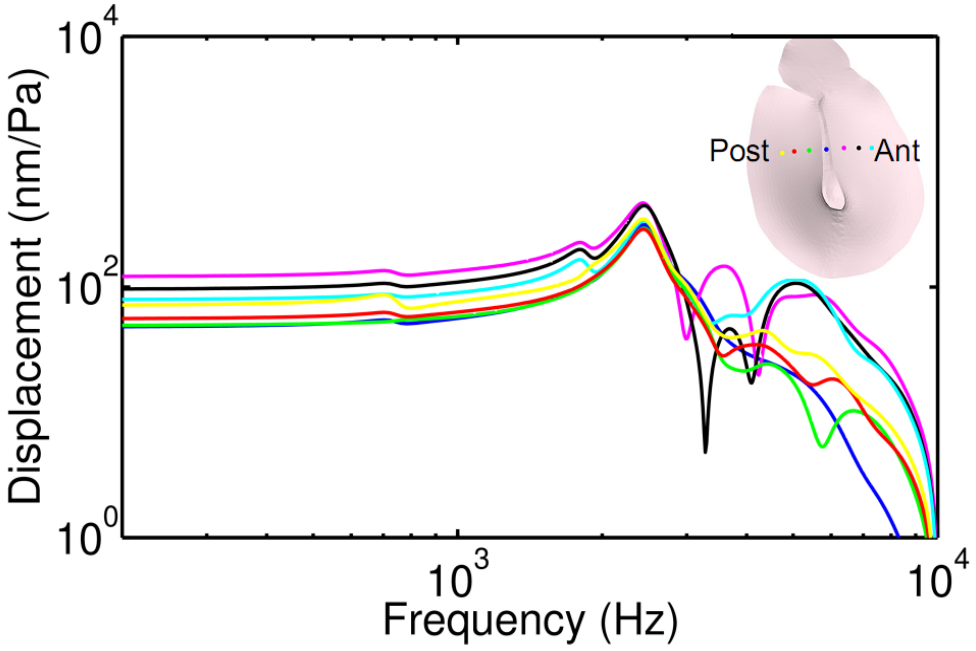

Figure 3.12: Simulated displacements (normalized by sound pressure) of several points across the PT. (Maftoon et al., 2011)

3.3 Conclusion

We have presented a review of both experimental and numerical studies relevant to our research. Experimental measurements of the TM vibration patterns in humans and other species using various techniques have shown qualitatively consistent results for the locations of maximum displacements, the frequency-dependent and sectional modes of vibration at high frequencies, the functional implications of the PF, and the existence of shifts in the ossicular rotational axis and possibly of bending of the manubrium tip at high frequencies.

Compared with the vibration measurements in gerbils, modelling studies have shown similar low-frequency responses of both the TM and the ossicles. However, high-frequency responses have not yet been well modelled, especially those of the PT. Although a number of experimental measurements have been performed at the umbo and at the stapes, there is a lack of experimental data for the entire vibration pattern of the gerbil TM. Measurements at multiple locations on the TM, especially at those closer to the annulus ring, would help to produce a more complete characterization of TM vibrations in gerbils. These measurements would also be useful to validate the middle-ear models so as to extend our understanding of TM vibrations to high frequencies. Furthermore, some experimental measurements have shown pronounced temporal effects in *post mortem* studies. This highlights the importance of *in vivo* measurements which are more representative of the normal state.

Chapter 4
Materials and methods

This chapter presents the experimental and numerical methods employed in this study. Specimen preparation is first discussed in Section 4.1, followed by a detailed discussion of the experimental set up in Section 4.2. An overview of the measurements is presented in Section 4.3. Finally, the finite-element modelling techniques for this study are discussed in Section 4.4.

4.1 Specimen preparation

The Mongolian gerbils used for this study were supplied by Charles River Laboratories (St-Constant, Québec).The animal-use protocol was approved by the Facility Animal Care Committee of the McGill University Health Centre. Twelve female gerbils with body weights between 60 and 84 g were used, with three of them being excluded from the results discussion due to intrinsic abnormalities (TM perforation) or experimental problems (unanticipated hemorrhage).

Each experiment lasted for several hours, the longest for fourteen hours. In order to enhance the viability of the gerbil during the experiment, a low flow of oxygen was provided through a tube near the nose of the gerbil, and a SnuggleSafe heating pad (Lenric C21 Ltd.) was placed underneath the gerbil to keep it warm. Moreover, a reflex check (e.g., foot pinch) was performed every 10 minutes to verify the depth of anaesthesia, and a long-lasting anaesthetic agent was injected every 20 to 25 minutes to maintain the gerbil in deep anaesthesia. At the end of each experiment, the gerbil was euthanized. Details of the anaesthetic drugs used in this study, including their functions, application methods, dosage and timing, are tabulated in Table 4.1.

Table 4.1: Details of the anaesthetic agents, application methods, dosage and timing.

Purpose	Route of Administration	Anaesthetic Agent	Dose [mg/kg]	Time
Pre-anaesthesia (tranquillizer)	Subcutaneous	Buprenorphine	0.05	At beginning of experiment
		Carprofen	5	
Main anaesthesia	Intraperitoneal	Xylazine	10	5 to 10 minutes after pre-anaesthesia
		Pentobarbital	35	
Anaesthesia re-dose	Intraperitoneal or intramuscular	Pentobarbital	5	Every 20 to 25 minutes
Analgesia	Intramuscular	Buprenorphine	0.05	7 to 8 hours after pre-anaesthesia
Local anaesthesia	On site	Lidocaine	1:8 (Lidocaine:Saline)	During surgery

About 10 minutes after the main anaesthesia was injected, the gerbil's respiratory rate and response to external stimuli were checked to ensure the depth of anaesthesia. Before starting the surgery, the state of the TM was briefly verified by using an ear speculum under the microscope. The following three steps were then performed to widely expose the TM according to our new method:

1) Compared with previous studies (Ellaham, 2007; Nambiar, 2009; Maftoon et al., 2011) a greater portion of the skin and soft tissue covering the bulla was surgically removed, with extreme care taken to avoid damaging a major blood vessel which lies over the anterior part of the bulla, ventral to the ear-canal entrance.

2) Since portions of the bulla, and of the bony ear canal close to the TM annulus, are lateral to the TM and obstruct the view of the PT, these bony structures were delicately drilled away almost to the annulus rim, leaving only two thin pieces of bone connecting the rim to the bulla wall, as shown in Figure 4.1-A.

3) Gaps between the annulus rim and the bulla wall lateral to the TM were then filled with a small amount of dental cement (Dentsply Caulk, IRM), as shown in Figure 4.1-B, so as to restore the closed-cavity acoustic environment of the middle ear.

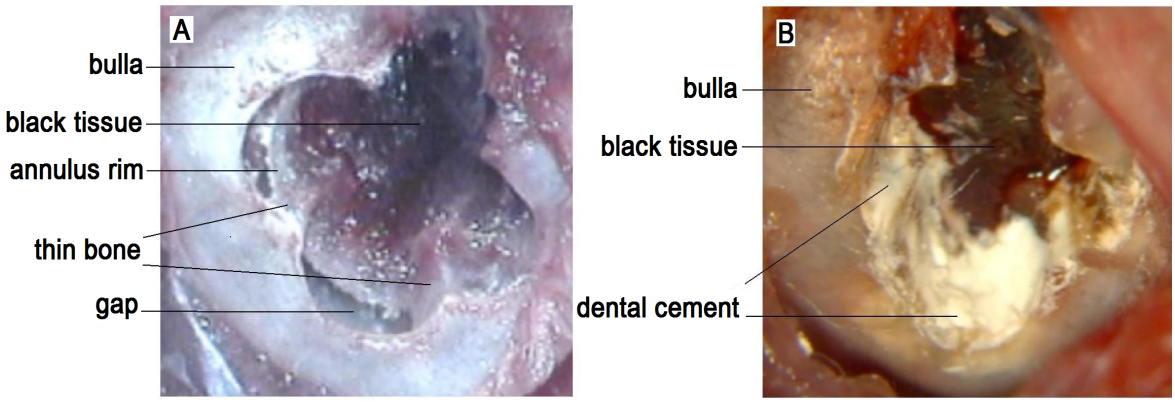

Figure 4.1: Surgical preparation of a gerbil TM. (A) Widely open bulla after done drilling; (B) gaps between TM annulus and the bulla filled with dental cement.

A black tissue overlying the canal wall all the way up to the TM annulus, which appears to be the continuation of the ear-canal epithelium, was kept intact during the preceding steps in order to keep the TM clean and moist. At this point, the black tissue was delicately removed to fully expose the TM, and the glass-coated plastic micro-beads (Sigma-Aldrich, model G4519) were then gently placed (with a fine paint brush that had been reduced to a single bristle) on desired locations on the TM, as illustrated in Figure 4.2-A. The smaller TM exposure in our previous study (Nambiar, 2009) is shown in Figure 4.2-B for comparison. Each micro-bead was approximately 120 microns in diameter and 1 μg in weight; it not only enhanced the reflected signals from the TM, but also allowed measurements to be repeatable at the same location on the TM. After placing micro-beads at all desired locations of the TM, the gerbil skull was glued to a wooden block (2 cm in length, 1 cm in width and thickness) which was then firmly screwed to a specimen-fixation device for measurements.

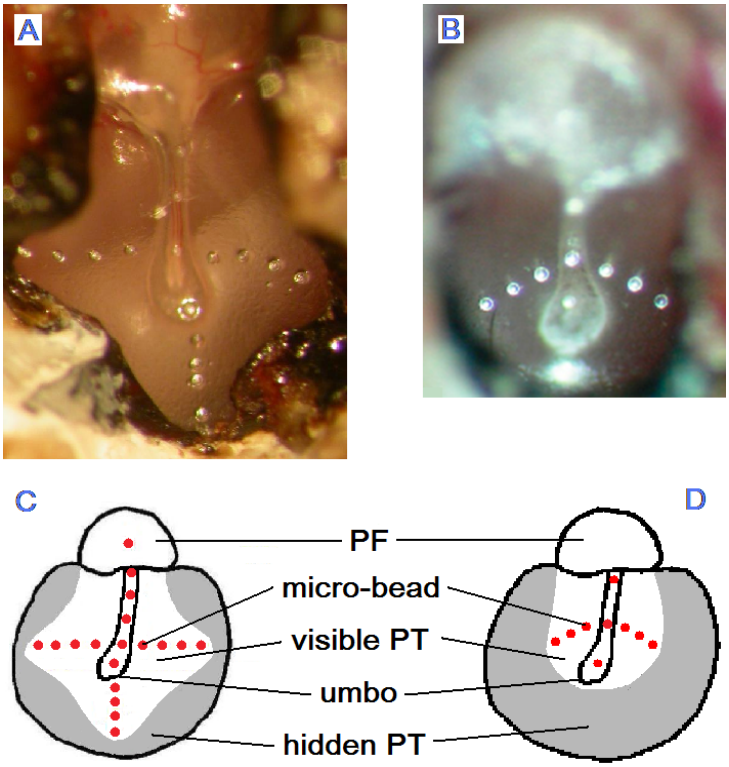

Figure 4.2: A comparison of the TM exposure in this study (A) and in the previous study (B); corresponding schematic illustrations are shown in (C) and (D), with the grey regions representing the remaining hidden regions of the PT. (Source for previous study: Nambiar, 2009)

Since the Eustachian tube cannot open regularly under anaesthesia, the middle-ear pressure must be artificially equalized to the ambient pressure to ensure normal vibrations of the TM during measurements. Hence, at the end of Step 1, a 1-mm ventilation hole was drilled on the bulla far away from the TM to release the middle-ear pressure. A 15-cm-long polyethylene tube with 1-mm outer diameter was then tightly inserted into the ventilation hole. It was narrow enough and long enough that it only allowed very low-frequency sound waves to pass through; in other words, it effectively blocked the hole in the auditory frequency range.

Unlike the practice in our previous *post mortem* gerbil experiments, no humidifier was used during the surgical preparation because no obvious drying effects were observed in the middle-ear structures of the living gerbil.

4.2 Experimental set-up

The main components of the specimen-fixation device are described in Section 4.2.1. The vibration-measurement device, a laser Doppler vibrometer (LDV), is discussed in Section 4.2.2. Section 4.2.3 explains the acoustical system set-ups and the choice of input stimulus.

4.2.1 Fixation device

The gerbil was placed directly under the microscope (OPMI 1-H, Zeiss) with its head stabilized by a specimen-fixation device, as shown in Figure 4.3.

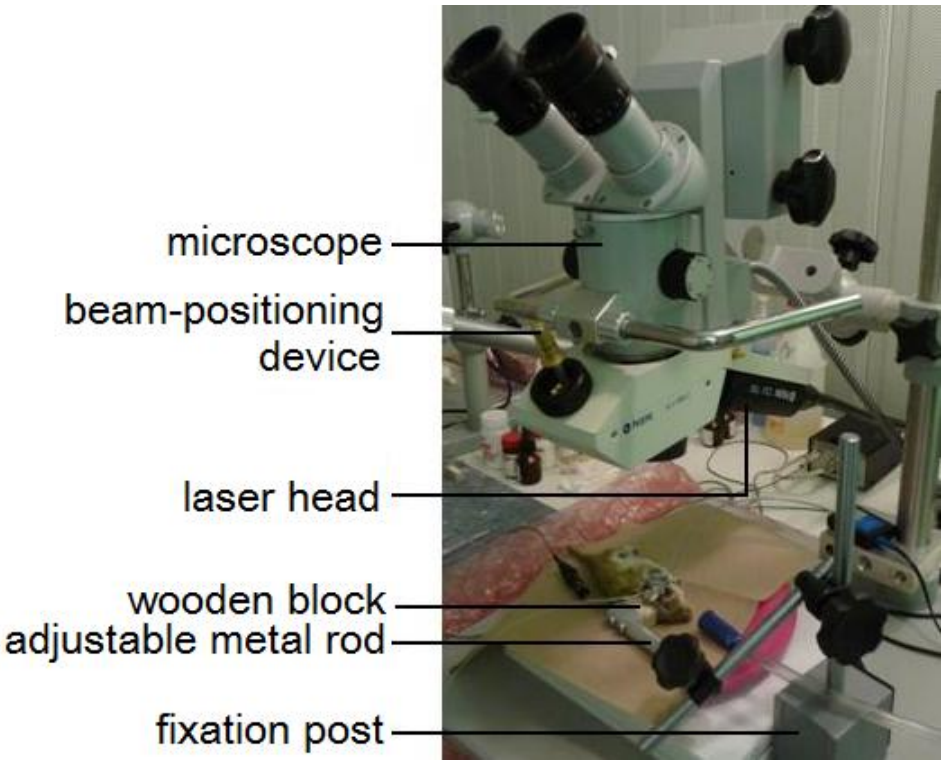

Figure 4.3: Microscope and fixation devices.

The fixation device contains two adjustable metal rods clamped onto a post mounted on a base containing a switchable magnet. Once the optimal view of the TM through the microscope was achieved, the metal rod and its clamp were tightened to maintain the desired position, thereby eliminating head movements during measurements. The magnet

in the base was not used since the weight of the base was itself enough to keep the specimen fixed. The laser head of the vibrometer was mounted on the microscope, and the laser beam was directed roughly perpendicular to the gerbil TM. Precise positioning of the beam was done by manually adjusting a joystick connected to a mirror.

4.2.2 Laser Doppler vibrometer

Among various techniques for surface vibration measurements, laser Doppler vibrometry (LDV) was selected for this study as it allows non-contact measurements on a small and delicate surface like the TM. Moreover, it provides adequate accuracy in vibration measurements by detecting displacements down to the order of nanometres. Hence, it is popular in middle-ear research and may become a useful tool for clinical hearing assessment in the future.

One basic principle behind LDV is the Doppler effect. When an observer is moving relative to a source emitting waves, the observed change in frequency of that wave is called the Doppler shift, or the Doppler effect. A simple example is when a car is passing by an observer standing still: the pitch of the car's horn sounds higher when the car is approaching than when it is receding. Each consecutive sound wave of the approaching car is emitted from a closer position and hence takes less time to reach the observer; the reduced time between arrivals of the consecutive waves therefore gives rise to a higher received frequency (Rosen & Gothard, 2009).

The other basic principle of LDV is optical interferometry. It involves combining two or more light beams in an optical instrument. The principle of superposition states that if the waves are in phase, the amplitude of the combined waveform is the sum of the amplitudes of the individual waves; in contrast, the waves cancel each other when they are out of phase. Hence, the resulting interference pattern maps out the phase differences between light waves, with bright fringes resulting from the in-phase interfering waves and the dark fringes formed by the out-of-phase ones (Hariharan, 2006).

A schematic diagram of the single-point heterodyne LDV used in this study is shown in Figure 4.4. The helium-neon laser beam of frequency f_0 is first projected from the LDV laser head and then split into a measurement beam and a reference beam. The measurement beam is pointed at the vibrating surface and reflected back from it; the reflected beam is then redirected towards the photodetecter though an optical lens and beam splitters.

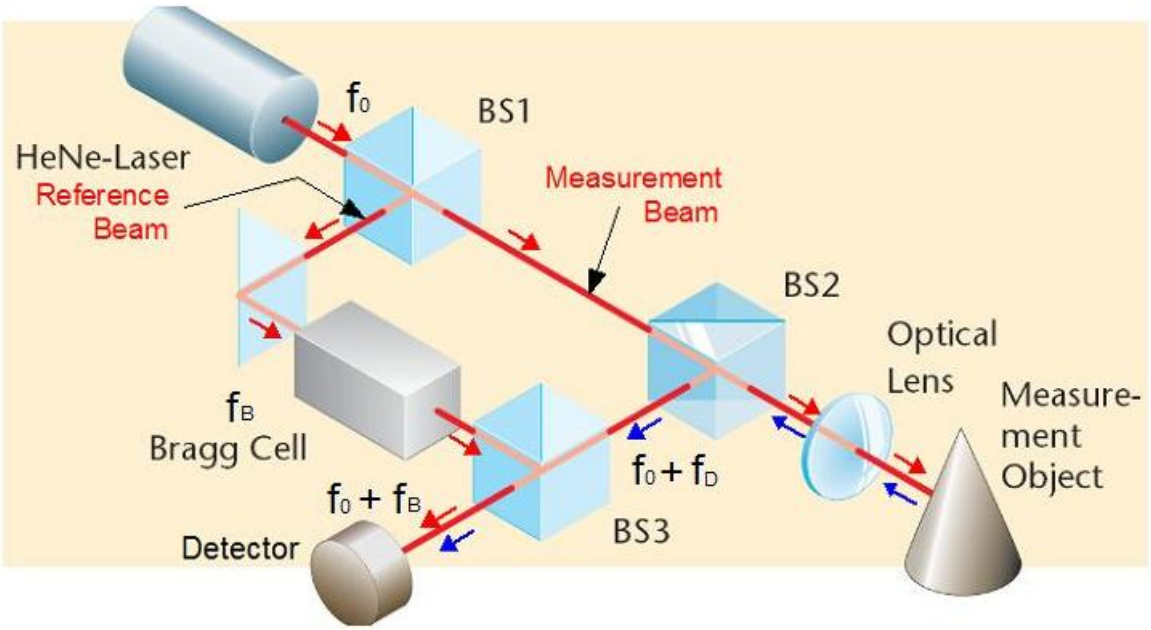

Figure 4.4: Schematic diagram of the LDV; BS1, BS2 and BS3 are beam splitters to split, redirect, and combine the laser beams. (After http://www.polytec.com/us/solutions/vibration-measurement/basic-principles-of-vibrometry/)

Due to the Doppler effect, the reflected measurement beam is subjected to a frequency shift f_D and becomes $f_0 + f_D$ as it reaches the photodetecter. The Doppler shift is a function of the velocity of the vibrating surface in the direction of the measurement beam, as shown in Equation 4.1:

$$f_D = 2v/\lambda \tag{4.1}$$

where λ is the wavelength of the laser beam and v is velocity of the vibrating surface. On the other hand, the reference beam passes through a Bragg cell (an acousto-optic

modulator) which adds a fixed frequency shift f_B (40 MHz in our LDV), and is then projected to the photodetecter with a carrier frequency of $f_0 + f_B$. Having low-pass filtered the incoming light beams, the photodetecter obtains a combined frequency shift of $f_B + f_D$ which can be digitally demodulated to retrieve velocity information about the vibrating surface. When the surface is at rest, a modulation frequency of f_B is generated, whereas when the surface is moving towards or away from the LDV, a resultant frequency lower or higher than f_B is detected. Hence, the Bragg cell plays an important role in determining the direction of the velocity ("Polytec: Basic Principles of Vibrometry," n.d.).

The LDV (HLV-1000, Polytec) employed in this study is designed for hearing research. It consists of a laser head connected to a vibrometer controller via fibre-optic cable. The laser head is mounted on an operating microscope to allow clear vision of the TM, and the laser beam can be directed manually by a beam-positioning device attached to the microscope as described in Section 4.2.1. The vibrometer controller is connected to a junction box (VIB-Z016, Polytec) allowing direct communication with the data-management system and the acoustical system. The input stimulus is generated by a software-controlled signal generator, and the data acquisition is controlled from the vibrometer software (VibSoft 4.3, Polytec).

4.2.3 Acoustical system

Two different acoustical set-ups were employed in this study, namely, a closed-sound-field system and an open-sound-field system. Four gerbils were measured in both types of sound field, and five gerbils were measured in only a single type of sound field (three in an open sound field, two in a closed sound field).

4.2.3.1 Closed sound field

The closed-sound-field acoustical system consists of an earphone and a microphone coupled into a small sound chamber sealed by an anti-reflective glass window, as illustrated in Figure 4.5.

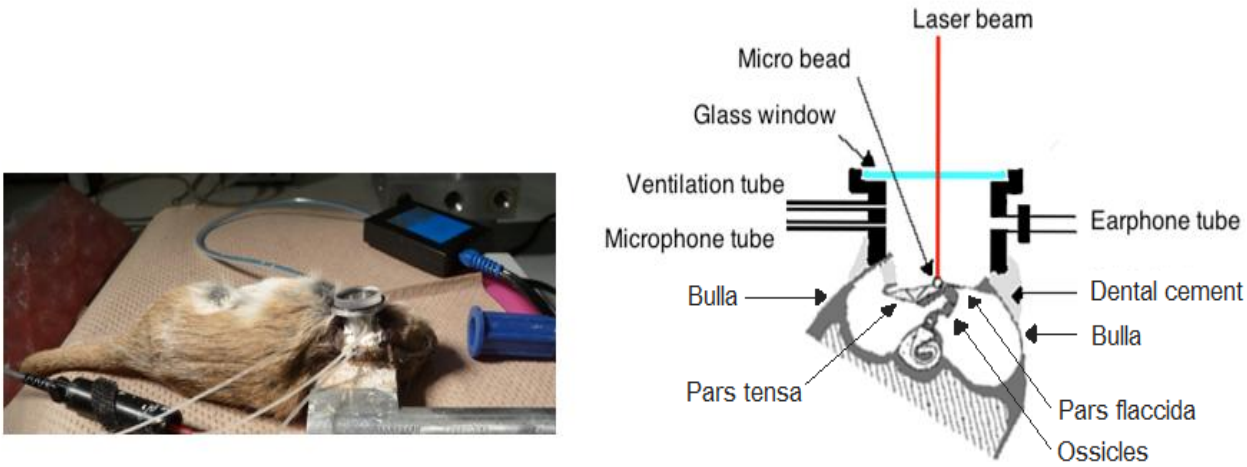

Figure 4.5: The closed-sound-field experiment (left) and a schematic of the set-up (right).(After Rosowski et al., 1997)

The input sound stimulus was delivered into the coupler by an earphone (ER-2, Etymōtic Research) and the sound-pressure level inside the coupler was monitored by a probe microphone (ER-7C, Etymōtic Research). Both ER-2 and ER-7C are specially designed for auditory research and provide flat frequency responses roughly from 100 Hz to 10 kHz (Etymotic Research, Inc. - ER-2, n.d., Etymotic Research, Inc. - ER-7C, n.d.); detailed technical specifications are shown in Figure 4.6. The earphone can only generate small volume velocities, which are not enough to generate an adequate free-field sound pressure level at the TM for low frequencies, so the sound field must be confined in the small volume of a coupler. This aluminum coupler was custom-made to match the size of our equipment and the widely exposed gerbil TM. It has three holes allowing tight coupling with the earphone, microphone and ventilation tube. Its bottom was glued onto the bulla wall using dental cement, and its top was covered by an anti-reflective glass window (T47-518, Edmund Optics) to obtain an acoustic seal while allowing excellent passage of the laser beam. Figure 4.7 shows the configuration of the coupler along with its detailed dimensions.

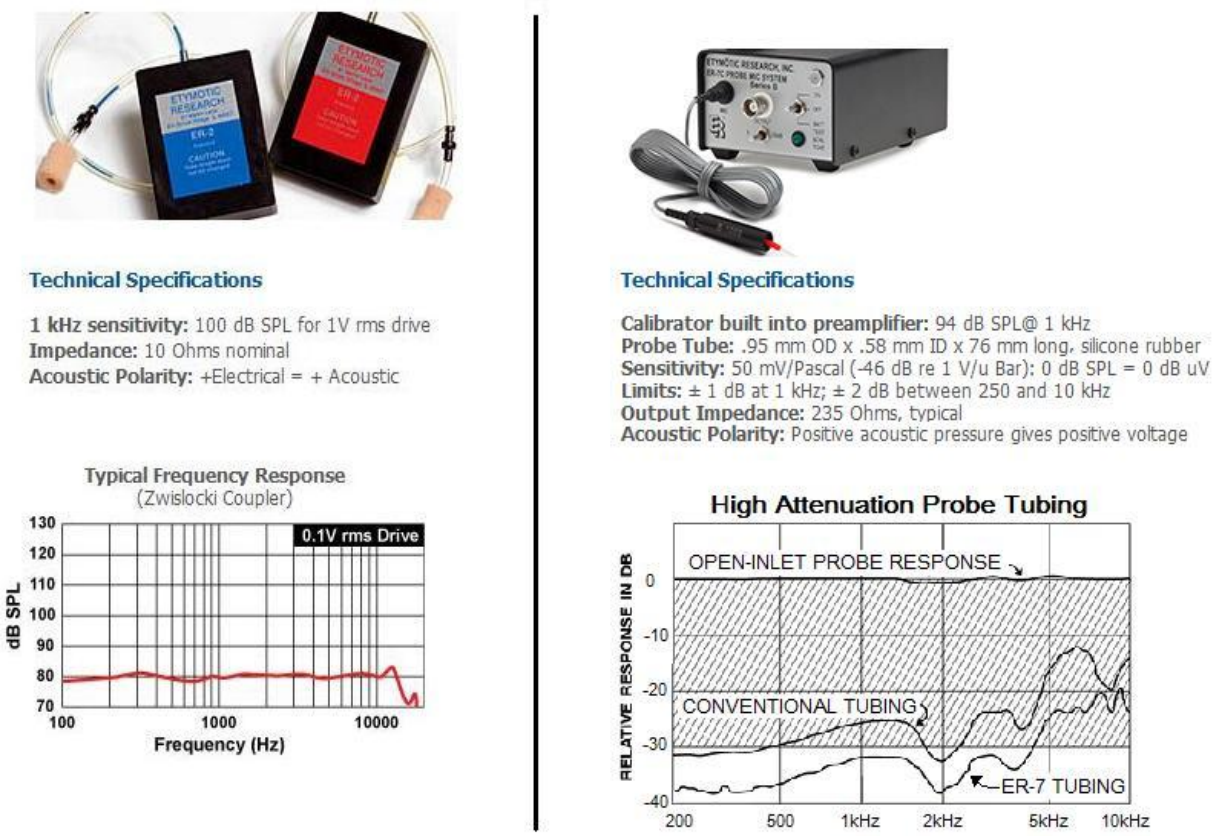

Figure 4.6: The earphone ER-2 with its frequency response curve (left) and the probe microphone ER-7C with its relative frequency response curve (right). (After http://www.etymotic.com/pro/er2-ts.aspx & http://www.etymotic.com/pro/er7c-ts.aspx)

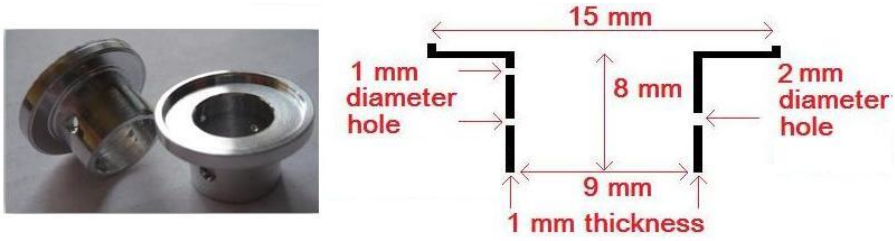

Figure 4.7: Custom-made aluminium coupler and its dimensions.

In this set-up, the sound-field is confined by the coupler so that the input sound pressure does not excite other objects nearby (e.g., the gerbil body, the heating pad and the fixation post). Moreover, the coupler along with the glass window helps to prevent contamination of the TM from dust or unexpected bleeding of the neighbouring soft tissue. However, from some viewing angles the exposed TM is slightly obstructed by the top inner edge of the coupler.

4.2.3.2 Open sound field

The open-sound-field acoustical system involves less equipment than the system mentioned previously; it only consists of a speaker and the same microphone as the closed-sound-field set-up, as illustrated in Figure 4.8.

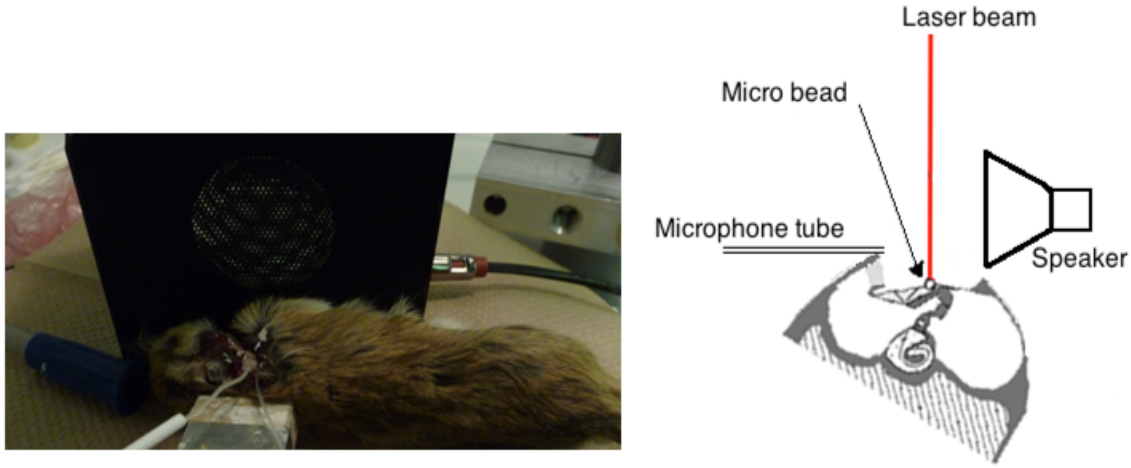

Figure 4.8: The open-sound-field experiment (left) and a schematic of the set-up (right).

The input sound stimulus was delivered by a speaker (Headrush Stereo Speaker for PC) providing a relatively flat frequency response from 20 Hz to 20 kHz. It was placed approximately 2 cm from the TM, ventral to the gerbil head. The sound pressure level at the TM was monitored by the ER-7C microphone placed approximately 1 mm above the bulla, superior to the PF. No coupler was used in this set-up because the volume velocities generated by this speaker were large enough to create adequate sound pressures at the TM.

Advantages of this set-up include: faster specimen-preparation time due to the simplicity of the set-up, a clear view of the TM from any viewing angle, and easy access to the TM during measurements due to the absence of the coupler. However, the sound signals generated by this speaker are reflected from everything nearby, and might directly stimulate the gerbil skull and body, causing signal contamination during measurements. Also, the TM is more prone to contamination from dust, hair or blood in this set-up. Results from the two systems will be compared in Section 4.2.2.5.

4.2.3.3 Sound-proof room

In order to reduce the effects of ambient noise, measurements were taken inside a double-wall audiometric examination room (model C-24, Genie Audio, St-Laurent, QC). Dimensions of this sound-proof room and a graph describing its sound attenuation are shown in Figure 4.9.

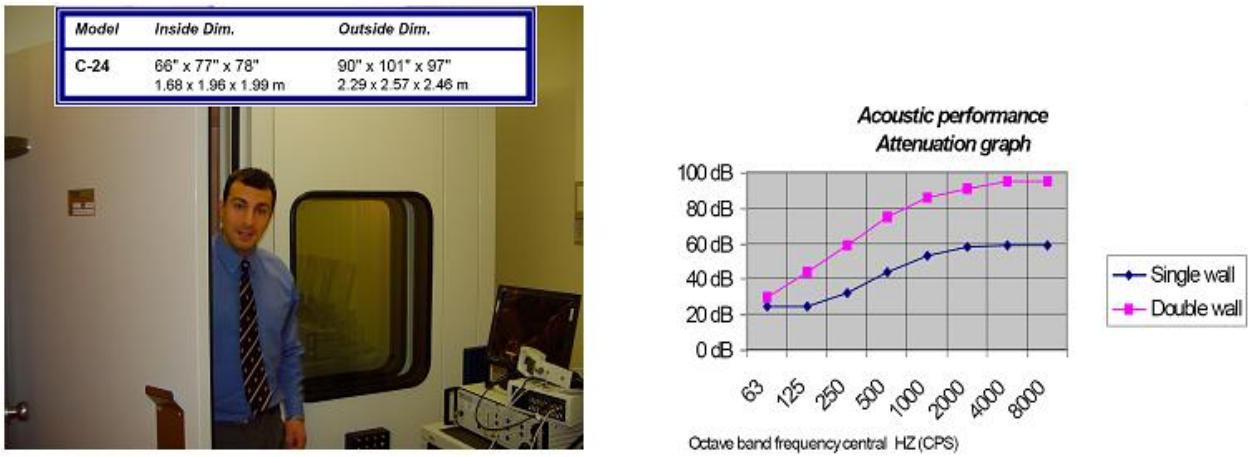

Figure 4.9: The dimensions (left) and the acoustic performance attenuation graph (right) of the sound-proof room (After Nambiar, 2009).

Most of the acoustical noise was attenuated by the sound-proof room. The remaining noise sources that potentially affect the quality of measurements are: the noise of the fan in the sound-proof-room; the electrical noise from the devices inside the sound-proof room; the optical noise of the laser head; and the vibrations of the building.

4.2.3.4 Input stimulus

Frequency resolution and signal-to-noise ratio (SNR) are two important factors to be considered when selecting an input stimulus. Pure-tone signals normally give very high SNR, but are not practical in our case as it would be very time consuming to achieve the desired frequency resolution. In order to quickly measure a broad spectrum with high frequency resolution, white-noise and sine-sweep input signals are better alternatives. White noise consists of random signals with energy equally distributed across the entire

spectrum. When white noise was chosen as the input signal in the vibrometer software (VibSoft 4.3, Polytec Inc.), the output signals displayed very low SNR, even after being averaged over 100 realizations; similar observations were reported by Ellaham (2007) and Nambiar (2009). Our experimental observations indicate much higher SNR's with sweeps even without averaging. Sine sweeps with the frequency of the signal changing linearly with time were chosen as the input stimulus, as also used in our previous studies (Akache, 2005; Ellaham, 2007; Nambiar, 2009).

In this study, sine sweeps over the range of 0.1 to 10 kHz with a period of 128 ms were used. Because of the noise at low frequencies (e.g., building vibrations) frequency responses over the range of 0.2 to 10 kHz were measured. According to the Nyquist-Shannon sampling theorem (Shannon, 1984), the sampling frequency must be at least 20 kHz to avoid aliasing; 32 kHz was chosen for our data acquisition. The frequency-domain responses were analyzed with 1600-point fast Fourier transforms over 10 kHz, resulting in a frequency resolution of 6.25 Hz (10 kHz/1600). In order to obtain optimal *in vivo* measurement results, all of the frequency responses were averaged over 50 realizations.

The sound pressure level of the input sound field for each experiment was measured with the ER-7C probe microphone placed very closed to the TM, eliminating the effects of the ear canal. Because all output responses were normalized by the corresponding sound-pressure values, the sound-pressure curve must be smooth enough to provide reliable normalization.

4.2.3.5 Acoustic system comparison

The sound pressure levels and the skull vibrations were measured at the beginning of each experiment with both open and closed sound field. Section 4.2.2.5.1 presents the sound pressure levels obtained in all the experiments, and the skull vibrations are discussed in Section 4.2.2.5.2.

4.2.3.5.1 Sound pressure level

The sound pressure level measured in both open- and closed-sound-field experiments, as well as a typical background noise measurement, are shown in Figure 4.10.

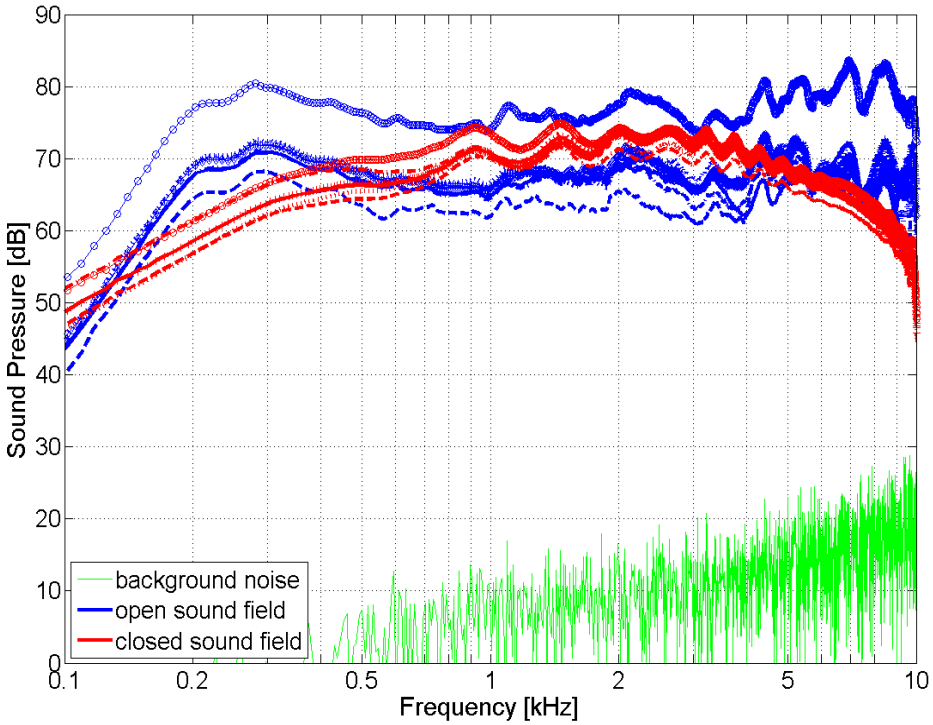

Figure 4.10: Sound pressure level measured near the TM in seven open-sound-field experiments (blue curves) and in six closed-sound-field experiments (red curves). The background noise (green curve) represents the noise inside the sound-proof room.

The sound-pressure-level curves (blue) in the open sound field show a linear increase of about 22 dB from 100 to 200 Hz, and then remain relatively flat in the range of 60 to 70 dB from 200 Hz to 10 kHz, with fluctuations of about ±3 dB at higher frequencies (> 6 kHz). These curves are very similar and lie within ±3 dB of the mean, except one (corresponding to the first open-sound-field experiment) that was about 10 dB higher than the others. A possible explanation might be that the speaker was powered by batteries in this experiment and via a USB port in the others. Batteries were not used to power the speaker in the later experiments because they were not durable enough to provide consistent sound pressure levels for lengthy experiments. In any case, this difference does

not affect the vibration measurements after they have been normalized by the corresponding sound pressure level values.

In the closed-sound-field experiments, the sound-pressure-level curves (red) show a gradual increase of about 15 dB from 100 to 300 Hz, remain very smooth in the range of 65 to 75 dB until 6 kHz, and then gradually drop to about 55 Hz at 10 kHz. These curves are very similar and lie within ±3 dB of the mean.

The sound pressure levels with both types of sound field are fairly smooth and the background noise is at least 40 dB lower than the input sound signals up to 8kHz, confirming that the output responses are not affected by the background noise. From 8 to 10 kHz, the sound pressure levels of the closed sound field gradually drop by 10 dB, whereas those of the open sound field stay roughly the same.

4.2.3.5.2 Skull vibrations

The skull vibrations were measured at a point on the bulla close to the TM. Ideally, nothing should be vibrating during measurements except the TM and the ossicles. Since the lateral part of the bulla was surgically exposed, the input sound pressure might directly stimulate the bulla, thereby affecting the TM vibrations. The bulla vibration is an important factor determining the quality of TM vibration measurements; it is a concern especially in the open-sound-field measurements where the bulla was directly exposed to the sound field.

The skull vibrations measured at the bulla in both open- and closed-sound-field experiments, as well as the typical umbo response corresponding to each sound field, are illustrated in Figure 4.11. The normalized bulla displacements in the open sound field (blue) show a more or less continuous drop from about 1000 to 0.1 nm/Pa as frequency increases from 0.1 to 10 kHz, with four peak values at about 280, 550, 5700 and 6400 Hz. These bulla vibrations are particularly high (> 100 nm/Pa) at low frequencies (< 300 Hz), which evidently affects the corresponding umbo response (black) at those frequencies.

These results indicate that bulla-vibration signal contamination exists in the open-sound-field measurements at the lowest frequencies and also to a small extent around 550 Hz where a peak of bulla vibration occurs.

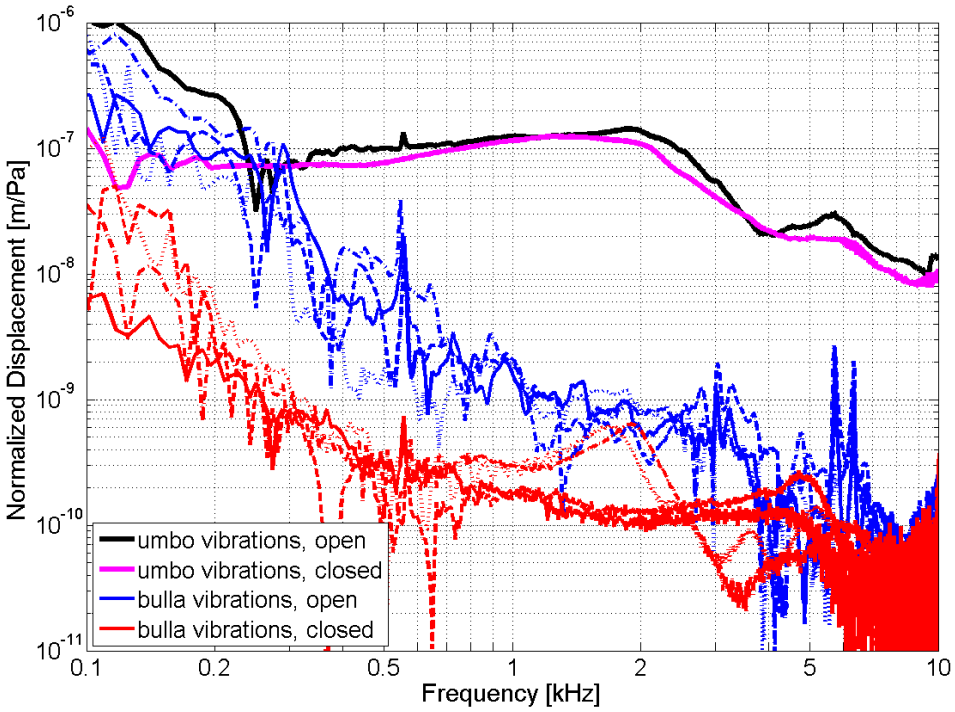

Figure 4.11: Normalized displacements measured at a reference point on the bulla in the closed-sound-field experiments are in red and those in the open-sound-field experiments are in blue. The corresponding umbo displacements measured in the closed and open sound fields are in magenta and black respectively.

In the closed-sound-field experiments, the bulla displacements again generally decrease as frequency increases, and at low frequencies are an order of magnitude less than those in the open-sound-field experiments. The bulla vibrations are considerably lower than the corresponding umbo displacements, confirming that the bulla vibrations are negligible in the closed-sound-field experiments.

In summary, the effects of bulla vibrations in both types of sound field are unimportant except at low frequencies in the open sound field. Taking this into account, all open-sound-field experimental data below 300 Hz are ignored in the following chapters.

4.3 Overview of measurements

All measurements were done on the right ear for consistency, except for one gerbil that had a perforation in its right TM. Frequency responses at multiple locations on the TM were measured: along the manubrium, across the PT regions inferior, anterior and posterior to the manubrium, and at the centre of the PF. The general arrangement of the micro-beads employed in all experiments is shown in Figure 4.12.

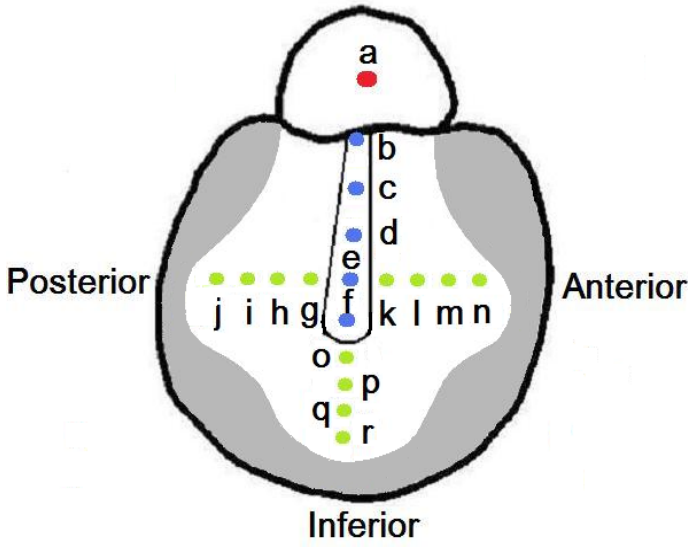

Figure 4.12: A schematic of the general layout of eighteen micro-beads on a right gerbil TM; the shaded area represents the remaining hidden region of the PT.

At the beginning and the end of each experiment, a point on the bulla close to the TM was measured as described in Section 4.2.3.5.2. All beads were measured in each round of measurement: starting at the umbo (f) first, moving along the manubrium to (b) and then to the centre of the PF (a), then across each PT region measuring from the manubrium towards the annulus. At the end of each round, the umbo response was acquired again to verify the consistency of the middle-ear behaviour. One such cycle of measurements took approximately 30 minutes.

As discussed in Section 4.2.3, two types of experiments were performed in this study. 'Single-sound-field' experiments included measurements with either an open or a closed sound field; 'double-sound-field' experiments included both open and closed sound fields. A single-sound-field experiment contains at least six consecutive rounds of measurements: three rounds to assess the effects of drying on the TM, followed by two rounds to compare the TM behaviour in open and closed MEC configurations (i.e., without and with insertion of the ventilation tube), and a last few rounds to measure the open-bulla TM responses while gradually enlarging the hole where the ventilation tube was initially inserted. The procedure for a double-sound-field experiment was almost the same except that two rounds of open-sound-field measurements (to assess the temporal effects) were followed by two rounds of closed-sound-field measurements; the closed-sound-field acoustical set-up is then used for the rest of the measurements. (If the closed-sound-field measurements were done first, removal of the coupler might cause damage to the specimen.)

The single-sound-field protocol does not require intermediate modification of the acoustical set-up and thus eliminates the risk of damaging the specimen. On the other hand, the double-sound-field protocol allows both open- and closed-sound-field measurements to be done with the same gerbil, so the comparison of TM behaviours with different sound fields is more convincing. However, changing the acoustical set-up during this experiment might cause dust, hair or tiny dental cement chips to fall on the TM, thereby affecting the quality of measurements.

Experimental details for each gerbil, such as the time for surgical preparation and vibration measurements, the arrangement of micro-beads, the number of rounds, the type of sound fields and so on, are summarized in Figure 4.13 and Table 4.2.

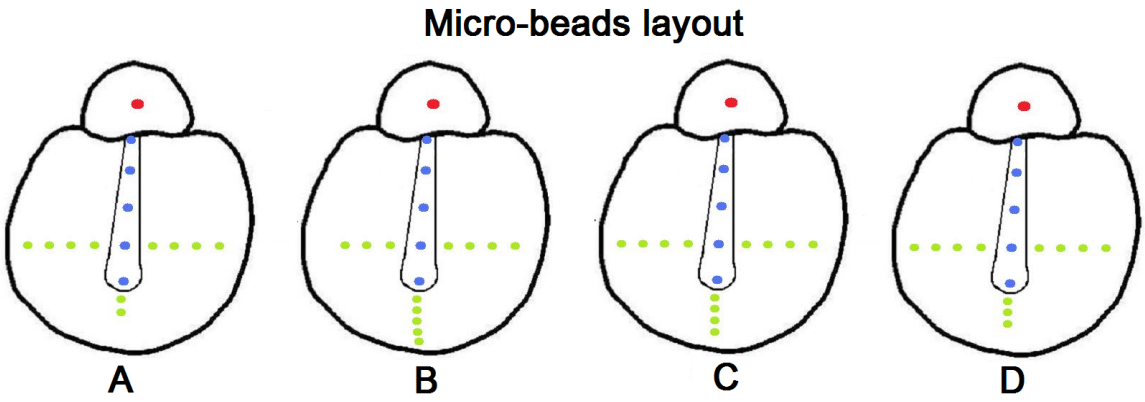

Figure 4.13: Four types of micro-beads layout employed in this study (green beads: PT; blue beads: manubrium; red bead: PF).

Table 4.2: Detailed information of all specimens.

Gerbil	Weight [g]	Ear	Prepara-tion time [hours]	Measure-ment time [hours]	No. rounds	Sound field	No. measurement points	Micro-beads layout
1	84	Right	6	5	7	Open	16	A
2	60	Right	6.5	4.5	6	Open	16	A
3	62	Right	6.5	6	7	Open	18	B
4	64	Left	7.5	5.5	7	Closed	18	C
5	66	Right	5.5	7	8	Closed	17	D
6	68	Right	6.5	7	7	Open & Closed	18	C
7	66	Right	6.5	6	8	Open & Closed	18	C
8	64	Right	6.5	4.5	8	Open & Closed	18	C
9	64	Right	6	6	8	Open & Closed	18	C

4.4 Modelling techniques

The middle ear is a very complex system involving non-uniform materials, interdependent structural parameters, and irregular geometries and boundary conditions. Its function and behaviour cannot be fully understood with a simple descriptive model, so a mathematical model based on realistic geometry and *a priori* knowledge of structural parameters and boundary conditions must be used to handle such a complex system.

4.4.1 The finite-element method

This section is based primarily on Funnell (n.d.). Among various mathematical modelling techniques, the finite-element method has become very popular in middle-ear research; finite-element models are extensively used to simulate the behaviour of the middle ear and to address issues that are difficult to evaluate experimentally. In finite-element analysis, any complicated geometry can be broken down into a number of two-dimensional (triangle, rectangle, etc.) or three-dimensional (tetrahedral, hexahedral, etc.) elements which connect one to another to form a mesh. A set of parameters including material properties, boundary conditions and loading is then assigned to each element. The behaviour of a single element can be easily analyzed in terms of the loads and the responses at each node of the element, resulting in an element matrix relating a vector of the applied nodal forces to a vector of the nodal displacements. Since all interconnected elements share nodes, the response of the whole system can be calculated by solving a large global matrix composed of individual element matrices. Figure 4.14 illustrates an example of a two-dimensional system composed of two triangular elements.

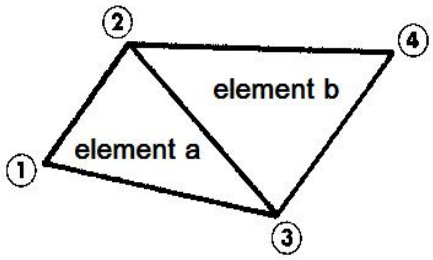

Figure 4.14: A system composed of two triangular elements. (After http://audilab.bme.mcgill.ca/AudiLab/teach/fem/fem.html)

The equations corresponding to each element as well as to the whole two-element system are shown in Equations 4.2 to 4.4 respectively. Matrices $[a_{ij}]$ and $[b_{ij}]$ are the stiffness matrices of the respective elements, $[w_j]$ is the vector of the nodal displacements, and $[f_i]$ and $[g_i]$ are the vectors of loads applied to each element:

$$\begin{pmatrix} a_{11} & a_{12} & a_{13} \\ a_{21} & a_{22} & a_{23} \\ a_{31} & a_{32} & a_{33} \end{pmatrix} \begin{pmatrix} w_1 \\ w_2 \\ w_3 \end{pmatrix} = \begin{pmatrix} f_1 \\ f_2 \\ f_3 \end{pmatrix} \tag{4.2}$$

$$\begin{pmatrix} b_{11} & b_{12} & b_{13} \\ b_{21} & b_{22} & b_{23} \\ b_{31} & b_{32} & b_{33} \end{pmatrix} \begin{pmatrix} w_2 \\ w_3 \\ w_4 \end{pmatrix} = \begin{pmatrix} g_2 \\ g_3 \\ g_4 \end{pmatrix} \tag{4.3}$$

$$\begin{pmatrix} a_{11} & a_{12} & a_{13} & 0 \\ a_{21} & a_{22}+b_{11} & a_{23}+b_{12} & b_{13} \\ a_{31} & a_{32}+b_{21} & a_{33}+b_{22} & b_{23} \\ 0 & b_{31} & b_{32} & b_{33} \end{pmatrix} \begin{pmatrix} w_1 \\ w_2 \\ w_3 \\ w_4 \end{pmatrix} = \begin{pmatrix} f_1 \\ f_2+g_2 \\ f_3+g_3 \\ g_4 \end{pmatrix} \tag{4.4}$$

4.4.2 The finite-element model

The finite-element model used in this study was originally presented by Elkhouri (2006) for a study of the gerbil middle-ear responses at low frequencies. The model geometry and boundary conditions were further refined based on X-ray micro-CT data (Gea et al., 2010) and histological images, and the application of the model was extended to higher frequencies (Maftoon et al., 2011).

Linear elastic material properties were used to model all middle-ear structures, with Rayleigh damping (Maftoon et al., 2011). Specific material properties were first chosen from *a priori* estimates. Maftoon et al. (2011) further adjusted these material properties based on the results of a sensitivity analysis of each property over its physiologically reasonable range. Thin-shell elements with variable thickness, based on the confocal microscopy data reported by Kuypers (2005), were used to model the TM. The boundary of the TM was clamped by constraining both displacements and rotations of the nodes located at the PT annulus, as well as along the rim of the PF, as shown in Figure 4.15. Moreover, displacements of the nodes at the tips of the anterior mallear process and posterior incudal ligament were also set to zero, fixing those tips to the imaginary cavity wall.

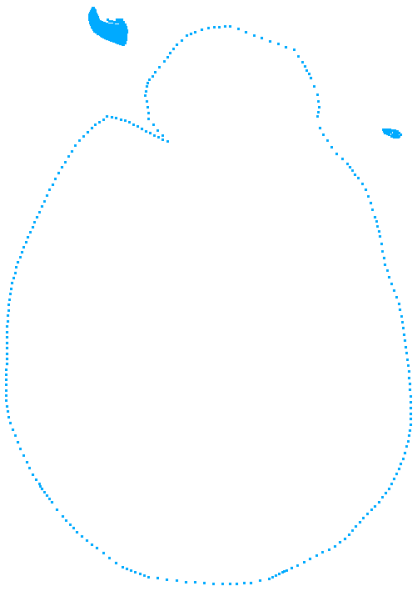

Figure 4.15: Boundary conditions of the model: the blue dotted line represents the TM boundary; the two irregularly shaped blue structures represent the tips of the anterior mallear process and the posterior incudal ligament respectively.

The MEC wall was not included in this model, so the model simulated the middle-ear behaviour with an open-bulla configuration. Hence, the simulation results were compared with the experimental measurements obtained without the ventilation tube or with a large hole in the bulla wall. Moreover, the incudomallear joint was modelled as being rigid, and the stapes is not yet included in this model, as shown in Figure 4.16.

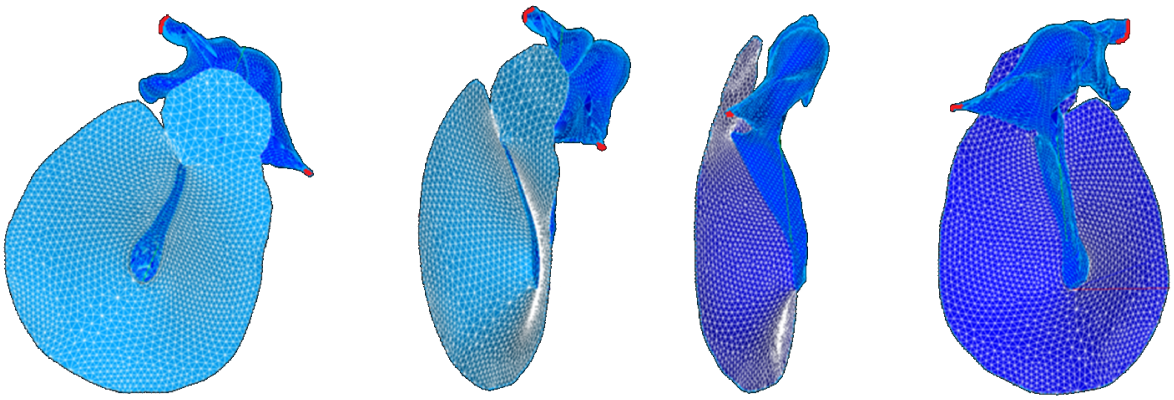

Figure 4.16: Multiple views of the model, showing the tympanic membrane, malleus and incus; the stapes is not included in the model. The fixed tips of the anterior mallear process and posterior incudal ligament are in red.

The uniformly distributed sound-pressure input was modelled as a step function of 1 Pa pressure applied on all the elements of the TM surface. The model was primarily used to evaluate the effects of micro-beads and of different measurement angles, which are presumably not very sensitive to the bulla configuration and ossicle articulations.

4.4.3 Software

Most of the model pre-processing was done by using a set of in-house software: Fie, to outline the contours of the middle-ear structures from stacks of micro-CT or histological images; Tr3, to generate surface meshes by three-dimensional surface triangulation between contours traced from the serial sections; and Fad, to assemble and modify meshes of the three-dimensional model. More detailed descriptions of the in-house software for model pre-processing were presented by Elkhouri (2006), and a complete list of the finite-element software used in our lab is available on the AudiLab Web site: http://audilab.bme.mcgill.ca/sw/.

Calculations were carried out using Code_Aster, a finite-element package developed by EDF (Électricité de France); the resulting time-domain responses were then converted into the frequency domain in MATLAB.

4.4.4 Time step

In the real physical world, everything happens in continuous time and not with discrete time steps. In digital computing we approximate continuous time by assuming finite time steps. Reducing the size of the time step can improve the accuracy of simulations, but will be computationally expensive. It is therefore important to verify that the time step is small enough to provide adequate accuracy and stability.

The time integration in our finite-element simulations is done using the Newmark method which is implicit and unconditionally stable, allowing the time step to be relatively large compared with those in explicit methods. However, this integration method low-pass filters the response to different extents depending on the size of the time step (Funnell et al., 1987). Since our experimental results indicate that the modes of TM vibrations are complex at high frequencies, it is important to select a time step small enough compared with the periods of those modes, in order to simulate the detailed resonance structures at high frequencies. Figures 4.17 and 4.18 show the simulated responses of the umbo and of a point at the centre of the posterior PT computed with four different values of the time step. Similar results are also seen in the anterior and inferior PT.

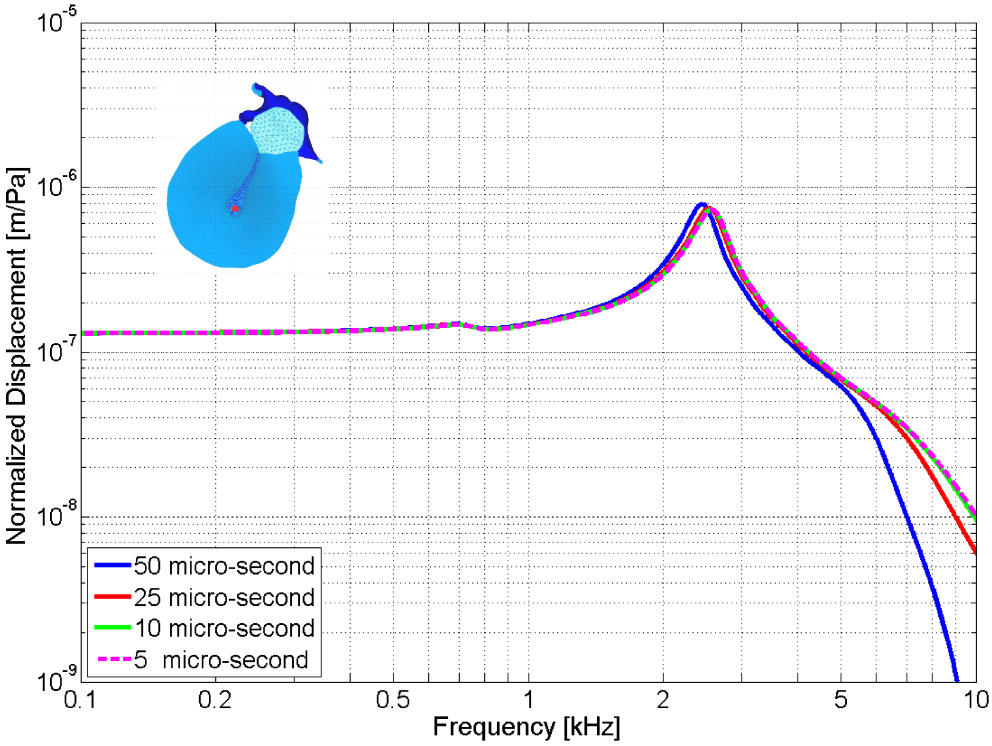

Figure 4.17: Normalized displacements of the umbo (red dot in the inset showing the TM) computed with four different values of the time step.

For both umbo and PT, the responses obtained with time steps of 5 and 10 μs are almost identical. Those with a time step of 25 μs show a similar shape with a slight leftward frequency shift at high frequencies (> 3 kHz). Those with a time step of 50 μs show a greater leftward frequency shift starting from about 1 kHz, and then fall off rapidly above about 5 kHz for the umbo and 7 kHz for the PT. The computation time for each simulation using time steps of 5, 10, 25 and 50 μs is roughly 5, 3, 1 and 0.5 hours respectively.

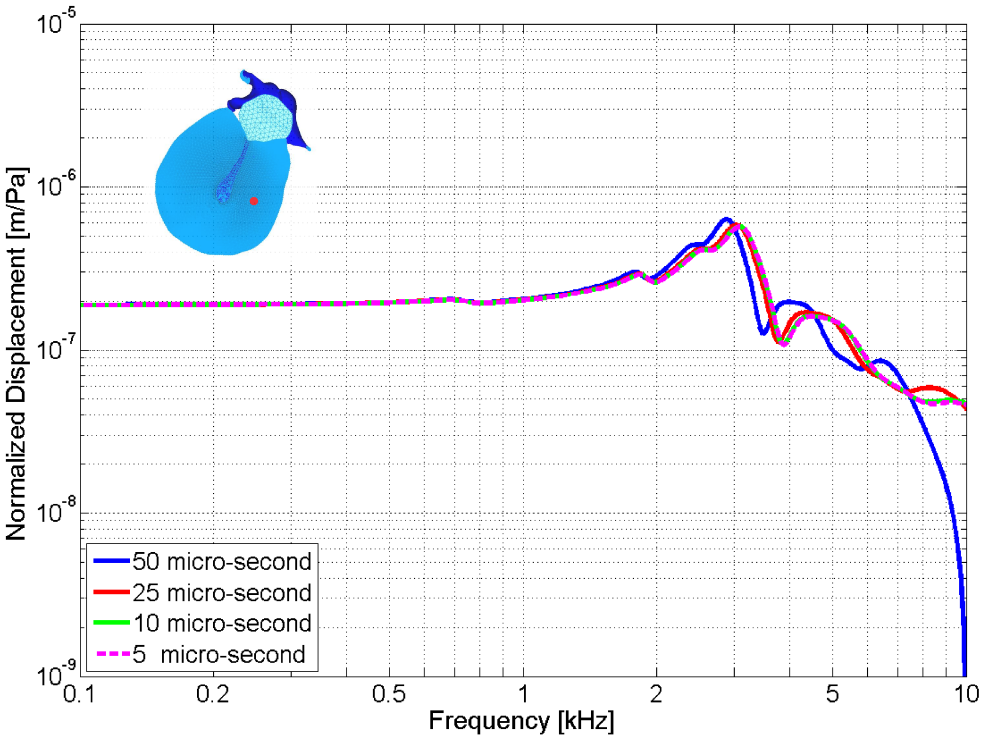

Figure 4.18: Normalized displacements at the centre of the posterior PT region (red dot in the TM figure) computed with four different values of time steps.

Based on these observations, the time step of 25 μs appears to be a reasonable choice for our analysis. It is small enough to simulate the fine resonant structures of the PT quite well at high frequencies, yet not too computationally expensive.

Chapter 5
Experimental Results

This chapter presents the vibration measurements performed at multiple locations on the TM's of nine gerbils. The frequency responses of the PF are presented in Section 5.1, with discussion of the effects of PF retraction. In Section 5.2, the frequency responses measured at the umbo are presented, addressing issues such as inter-specimen variability, temporal effects, the responses for both closed and open middle-ear configurations, and a comparison with previous studies. Section 5.3 presents the frequency responses along the manubrium. In Section 5.4, the responses measured in the anterior, posterior and inferior regions of the PT are presented, with detailed discussion of the responses in each region, as well as the temporal effects on the PT. Key observations are then summarized in Section 5.5.

5.1 Pars-flaccida vibrations

Two states of the PF were observed in this study, namely flat PF and retracted PF, as illustrated in Figure 5.1.

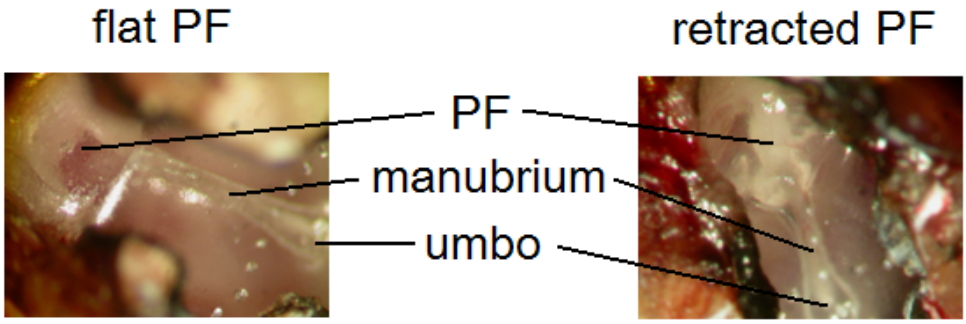

Figure 5.1: Pictures of the gerbil TM with flat PF (left) and retracted PF (right).

The flat PF reflects the physiologically normal state of the PF with zero pressure difference across the TM. Under the microscope, it appears a bit more opaque than the PT and blurs the view of objects behind it. On the other hand, the retracted PF appears slightly more transparent and therefore the malleus head can be seen clearly through it.

Although it is difficult to judge the flatness of an almost transparent membrane, the retracted PF normally shows a cone of light close to its periphery, which is a result of the incoming microscope light reflected from a concave surface. As discussed below, the flatness of the PF can be further confirmed when placing a micro-bead on it. The PF responses are presented in Section 5.1.1, and the temporal effects are presented in 5.1.2.

5.1.1 Flat vs. retracted pars flaccida

Among nine gerbils measured in this study, a flat PF was only observed in two of them: gerbils 1 and 8. A possible explanation of PF retraction might be the accumulation of negative middle-ear pressure during the hours of surgical preparation. The pressure could retract the PF to the extent that the PF touches the malleus head. Although the negative middle-ear pressure is later released through a ventilation tube, the contact between the malleus head and the medial side of the PF might still remain due to the surface tension of the mucosal lining, partially immobilizing the PF during measurements. This phenomenon of adhesion was observed by Rosowski & Lee (2002) when measuring TM responses while varying the middle-ear pressure from −30 to +30 cm H_2O.

The PF displacements measured at approximately the centre of the PF in the nine gerbils are illustrated in Figure 5.2. In particular, the responses of gerbils 1 and 8, both with flat PF, are quite distinct from the other gerbils. They both have a resonance peak at about 600 Hz; their overall displacements are very similar and are about 20 to 40 dB higher than the retracted-PF displacements below 1 kHz, and about 15 dB higher above 1 kHz; and their high-frequency displacements (> 2 kHz) generally drop off at about −12 dB/octave. Compared with gerbils 1 and 8, the gerbils with retracted PF are less consistent. However, some common features are found in these results: the displacements below 0.5 kHz are generally flat; two or three relatively broad peaks can be seen between 0.8 to 3.5 kHz; and the displacements drop off at about −12 dB/octave from 2 to 5 kHz. Some of these features are not seen in gerbils 2 and 3; moreover, big valleys are seen in their low-frequency responses. This is because gerbils 2 and 3 were measured in an open sound

field where low-frequency noise was approximately at the same level as their PF responses at those frequencies; details about this low-frequency noise can be found in Section 4.2.3.5.2.

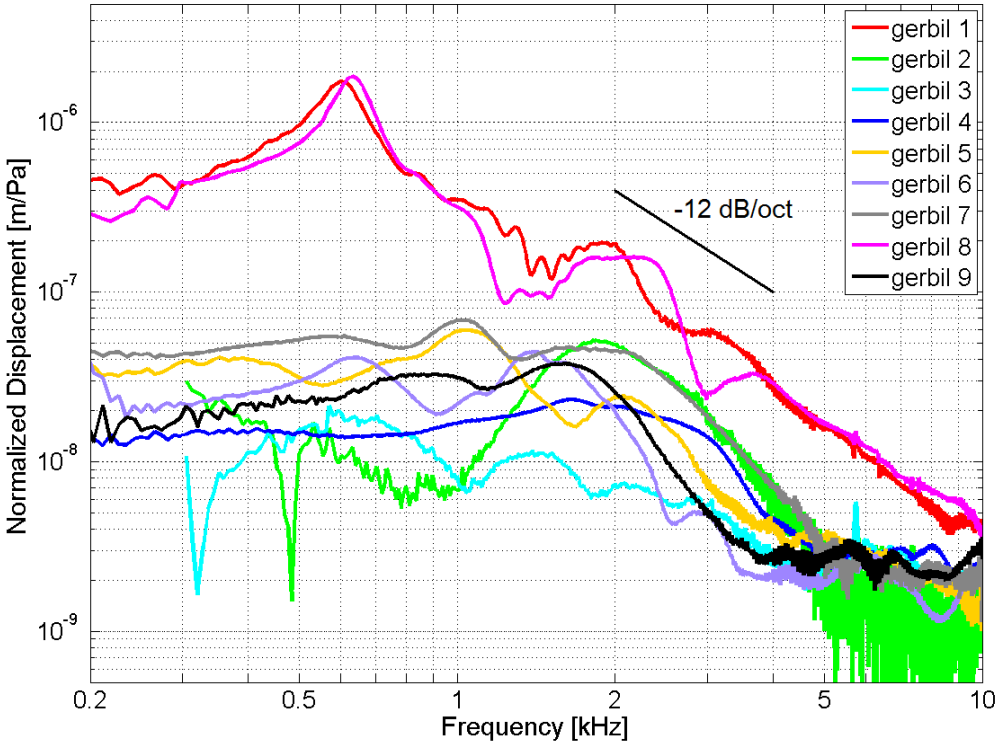

Figure 5.2: Normalized displacements of the PF in nine gerbils (gerbils 1 and 8 with flat PF, other gerbils with retracted PF). Results for gerbils 1, 2 and 3 were the first round of open-sound-field measurements, and those of the other gerbils were the first round of closed-sound-field measurements.

5.1.2 Temporal effects

PF responses (blue curves) along with the corresponding umbo responses (grey curves) are presented for gerbils 5, 1 and 8 in Figures 5.3 to 5.5, demonstrating the effects of time with different PF states. The PF's in gerbils 2, 3, 4, 5, 6, 7 and 9 were all retracted and revealed similar temporal effects; therefore, only the results of gerbil 5 are shown in Figure 5.3 as a typical illustration. In this gerbil, the overall PF displacements are lower

than the umbo displacements. The absence of the PF resonance is associated with a relatively flat umbo response at low frequencies. As time increases, the 1 kHz broad peak in the PF response shifts to higher frequencies: it shifts by about 200 Hz over the first 65 min, changes little over the next 65 min, then shifts again by about 300 Hz over the next 140 min. Moreover, the magnitudes at frequencies below that peak decrease gradually, while the high-frequency PF responses (> 3 kHz) change very little. Regardless of the temporal effects seen in the PF response, no significant change is observed in the corresponding umbo response, implying that the vibration of the PF does not influence the umbo response in the case of a retracted PF.

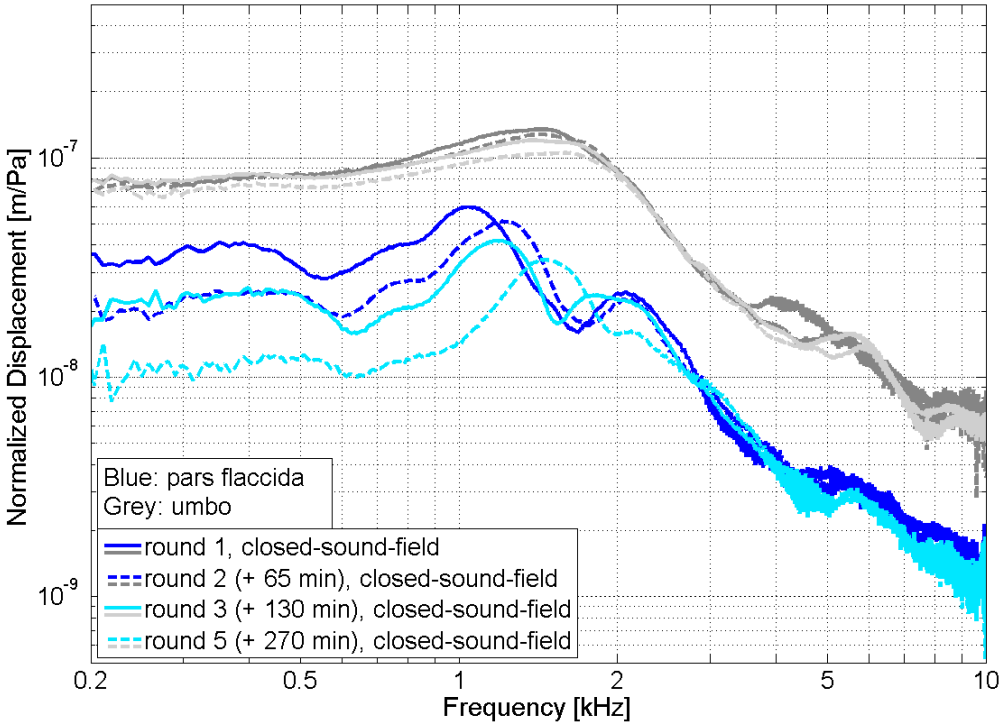

Figure 5.3: Temporal effects of the PF (blue curves) and the corresponding umbo response (grey curves) measured in gerbil 5 with retracted PF.

Figure 5.4 shows the results for gerbil 1, which had a flat PF. The PF displacements below about 1.5 kHz are significantly higher than the corresponding umbo displacements. In round 1 the PF resonance occurs at 600 Hz and is associated with a minimum in the

umbo response. As time increases, this PF resonance shifts to higher frequencies and there is a gradual decrease in magnitude below 1.5 kHz. There is actually little change in the first 30 min but in the next 30 min the PF resonance shifts by 100 Hz, and the displacements at frequencies up to this resonance generally decrease by about 8 dB, resulting in a magnitude increase in the corresponding umbo minimum. In fact, there appear to be three PF resonances (at 0.7, 1.2 and 2 kHz) in round 3 (the second 30 min), with the first two of them (700 Hz and 1.2 kHz) being reflected in the umbo response as two minima. Above 1.5 kHz, the temporal effects are less pronounced in the PF response, and the corresponding umbo response changes very little. In summary, regardless of all the temporal effects seen in the response of a flat PF, the corresponding umbo response is only affected in the frequency range in which a PF resonance is present.

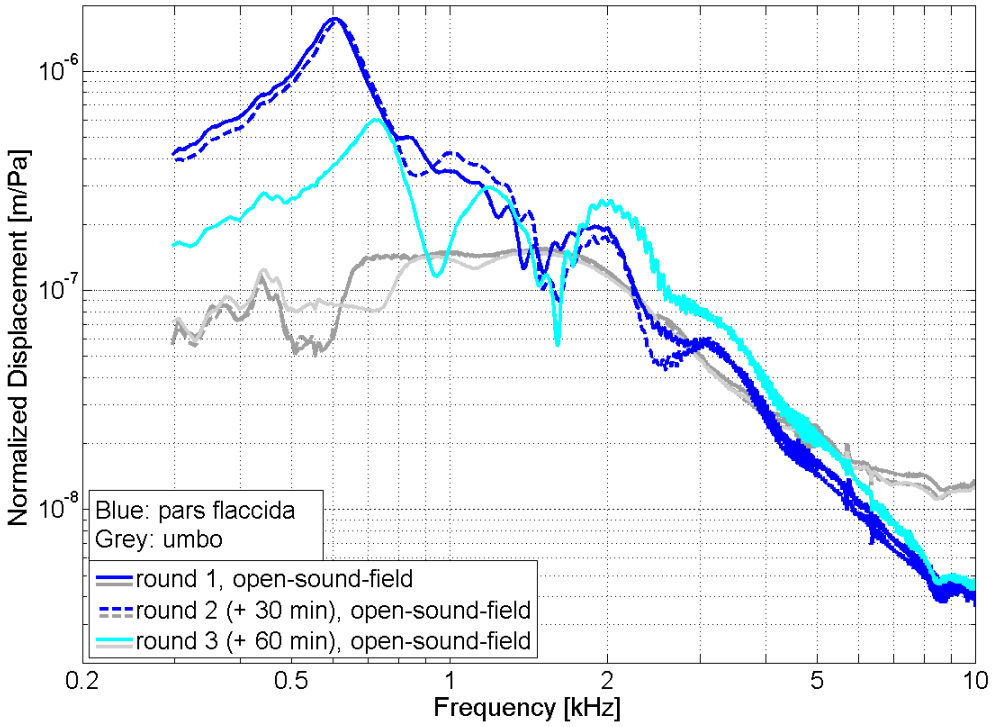

Figure 5.4: Temporal effects of the PF (blue curves) and the corresponding umbo response (grey curves) measured in gerbil 1 with flat PF.

In gerbil 8, with a flat PF, the shapes and magnitudes of both the PF and umbo responses are similar to those of gerbil 1, except that the temporal effects are more pronounced in gerbil 8. As shown in Figure 5.5, the overall PF response shifts to higher frequencies as time increases. The magnitudes of the PF responses generally decrease slightly with time, except that they increase between rounds 3 and 4. At the end of round 3, a tiny bone chip fell onto the TM close to the manubrium; the middle-ear behaviour might have been somehow altered after the removal of this bone chip, resulting in an overall magnitude decrease in the umbo response (in rounds 4 and 6) and the corresponding magnitude increase in the PF response. For the umbo responses, the frequency shifts are similar to those observed in the PF response. The PF resonance in each round of measurements is consistently at a slightly higher frequency than the corresponding umbo minimum. Since the PF was normally measured 10 to 20 min after the umbo, these frequency offsets may reflect temporal effects between measurements in each round. In fact, gerbil 8 died right at the beginning of measurements, so *post mortem* effects probably explain why the temporal effects are so large in this animal. The temporal effects observed in these results are consistent with those in *post mortem* gerbil measurements by Nambiar (2009) and demonstrate the relatively poor consistency of *post mortem* measurements compared with *in vivo* ones.

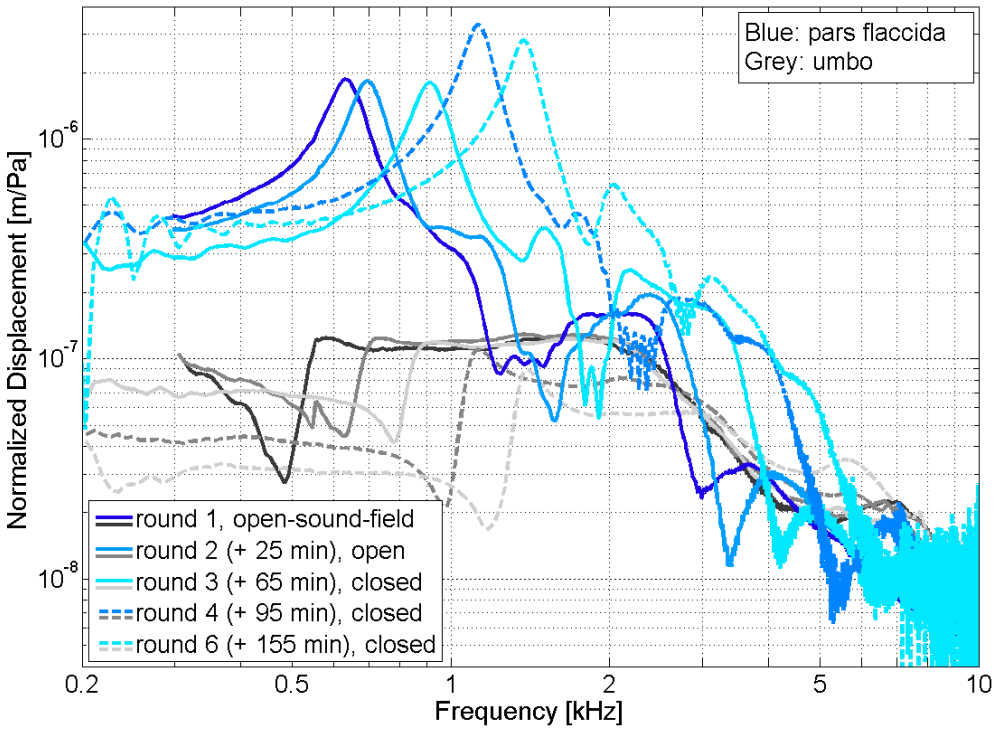

Figure 5.5: Temporal effects of the PF (blue curves) and the corresponding umbo response (grey curves) measured in gerbil 8 with flat PF. Gerbil died right at the beginning of measurements.

In conclusion, the PF resonance at around 600 Hz in the flat-PF response is associated with a minimum followed by a sharp rise in the corresponding umbo response. When the PF is retracted, the PF resonance is absent and the overall PF response is smaller, implying a stiffening effect due to the retraction of the PF. Regardless of the state of the PF, the umbo responses at frequencies above 800 Hz are unaffected by changes in the PF response. In gerbil 1, the umbo response below 500 Hz was contaminated by the low-frequency noise in the open sound field which obscures the PF-umbo interactions at low frequencies. In gerbil 8, the pronounced *post mortem* effects result in some frequency offset between the PF resonances and the umbo minima. Taking these issues into account, our observations generally agree with the hypothesis proposed by Rosowski et al. (1997) that the normal flat PF provides an acoustic shunting function at low frequencies.

5.2 Umbo vibrations

The umbo can be easily recognized on the TM and is often taken as the location for vibration measurements. Accordingly, measurements were taken at the umbo of each gerbil as a reference point. Those measurements not only allow assessments of the inter-specimen variability (Section 5.2.1) and of the effects of time (Section 5.2.2), and comparison of the responses with closed and open MEC (Section 5.2.3), but also permit a comparison with previous studies (Section 5.2.4).

The normalized umbo displacements measured in the first round of measurements in all nine gerbils are shown in Figure 5.6. As discussed in the previous chapter, the open-sound-field measurements at frequencies below 300 Hz are contaminated by the open-sound-field skull vibrations and are therefore ignored. All of these displacement curves are relatively flat below about 400 Hz, indicating the stiffness-dominated behaviour of the gerbil middle ear at low frequencies. Above 400 Hz, the overall umbo displacements (except for the PF effects in gerbils 1 and 8, as discussed in the previous section) gradually increase by about 4 dB until a broad peak at around 1.5 to 2 kHz, and then drop off at about −12 dB/octave until about 4 kHz. Above 4 kHz, the umbo displacements continue to drop at about the same rate but with large and fairly broad magnitude peaks that differ greatly among gerbils.

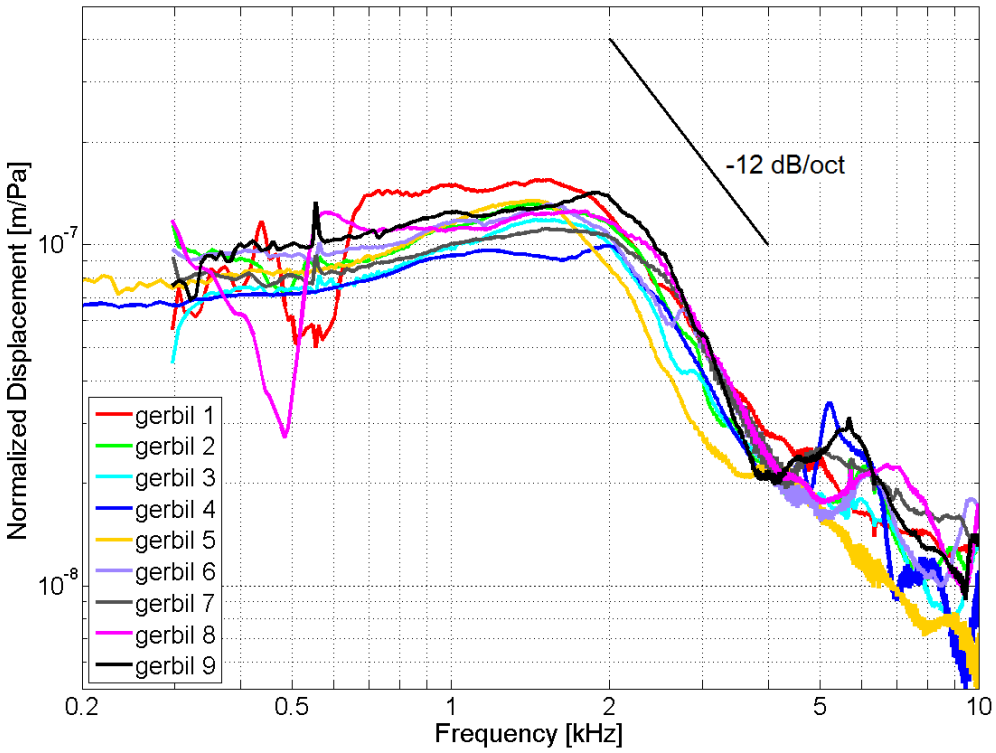

Figure 5.6: Normalized umbo displacements obtained at the first round of measurement in nine gerbils (gerbils 1, 2, 3, 6, 7, 8, 9 in the open sound field; gerbils 4 and 5 in the closed sound field).

5.2.1 Inter-specimen variability

Inter-specimen variability is one of the main concerns in experimental studies. As shown in Figure 5.6, the shapes of all of the umbo response curves (except those of gerbils 1 and 8) are consistent over the frequency range of 300 Hz to 4 kHz with a variation of approximately ±2 dB. From 4 to 9 kHz, the variability increases to ±5 dB as the two broad peaks in each gerbil occur at different frequencies.

The inter-specimen variability observed in this study is comparable with that of other experimental studies of TM vibrations in gerbils or human. For example, a variability of ±3 to ±8 dB was estimated by Cohen et al. (1993) based on umbo displacements averaged over five or six gerbils in each of eight age groups. More recently, Nambiar (2009)

reported a variation of approximately ±5 dB (excluding the frequency region where the minimum and sharp rise occur) in *post mortem* umbo displacements of eight gerbils; in another four gerbils, there were magnitude differences of 20 to 30 dB at high frequencies (> 6 kHz). In humans, an inter-subject variation of ±10 dB in umbo velocity measurements among eighty normal ears was observed by Whittemore et al. (2004). Recently, in a study of sixty-two normal human ears, Arechvo et al. (2009) reported that the variation in umbo displacements increased with frequency: the deviation pattern covered a band of ±5 dB over the frequency range of 500 to 2000 Hz, and then broadened to a range of ±10 dB from 2000 to 3700 Hz.

5.2.2 Effects of time

The experimental preparations in this study required a considerable amount of time (5.5 to 8.5 hours) during which the TM as well as other middle-ear structures might have become dehydrated, leading to changes in their material properties; however, temporal effects before the first measurement are difficult to evaluate experimentally. Moreover, the TM was widely exposed during the lengthy measurements (4.5 to 7 hours), which might make it more prone to temporal effects; it is therefore important to verify the consistency of the measured responses within a given experiment. In our previous *post mortem* study (Nambiar, 2009), small pieces of moist tissue paper were placed on the outer wall of the bulla for passive re-hydration. In that study, the short-term variability observed in the umbo displacements within 30 min was about 1 to 2 dB except at the lowest and highest frequencies; the long-term variability (up to 200 min between measurements) showed obvious temporal effects, with a gradual decrease in response magnitude at frequencies up to 2.2 kHz, and a positive frequency shift of the response curve.

In this study, the temporal effect should be less pronounced as all measurements were performed with living gerbils (except gerbil 8 which died at the beginning of measurements, possibly due to an overdose of anaesthesia). Moreover, the periodically

applied long-lasting anaesthesia contained a substantial volume of saline solution which helped to protect the gerbils from dehydration during the experiment; the fact that they were not dehydrated could be confirmed by the fact that no gerbil lost more than 2 g of weight (about 2-3% of body weight) over the course of an experiment, including the weight of surgically removed soft tissue and bone. Nevertheless, the TM surface might still be vulnerable to dehydration over time, especially because it was widely exposed in this study. Therefore, the passive re-hydration method from the previous study using small pieces of moist tissue paper was also employed in this study during the open-sound-field experiments. In the closed-sound-field experiments, the exposed bulla surface was almost completely covered by the coupler and the dental cement, leaving only a small space in the area where the ventilation tube was inserted; therefore, it was impractical and presumably unnecessary to apply moist tissue paper during the closed-sound-field experiments, as the TM was not directly exposed to air flow.

The temporal effects in gerbils 2, 3, 4, 5, 6, 7 and 9 are similar within the time range up to 305 min. Therefore, only the results of gerbil 7 are presented here as a typical illustration. The normalized umbo displacements measured in gerbil 7 at multiple time points are shown in Figure 5.7. The time at the first round of measurement is considered as a reference point, and several consecutive measurements are plotted and labelled with their corresponding time differences. There is a small localized dip at about 1.7 kHz in the third round of measurements, and a slight rise at about 5 kHz disappears after the first round of measurements. In general, the variations in response magnitudes over the entire measurement period for all gerbils (except gerbils 1 and 8) are within the range of 1 to 2 dB at frequencies below 5 kHz and rise up to 4 dB at higher frequencies. This is comparable to the short-term variability observed in the previous study (Nambiar, 2009), indicating the improved consistency of *in vivo* measurements.

The temporal effects of gerbils 1 and 8 are further complicated by the state of the PF and have already been discussed in Section 5.1.2.

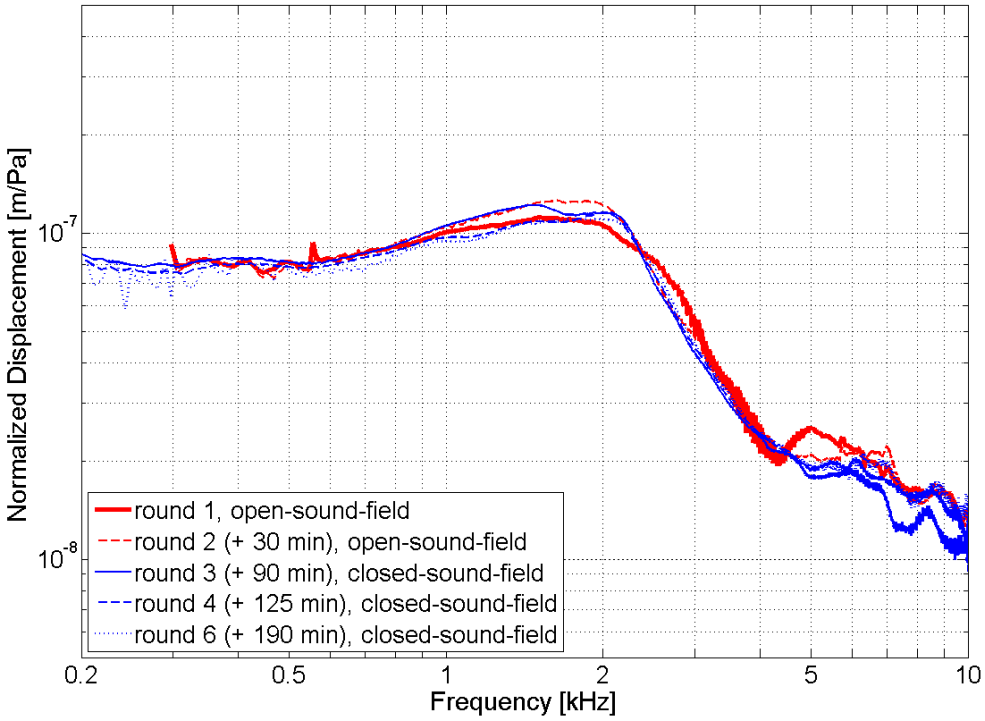

Figure 5.7: Temporal effects of umbo responses in gerbil 7.

5.2.3 Closed and open middle-ear cavity

In all closed-sound-field experiments, measurements were first taken in the closed MEC configuration and then the preparation was changed to the open-MEC configuration. In order to verify the repeatability of measurements when switching between different configurations, the ventilation tube was always inserted back into the bulla for another round of measurement right after the measurements without the ventilation tube.

The umbo displacements with both open and closed MEC configurations were measured in gerbils 4 to 9. All measurements except those of gerbil 8 (due to *post mortem* effects) are very similar; therefore, results for gerbil 7 are shown in Figure 5.8 as a typical illustration. In these gerbils, measurements with the initial closed MEC configuration and then with the tube inserted back in the bulla are roughly the same (magnitude difference < 2 dB), confirming the repeatability of those measurements. Removal of the

ventilation tube results in an overall increase of response magnitude below about 1.2 to 1.5 kHz and a sharp minimum at about 1.8 to 2.2 kHz. As the ventilation hole is widened, this minimum shifts towards higher frequencies and further decreases in its magnitude. Some variations in the displacements occur at low frequencies (< 800 Hz), but the displacements above the anti-resonance remain almost unaffected, with less than 2 dB of variations. In gerbil 7, a slight drop in magnitude is found at around 1 to 1.7 kHz when the tube is inserted back in the bulla; this change might be attributable to temporal effects and not to the removal and replacement of the tube. For gerbil 8, apart from the *post-mortem* effects and the presence of a PF resonance, opening the MEC leads to results similar to those in the other gerbils. In general, our observations regarding the TM response in open MEC configuration are in agreement with those observed in previous studies (Rosowski et al., 1997; Nambiar, 2009).

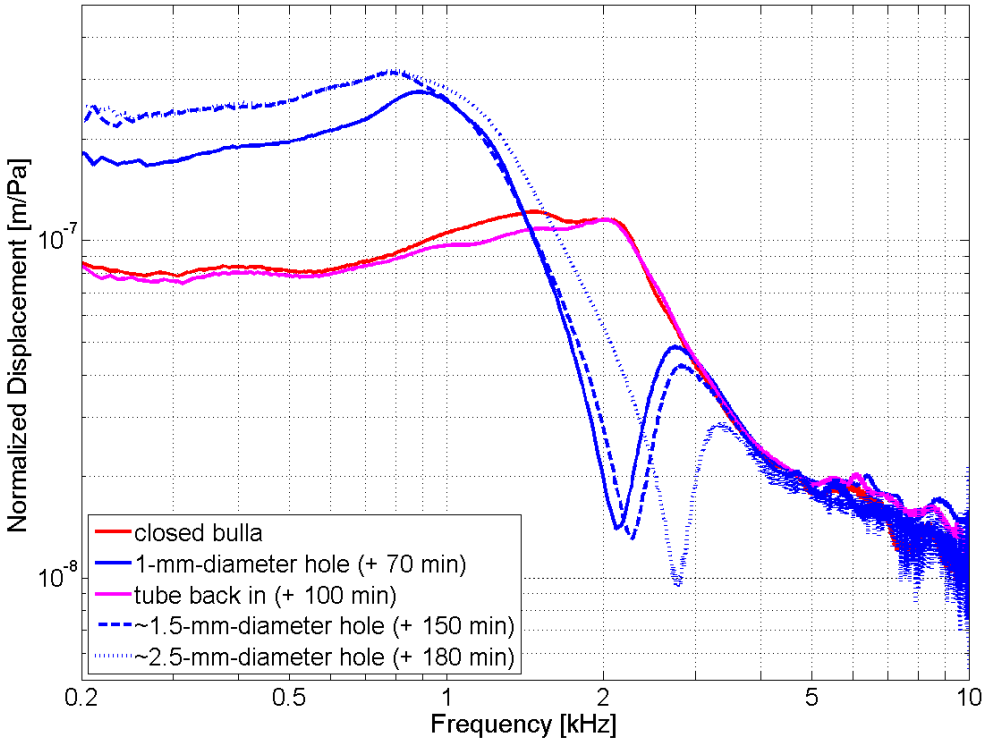

Figure 5.8: Comparison of the umbo responses in closed (red curves) and open (blue curves) MEC configurations, measured in gerbil 7.

The effects of the size of the ventilation hole on the low-frequency umbo response in these gerbils are shown in Figure 5.9, from which gerbil 6 is excluded because only one round was measured with the open MEC configuration. The normalized umbo displacements at 400 Hz are plotted versus time, with different hole sizes indicated by different markers. The low-frequency magnitude variations with increasing hole size are not as consistent as the frequency shift, but a common phenomenon can be observed: the displacement reaches a plateau at the smallest hole size (1 mm in diameter). The exception seen in gerbil 7, in which the plateau is reached only with the second hole size (1.5 mm) might be due to some mucous membrane left inside the hole when pulling out the ventilation tube from the bulla, which would reduce the effective size of the hole to less than 1 mm in diameter.

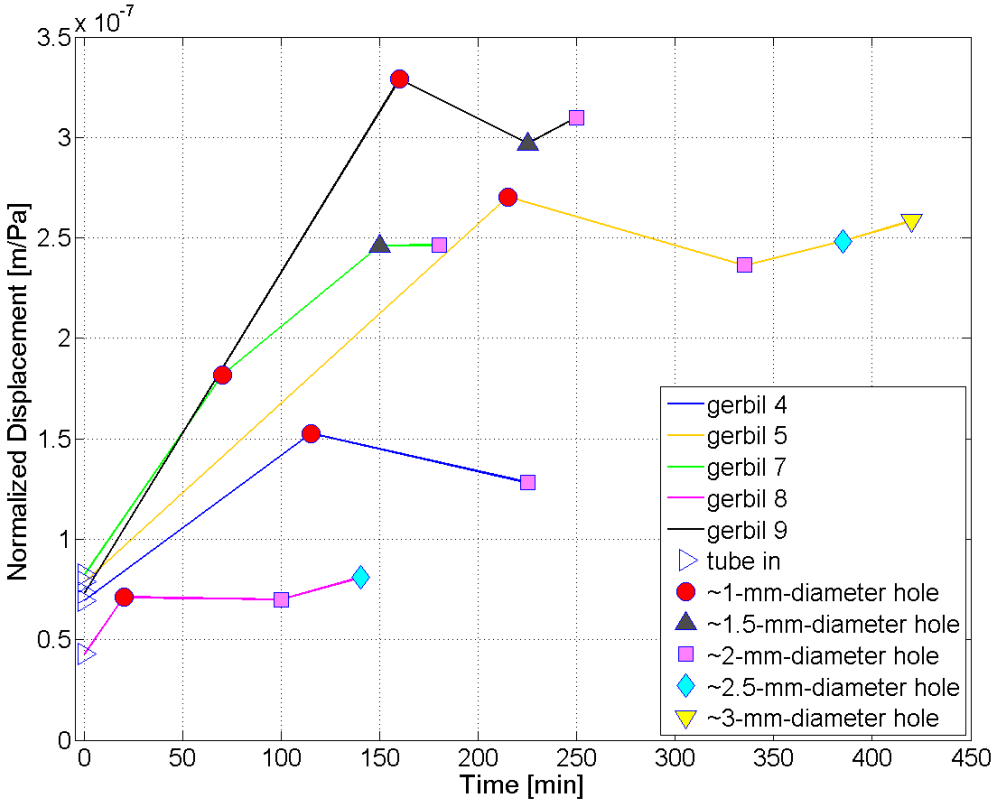

Figure 5.9: The effects of the size of ventilation hole on the low-frequency umbo displacements in five gerbils; all measurements were taken at 400 Hz.

5.2.4 Comparison with previous studies

Since the umbo is the location where people have often measured TM vibrations, the reliability and accuracy of our experimental results can be verified by comparing our umbo responses with those from previous studies. In this section, our umbo measurements are compared with those reported by Rosowski et al. (1997; 2002) and Nambiar (2009). The umbo velocities reported by Rosowski et al. are divided by the corresponding angular frequencies to provide displacement values for comparison.

As mentioned earlier, the umbo minimum corresponding to the PF resonance was absent in gerbils 2, 3, 4, 5, 6, 7 and 9, which had retracted PF's. The absence of this umbo minimum was also observed in gerbils with experimentally immobilized PF's (Rosowski & Lee, 2002; Rosowski et al., 1997). Hence, it is likely that the retracted PF is stiffer than the flat PF. Figure 5.10 shows the first round of umbo measurements of the gerbils with retracted PF in this study, and the umbo displacement averaged over ten gerbil ears with immobilized PF, as well as the 95% confidence limits, reported by Rosowski & Lee (2002). Below 5 kHz, the magnitudes of our measurements are 2 to 4 dB higher than those obtained by Rosowski and Lee.. One possible explanation for such a magnitude increase may be the difference in the measurement angles. According to Rosowski & Lee, the angle between the laser beam and the annulus plane was around 60º in their experiments, whereas the umbo plane could be oriented perpendicular to the laser beam in our experiments due to the wide exposure of the TM. The effects of different measurement angles are further studied with our numerical model and the results are presented in Chapter 6. Above 5 kHz, the results of Rosowski and Lee appear smoother than our results, presumably because any sharp differences in high-frequency magnitudes are muted by averaging in their results; moreover, their results are about 4 to 18 dB lower than ours.

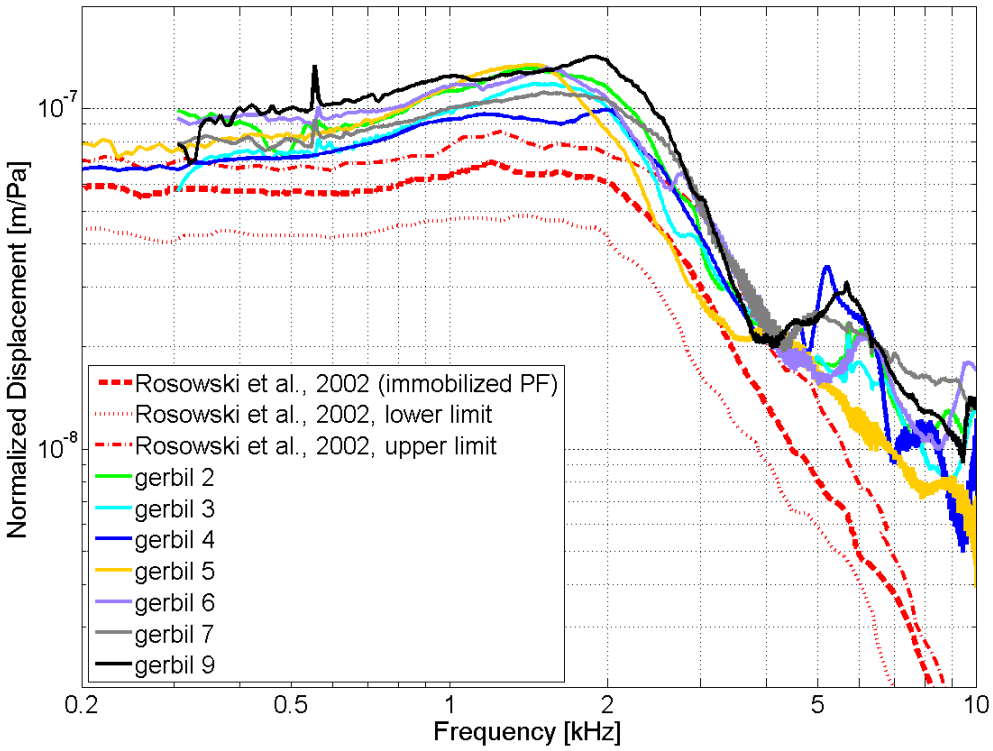

Figure 5.10: Comparison of our umbo displacements with those with immobilized PF obtained by Rosowski & Lee (2002). Limits with 95% confidence are also shown for the averaged data reported by Rosowski et al. (2002).

The umbo displacements measured in gerbils 1 and 8 and those obtained by Rosowski et al. (2002; 1997) and Nambiar (2009) from gerbils with normal PF are illustrated in Figure 5.11. The shapes of our response curves are comparable to those of the previous studies, with an overall magnitude increase of 2 to 4 dB above 800 Hz. All the PF-related umbo minima can be found in the range from 350 to 630 Hz, with those in this study being in the middle of that range and the one obtained by Nambiar being at the highest frequency (~630 Hz). Such differences in the PF resonance may be due in part to the temporal effects of the PF, especially in the *post mortem* measurements by Nambiar where dehydration of the middle-ear structures was more pronounced. The frequencies of the umbo minima in our study are within the limits of the data of Rosowski et al..

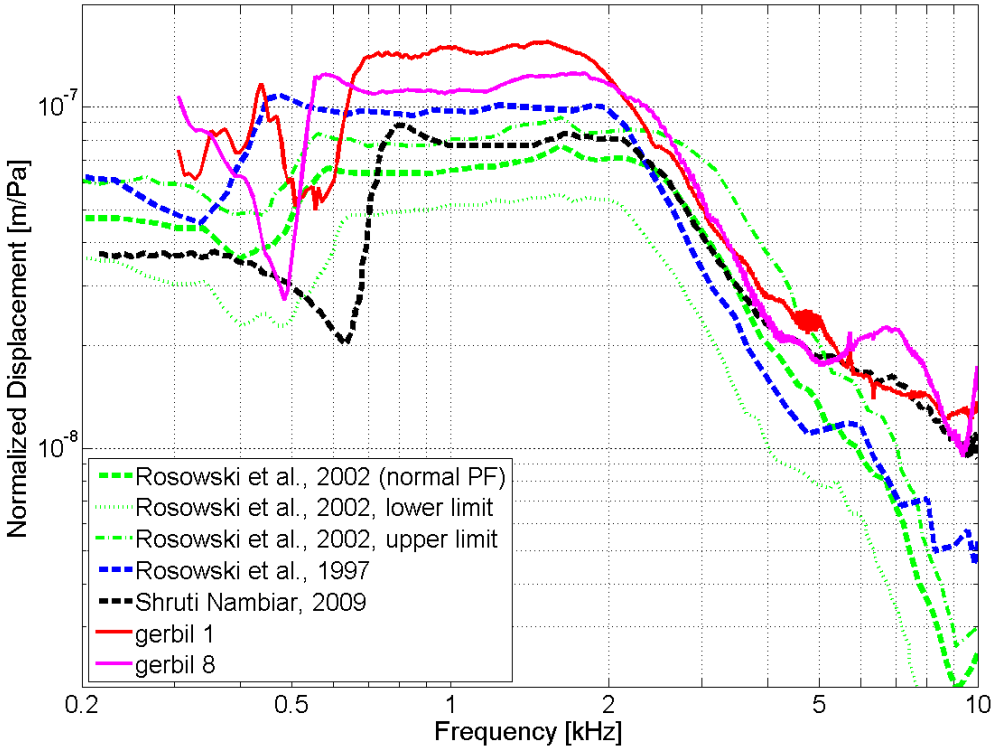

Figure 5.11: Comparison of our umbo displacements with those with normal PF obtained by Rosowski et al. (2002; 1997) and Nambiar (2009). Limits with 95% confidence are also shown for the averaged data reported by Rosowski et al. (2002).

5.3 Manubrium vibrations

Regardless of the PF state and the type of sound field, similar manubrium vibration patterns are seen in all gerbils, so only the first round of closed-sound-field measurements for gerbil 7 are presented in Figure 5.12 as a typical illustration. A schematic drawing of the measurement points on the manubrium is also included in Figure 5.12, with points *f* and *b* indicating the umbo and the lateral process of the malleus respectively. A comparison of the manubrial displacements of all gerbils measured at 1 kHz from point *b* to point *f* can be found in Figure 5.16.

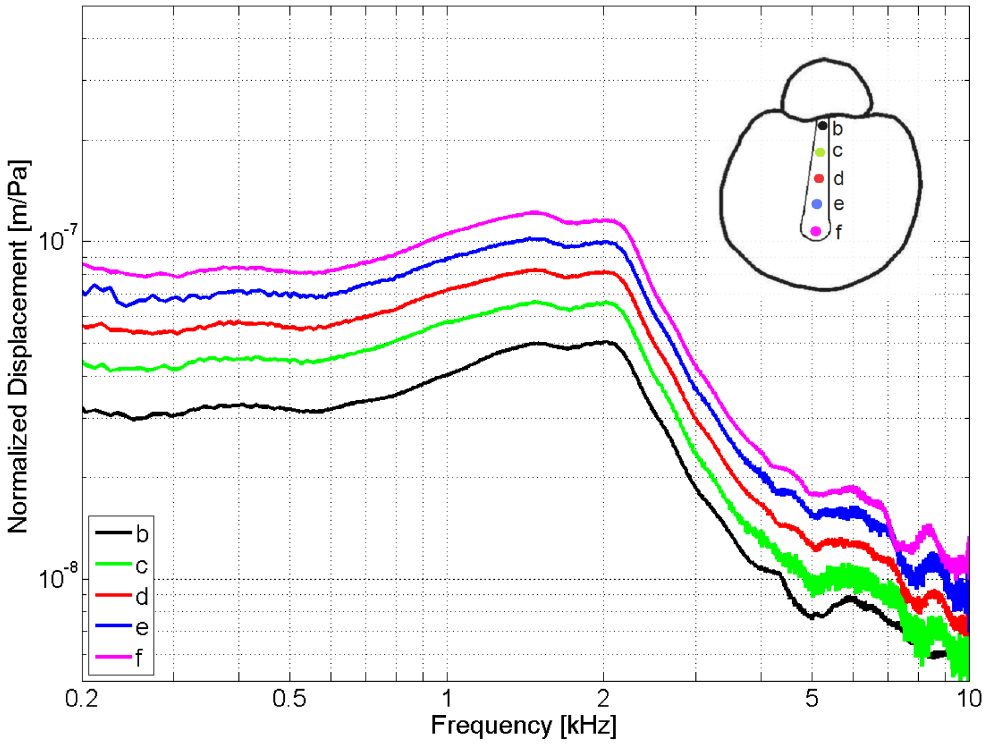

Figure 5.12: Normalized displacements of the manubrium measured in gerbil 7 (retracted PF, closed-sound-field experiment). Measurement points are shown in the top right TM figure.

Displacements of the umbo are about 2 to 3 times as large as those of the lateral process of the malleus. Displacement increments from point to point are more or less consistent

for frequencies up to about 7 kHz. In general, the frequency responses measured at each point along the manubrium follow almost the same pattern as those measured at the umbo, with a gradual magnitude decrease at points higher up on the manubrium, towards the lateral process of the malleus. These vibration patterns suggest that the manubrium rotates around an axis somewhat superior to the manubrium.

At higher frequencies, fairly small magnitude changes and frequency shifts were observed in the manubrium responses from round to round, as shown for four rounds for gerbil 7 in Figure 5.13. This is true for all gerbils except gerbil 8 which shows pronounced *post-mortem* temporal effects, consistent with our observations on temporal effects of the umbo response (already discussed in Section 5.1.2).

Frequency shifts and inconsistent magnitude increments are especially seen in the umbo response. Besides experimental errors, possible explanations for this observation may be a shift in rotational axis or manubrial bending at high frequencies, which have also been suggested in some previous experimental (Decraemer & Khanna, 1994; de La Rochefoucauld & Olson, 2010) and numerical (Funnell et al., 1992) studies (as discussed in Section 3.1.2). However, the data obtained in this study are not repeatable enough to permit such conclusions; measurements from different angles to reconstruct the three-dimensional motion of the manubrium, as well as phase data, are required in order to clarify this point.

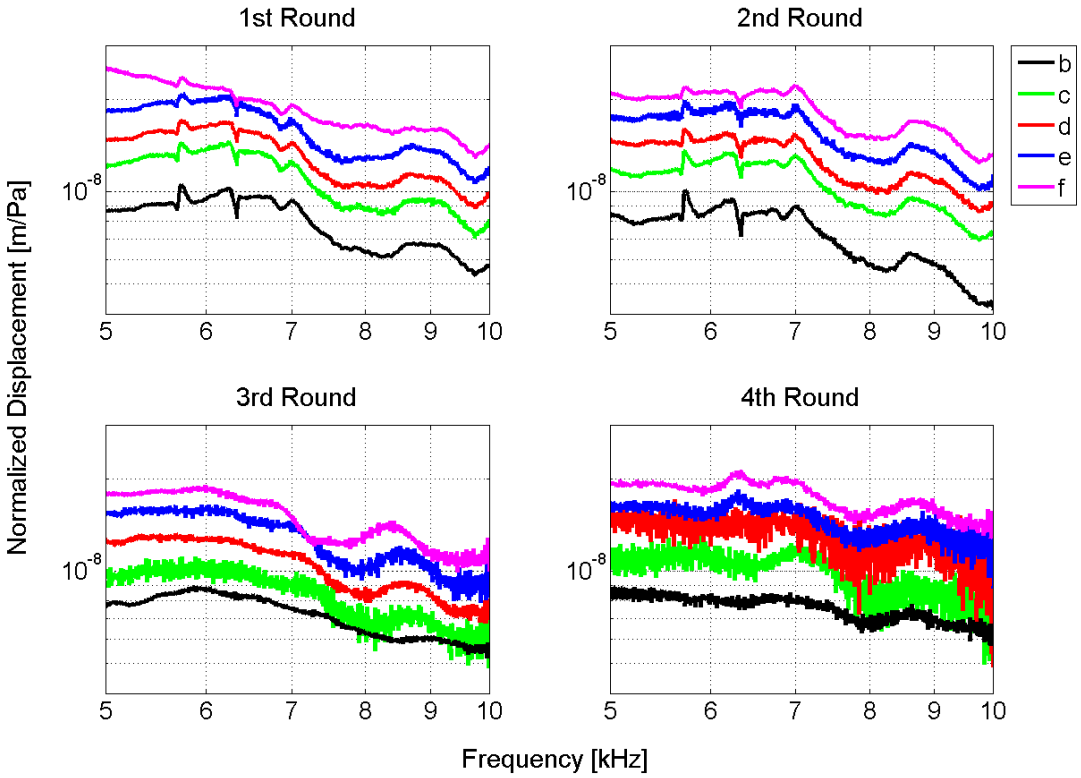

Figure 5.13: High-frequency manubrial displacements of gerbil 7 measured in four consecutive rounds (each round takes approximately 35 min).

5.4 Pars-tensa vibrations

The measurement points in the posterior, anterior and inferior regions of the PT for three gerbils are shown in Figure 5.14. Apart from the effects of PF state and skull vibrations, the PT responses obtained in this study reveal similar characteristics among all gerbils, except for gerbil 8 due to its *post mortem* effects. Hence, gerbil 7 is chosen to illustrate the typical PT behaviour observed in this study.

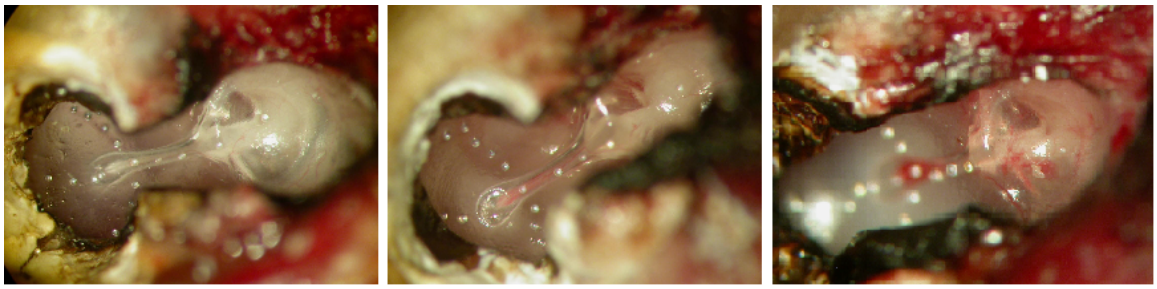

Figure 5.14: Photos of the gerbil TM showing the measurement points on the PT.

5.4.1 Overview of pars-tensa vibrations

Normalized displacements measured at multiple points in the anterior, posterior and inferior regions of the PT of gerbil 7 are shown in Figure 5.15. A schematic drawing is also included in the figure to illustrate the locations of the measurement points.

Below 2 kHz, the PT vibration patterns in all three regions have similar shapes, with the highest displacement magnitude being in the posterior PT (point *i*). In each region, the displacements gradually increase from the point closest to the manubrium (points *o*, *g* and *k*) to roughly halfway to the annulus (points *r*, *i* & *m*). Above 2 kHz, the PT vibration patterns in all three regions become very complex. In each region, displacements vary greatly from bead to bead and oscillate dramatically with frequency, indicating that the PT responses are spatially complex and highly frequency dependent. These observations are consistent with a description suggested by others (discussed in Section 3.2.2) that the PT generally undergoes simple in-and-out motions in phase with the manubrium at low

frequencies, but that the high-frequency behaviour is dominated by more complex, frequency- and location-dependent wave-like motions.

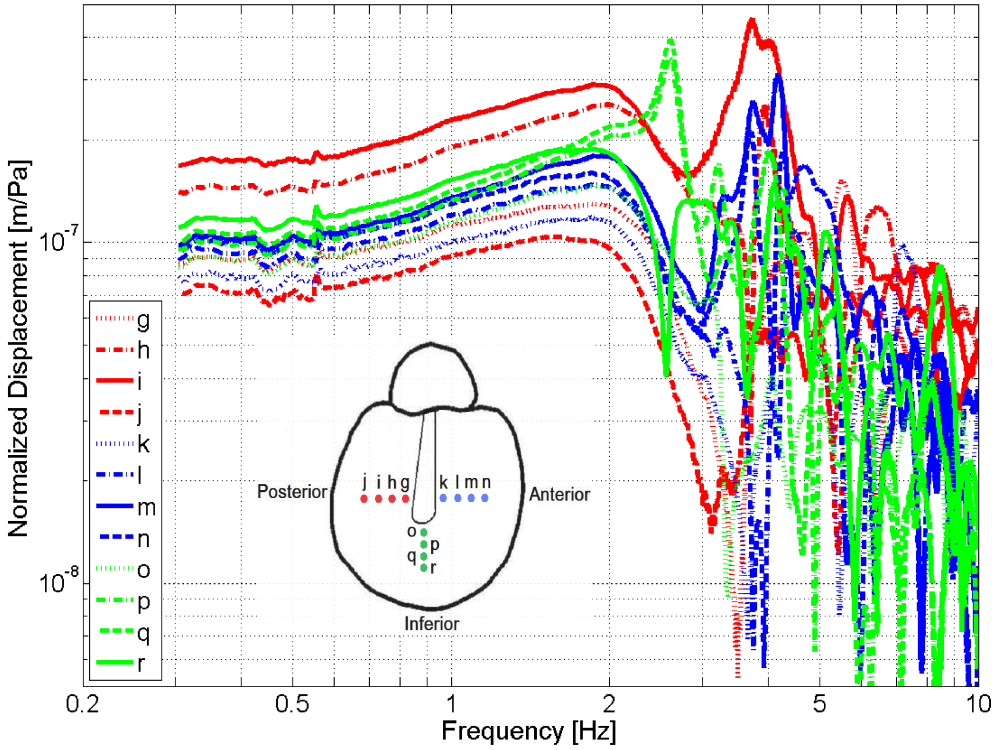

Figure 5.15: Normalized displacements measured at multiple points on the PT of gerbil 7; the responses of anterior, posterior and inferior PT are in blue, red and green respectively, as indicated in the TM figure. Solid line is used for location with largest low-frequency displacement in each region.

5.4.2 Pars-tensa vibrations in different regions

In this section, the low-frequency displacement amplitudes along the rows of micro-beads in the different regions of the TM are presented. The displacements at 1 kHz measured in all gerbils are presented in two figures: Figure 5.16 shows the TM displacements on a line along the manubrium (points *b*, *c*, *d*, *e*, *f*) and in the inferior region of the PT (points *o*, *p*, *q*, *r*), and Figure 5.17 shows the displacements along a line perpendicular to the manubrium, crossing at point *e* (about one quarter of the way up the manubrium), and

extending to the anterior (points *k*, *l*, *m*, *n*) and posterior (points *g*, *h*, *i*, *j*) regions of the PT. These figures provide an overall comparison of the PT responses in different regions.

In Figure 5.16, the manubrial displacements increase almost linearly in all gerbils from the lateral process of the manubrium (point *b*) to the umbo (point *f*), consistent with rotation of the manubrium as a rigid body around an axis superior to the lateral process of the manubrium, as discussed above in Section 5.3. Except in gerbil 4, TM displacements in the inferior region continue to increase from the umbo to approximately the centre of the inferior PT (point *r*). In gerbil 4, the PT displacements are roughly the same as those at the umbo. In gerbil 3, there was an extra measurement point *s* closer to the annulus and the displacement there was less than at point *r*, indicating that the displacement maximum in the inferior region is located around point *r*.

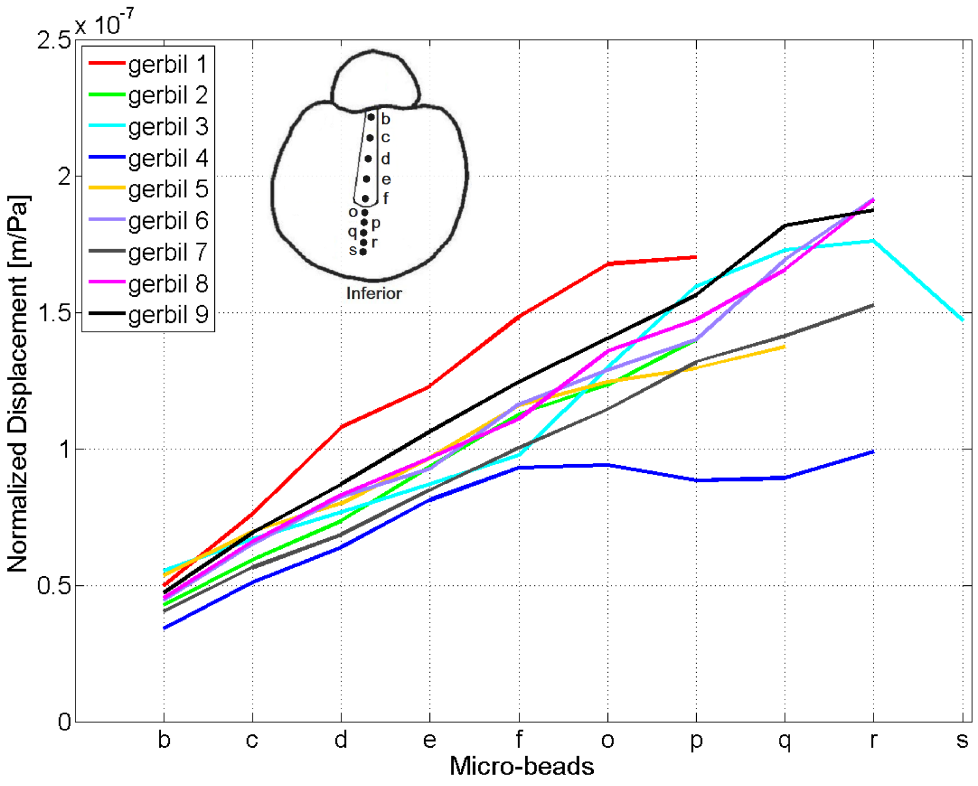

Figure 5.16: Vibration patterns of the TM at 1 kHz measured along the line of the manubrium and in the inferior region of PT in nine gerbils. Approximate locations of the micro-beads are indicated in the TM figure.

In Figure 5.17, for all gerbils the displacements are lowest at the manubrium (point *e*), then gradually increase towards the annulus and reach maximum values at approximately midway between manubrium and annulus (point *m* in the anterior PT; point *i* in the posterior PT). The PT displacements in gerbil 4 are lower than in the other gerbils, as also seen for the inferior region in Figure 5.16. In most cases the displacements drop at the measurement points furthest away from the manubrium (point *n* in the anterior PT; point *j* in the posterior PT), indicating that the exposure of the TM in this study is wide enough that the approximate locations of the displacement maxima in both anterior and posterior regions can be determined. For each gerbil, the value of the maximum displacement in the posterior region is significantly higher than those in the anterior and inferior regions, which are more or less the same.

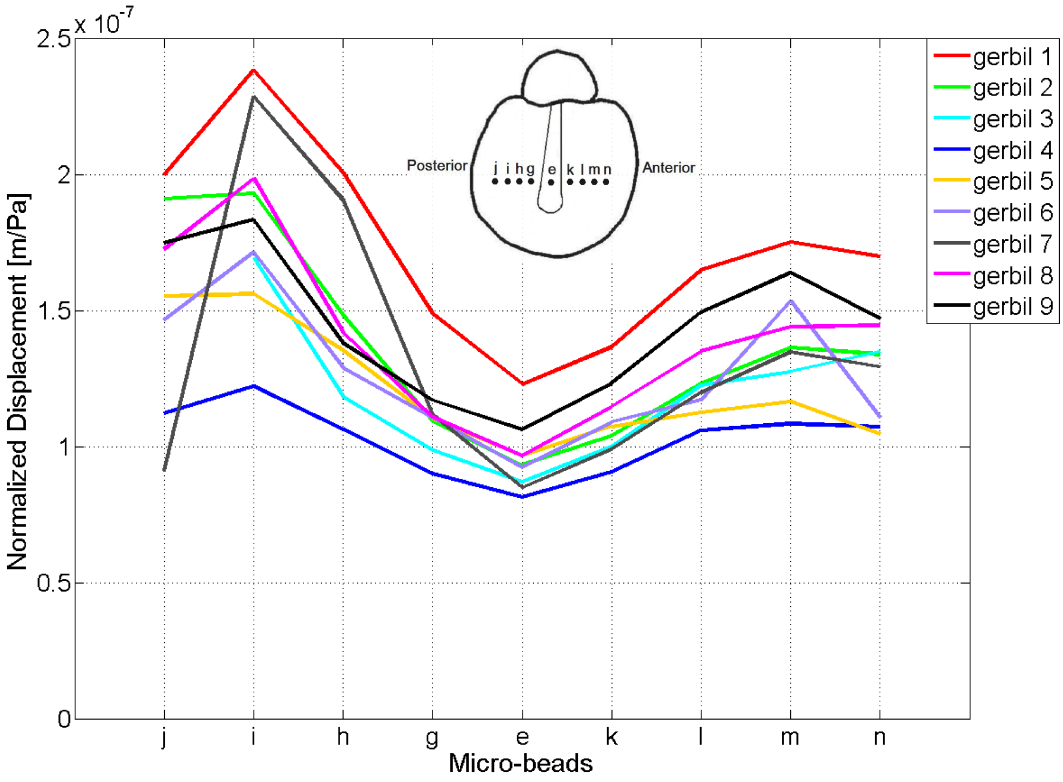

Figure 5.17: Vibration patterns of the TM at 1 kHz measured along lines in the anterior and posterior regions of the PT in nine gerbils. Approximate locations of the micro-beads are indicated in the TM figure.

5.4.3 Temporal effects on pars-tensa vibrations

The PT is such a delicate physiological structure that its responses might be highly sensitive to any dehydration of the membrane during experiments, especially in the case of a wide exposure of the TM. Possible factors accelerating the dehydration of the TM surface in this study might be: the complete removal of the external ear canal, which normally provides a relatively humid environment lateral to the TM and reduces the air flow across the TM surface; the heat from the microscope light shining directly on the widely exposed TM; and the relatively low ambient humidity, since no humidifier was used.

In all gerbils, similar temporal effects on the PT were observed at low and mid frequencies, except for gerbil 8 as its responses were further complicated by *post mortem* effects as discussed earlier. Moreover, no substantial difference was observed between the temporal effects of open-sound-field and closed-sound-field measurements. Therefore, results for one measurement point from gerbil 5 at different measurement times over 270 min are shown as typical observations in Figures 5.18. Point *m* is chosen as it represents the low and mid-frequency displacement maximum in the anterior region of the PT. As shown in this figure, the temporal effects are small below 3 kHz (ignoring the noise effects), with the overall magnitude dropping by less than 3 dB with time. This is comparable to the temporal effects observed in the umbo response discussed in Section 5.1.2, and indicates that the PT response is relatively stable at low and mid frequencies. Above 3 kHz, significant temporal effects can be seen in all gerbils, as the fine structures of the PT responses change dramatically with time. The details of the high-frequency temporal effects vary among gerbils, but a few common characteristics can still be seen in Figure 5.18:

- In some gerbils there is a greater drop in the high-frequency displacement magnitudes, especially when comparing the values of resonance peaks in the last round of measurement with those in the first round.

- The responses shift towards higher frequencies, with the individual peaks not all shifting by the same amounts, resulting in changes in the shapes of the frequency-response curves. For example, in gerbil 5 the resonance peak at around 3.3 kHz in round 1 shifts to around 4.2 kHz in round 5, whereas the peak at around 5.5 kHz in round 1 shifts only to around 5.8 kHz in round 5.

- There seem to be some smoothing effects at some frequencies, as some small resonance structures become weaker or indistinguishable. For example, in gerbil 5 there is a small peak at about 2.8 kHz in the first two rounds of measurements but it disappears in later measurements.

Although the temporal effects are very noticeable in the PT responses at high frequencies, they do not significantly affect the manubrium response, as discussed in Section 5.3.

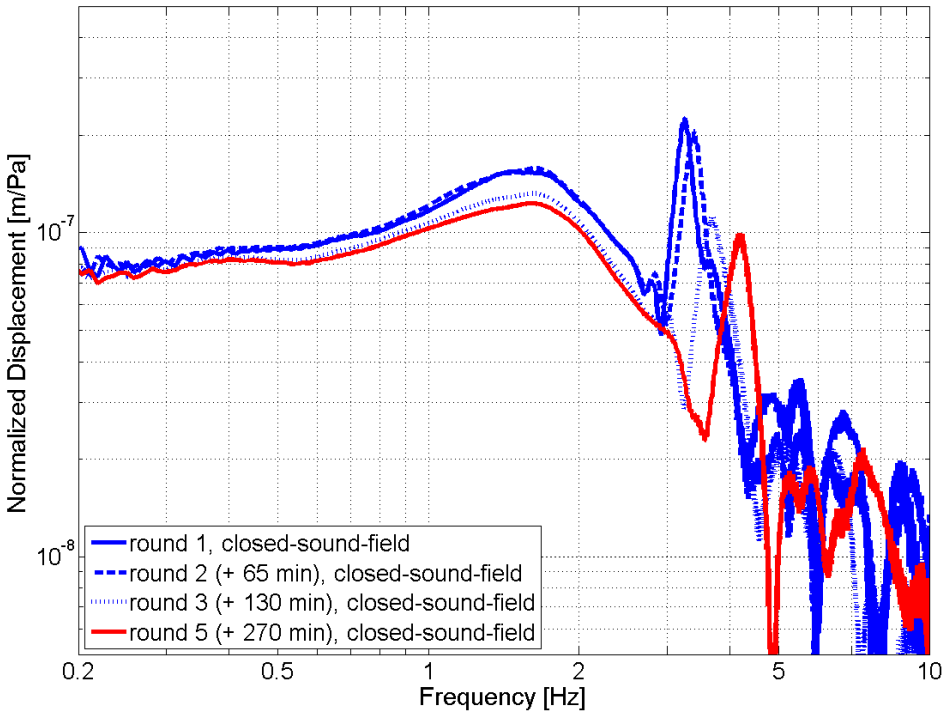

Figure 5.18: Long-term intra-specimen variability of the anterior PT response at point m in gerbil 5. All measurements were taken in closed sound field, with the red curve indicating the last measurement.

5.5 Summary

For the PF response, a resonance at about 600 Hz can be seen in the case of a flat PF, but such a resonance is absent in the case of a retracted PF. Above 800 Hz, no substantial difference can be seen between the responses of flat and retracted PF's. The results with retracted PF's show relatively large variability, presumably due to differences in the nature of the retraction and adhesion. Moreover, the PF responses generally reveal pronounced temporal effects, but the corresponding umbo responses are not affected except where the PF resonance occurs.

In the case of a flat PF, the umbo response shows a minimum followed by a sharp rise at the frequency where the PF resonance occurs. In the case of a retracted PF, the umbo response was relatively flat at low frequencies, resembling umbo responses with immobilized PF's as measured by other researchers. Above 800 Hz, the umbo responses are not affected by the state of the PF. Opening the MEC with a small hole (~1 mm in diameter) increases the umbo displacements below about 1.5 kHz and introduces a sharp minimum at about 2 kHz. Increasing the size of the MEC opening shifts this minimum to higher frequencies. The umbo displacements at frequencies below this minimum reach a plateau at the smallest size of MEC opening. In general, the umbo responses are similar to those seen in previous studies, suggesting a similar degree of reliability and consistency for our measurements in other parts of the TM. Furthermore, the long-term variability of the umbo responses are comparable to the short-term variability reported in the previous *post mortem* study in our lab, indicating the improved consistency of *in vivo* measurements.

The displacements measured along the manubrium follow a consistent pattern, with decreasing magnitude from the umbo to the lateral process of the malleus, suggesting that the manubrium rotates around an axis superior to the manubrium. Slight magnitude variations and frequency shifts are seen at high frequencies in some gerbils, possibly due to the changes in rotational axis and bending of the manubrium tip that have already been

suggested for other species.

The PT responses at low and mid frequencies generally follow the same pattern (with greater magnitudes) as those of the umbo and manubrium. The maximum low- and mid-frequency displacements are found at approximately the centre of the posterior PT. At about 2 kHz, the PT response breaks up into a series of resonances at different frequencies and also varies greatly from bead to bead. Temporal effects of the PT response are small at low and mid frequencies, then become more pronounced at high frequencies. Nevertheless, the pronounced temporal effects in the high-frequency PT response do not influence the behaviour of the umbo and the manubrium.

Chapter 6
Modelling Results

In order to address issues that are difficult to evaluate experimentally, this chapter discusses the results obtained from numerical simulations using a finite-element model being developed in our lab. The MEC and the stapes are currently not included in our model and the incudo-mallear joint is modelled as being rigid. In this study, the model is only used to address issues that are not sensitive to those missing features. In particular, we explore the effects of various measurement angles in Section 6.1, and the effects of the mass of the micro-beads in Section 6.2. Compared with the experimental results in Chapter 5, the model frequency responses exhibit less damping at around 2 to 3 kHz but more damping at higher frequencies. Further work is required on setting appropriate damping parameters, but this does not affect the issues considered here.

6.1 Measurement angle

In previous studies (Rosowski et al., 1997; Rosowski & Lee, 2002; Nambiar, 2009), the angle between the laser beam and the plane of the annulus was around 45º to 60º. In this study, since the TM was widely exposed by removing a portion of the bulla lateral to the TM, the laser beam could be more perpendicular to the plane of the annulus, as illustrated in Figure 6.1. The effects of various measurement angles are explored using our finite-element model.

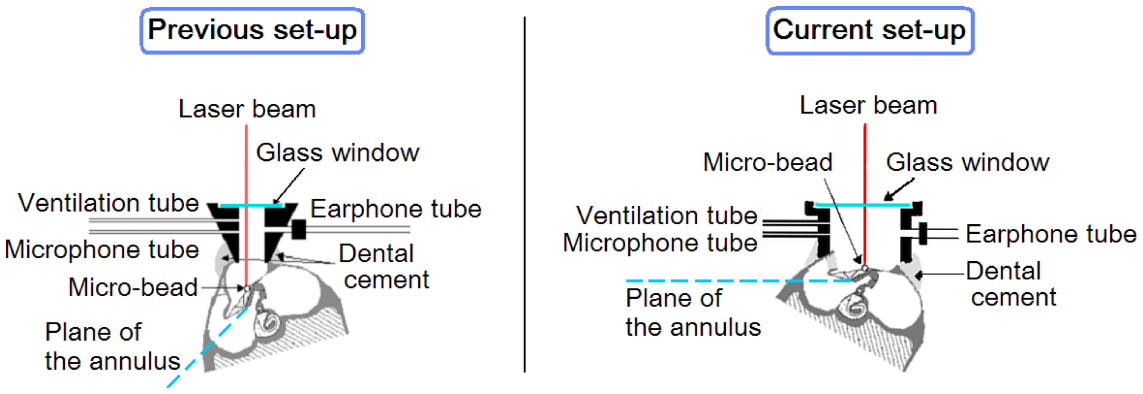

Figure 6.1: Schematic illustration of the previous set-up (left) and the currents set-up (right) in which the TM is widely exposed. The angle between the laser beam (red line) and the plane of the annulus (blue dashed line) was about 45° in the previous experiment and about 90° in the current experiment.

Simulations with measurement angles of 0º, 30º, 45º, 60º, 90º, 120º, 135º, 150º and 180º were performed and the responses are shown for four locations: at the umbo, and at the centres of the posterior, anterior and inferior regions of the PT. Results for the umbo are shown in Figure 6.2; Figures 6.3 to 6.5 present the results for the posterior, anterior and inferior PT respectively.

For each location, the response for most or all frequencies is maximal at the 90º measurement angle, then generally decreases with decreasing or increasing angle and usually reaches a minimum at 0º and 180º (which are equivalent in terms of magnitude). This indicates that the movements of the TM at these locations are mainly perpendicular to the plane of the annulus. Specifically, changing the angle from 45º to 90º (or from 135º to 90º) results in an overall magnitude increase of about 2 to 6 dB for most frequencies. This agrees with the magnitude differences between our experimental results and previous ones, as discussed in Chapter 5.

All the response curves (except those at 0º and 180º) are very similar in shape below about 1.5 kHz, consistent with a simple mode of vibration across the whole TM at low frequencies. The shapes of the response curves change slightly with the measurement

angle above 1.5 kHz and more so above 3 kHz, suggesting that the modes of TM vibration become more complex at high frequencies and increasingly involve some displacements parallel to the plane of the annulus. Moreover, these shape changes occur at different frequencies depending on the location on the TM, confirming that the high-frequency TM response is both frequency- and location-dependent.

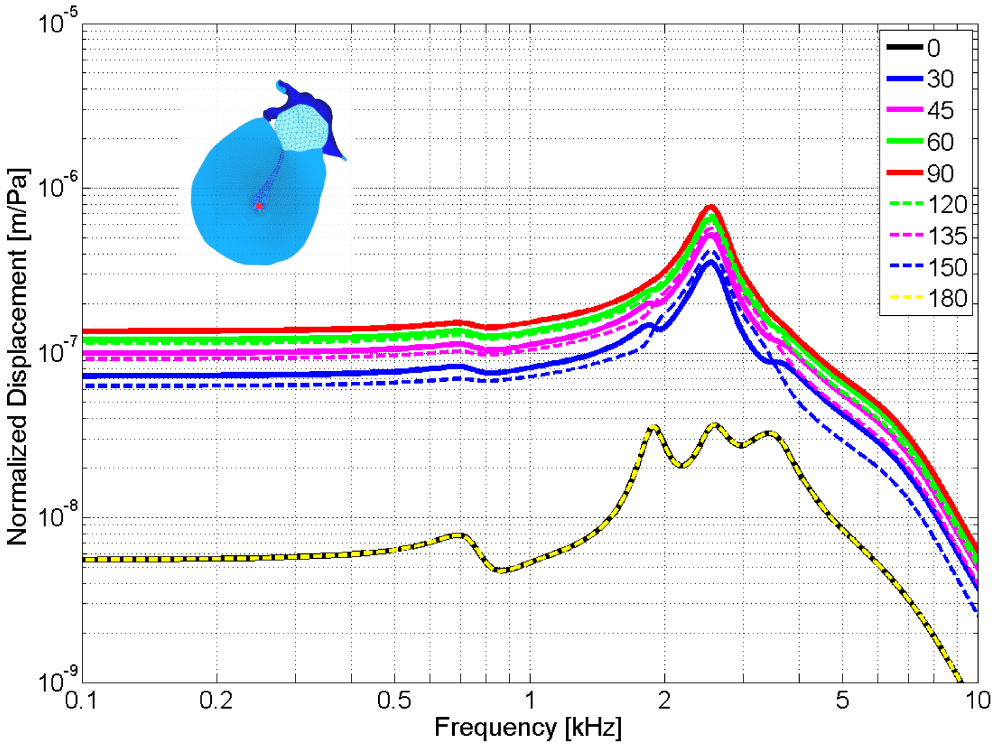

Figure 6.2: Simulated normalized displacements at the umbo (red dot in the TM figure) with different measurement angles between the laser beam and the plane of the annulus. Measurement angle varies from 0° to 180°.

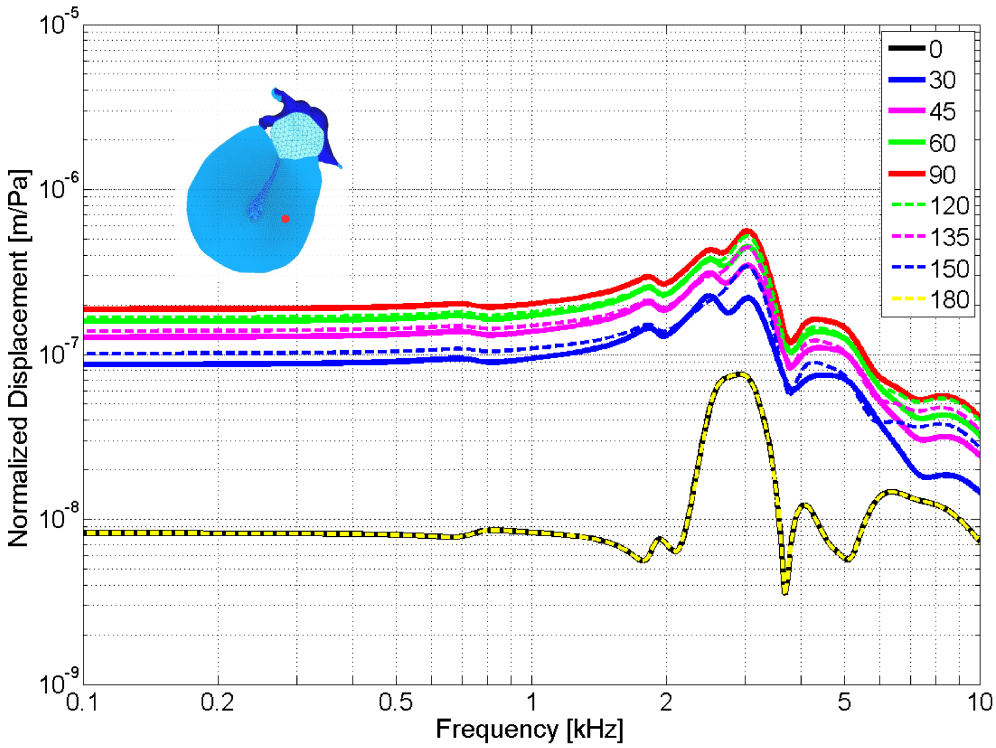

Figure 6.3: Simulated normalized displacements at the centre of the posterior PT (red dot in the TM figure) with different measurement angles between the laser beam and the umbo plane. Measurement angle varies from 0° to 180°.

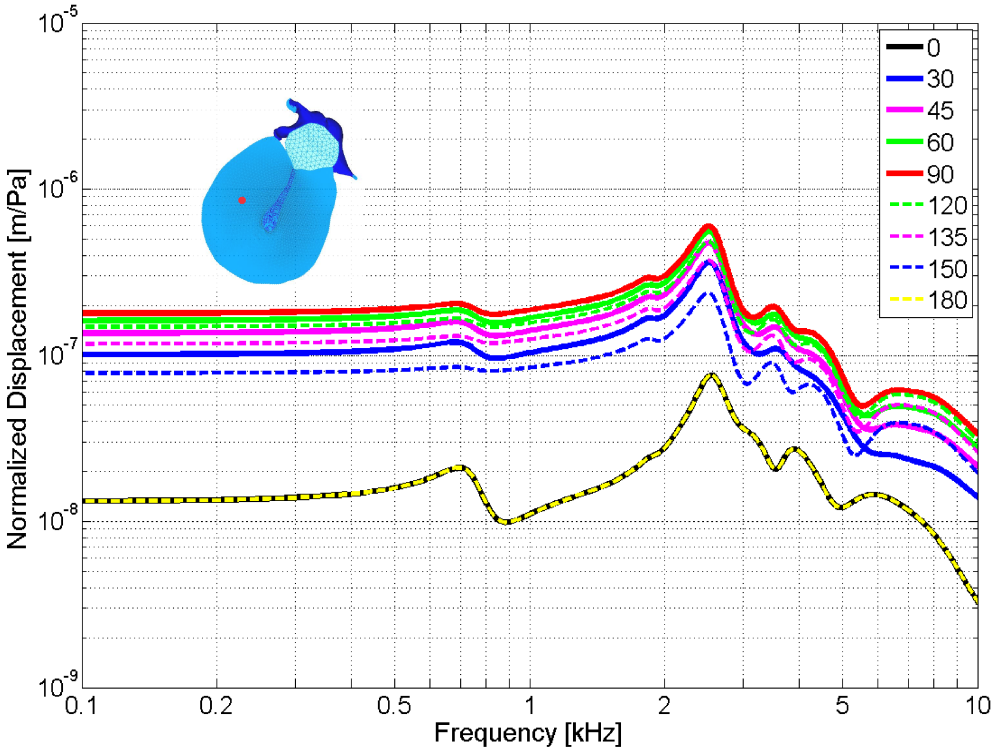

Figure 6.4: Simulated normalized displacements at the centre of the anterior PT (red dot in the TM figure) with different measurement angles between the laser beam and the umbo plane. Measurement angle varies from 0° to 180°.

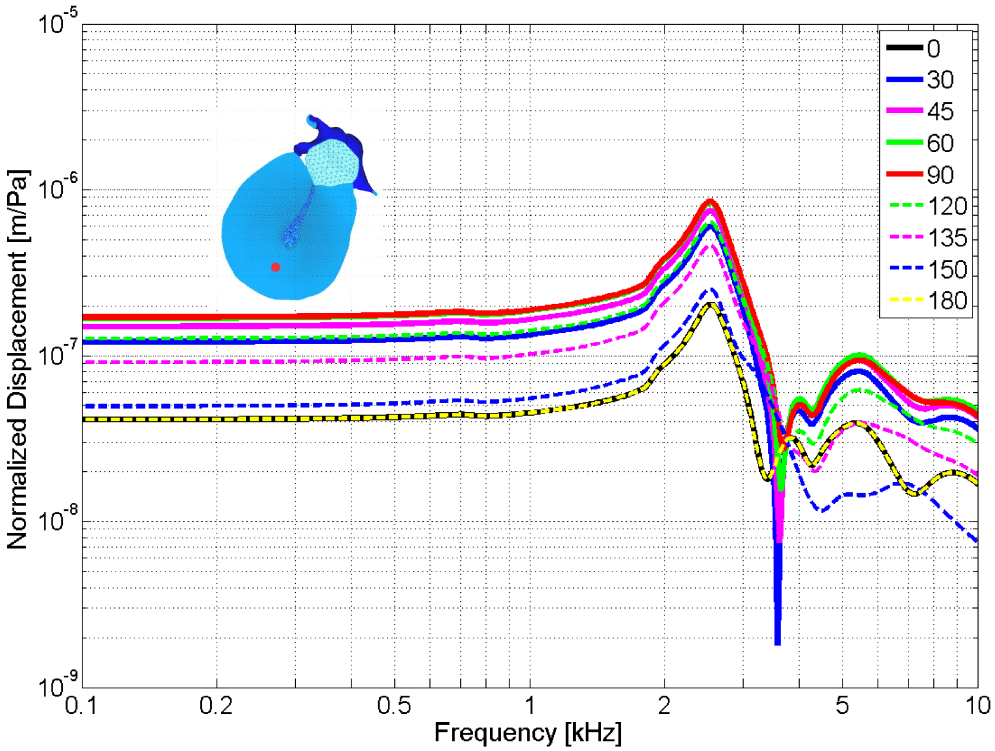

Figure 6.5: Simulated normalized displacements at the centre of the inferior PT (red dot in the TM figure) with different measurement angles between the laser beam and the umbo plane. Measurement angle varies from 0º to 180º.

The shape variations in the PT responses (Figures 6.3 to 6.5) are greater than those in the umbo responses (Figure 6.2). The magnitude difference between the maximum (90º) and minimum (0º and 180º) responses are considerably smaller in the inferior PT (as shown in Figure 6.5) than in the anterior and posterior regions, indicating that the TM movements inferior to the umbo are relatively large in directions parallel to the plane of the annulus. This is presumably due to the orientation between the annulus plane and the TM surface in this region, with the assumption that the maximum TM movements are perpendicular to the membrane surface.

6.2 Mass of micro-bead

The effects of the micro-beads are difficult to verify experimentally and have not been explicitly evaluated, so here we present a preliminary study of those effects using our finite-element model. Simulations are presented for cases where only one bead is present, modelled as a point mass either on the umbo or at the centre of the posterior PT (analogous to the points *f* and *i* in our experiments). Each glass-coated plastic micro-bead used in our experiments is estimated to have a mass of about 1 μg, as discussed in Section 4.1. Therefore, the mass of each simulated bead is varied from 0 to 10 μg, with zero mass representing the initial situation with no bead and the 10 μg mass being equivalent to having about ten beads at the same location. The bead mass is gradually increased by 1 μg (equivalent to the mass of one bead) at a time. Regardless of the bead location, responses at both the umbo and the centre of the posterior PT are computed in each simulation for comparison.

Figure 6.6 demonstrates the effects when a micro-bead is placed at the umbo, with the umbo responses plotted in magenta (0 bead mass) and blue curves and the PT responses in green (0 bead mass) and red curves. Both PT and umbo responses appear unchanged as the bead mass increases, implying that the micro-bead will not affect the TM responses if it is placed at the umbo, that is, at the inferior tip of the manubrium. Evidently the bead mass is negligible compared with that of the manubrium. This result also suggests that placing multiple micro-beads along the manubrium will not affect the TM response, given the fact that the manubrium is thinnest at its inferior tip.

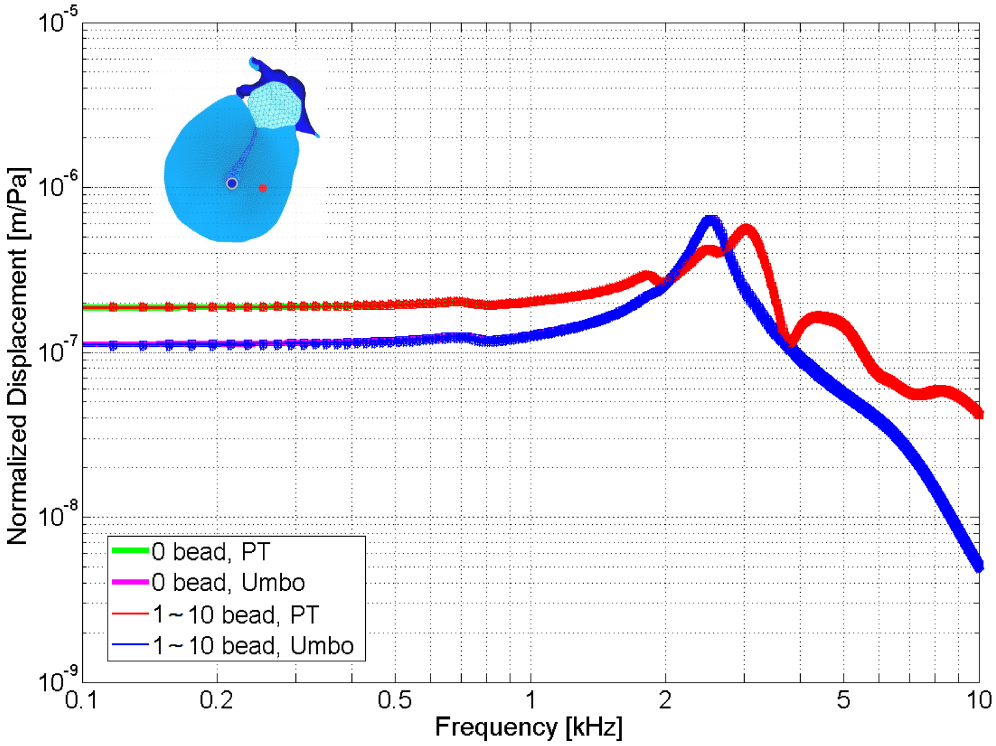

Figure 6.6: Simulated normalized displacements at the umbo (magenta and blue curves) and the centre of the posterior PT (green and red curves), with zero to ten micro-beads placed at the umbo (different markers representing different number of micro-beads). The curves for 1 to 10 beads are almost indistinguishable. The umbo (blue dot) and PT (red dot) locations are indicated in the TM figure.

Similar simulations with a micro-bead placed at the centre of the posterior PT were performed and the results are shown in Figure 6.7. As the bead mass increases from 0 to 10 μg, the umbo responses are almost identical but the PT responses change dramatically. This is presumably because the local mass of the PT at this location is small compared with the mass of the micro-bead. This location is the thinnest part of the posterior PT, approximately in the middle between its boundaries (annulus and manubrium), making it one of the most likely regions of the TM to be affected by the micro-beads. Comparing the PT responses, one can observe that the low-frequency response remains unchanged, but there is a resonance that shifts to lower frequencies and the magnitudes of the high-frequency response gradually decrease as the bead mass increases; this is expected when a

mass is added to a mass-spring system. Furthermore, the resonance peak originally located at 3 kHz (with zero bead mass) shifts towards lower frequencies with increasing bead mass, suggesting that a new resonance at about 3 kHz is added to the PT response due to the addition of a bead at this particular location on the TM. In this particular case, placing one bead on the PT results in the intriguing fact that the PT resonance peak shifts to about the same frequency where the umbo peak occurs; superposition of these peaks therefore gives rise to a strong resonance at that frequency (~2.6 kHz). In spite of the significant variations in the PT responses, however, the umbo remains unaffected. The local effects on the PT are still not large enough to induce corresponding effects on the umbo and the ossicular chain.

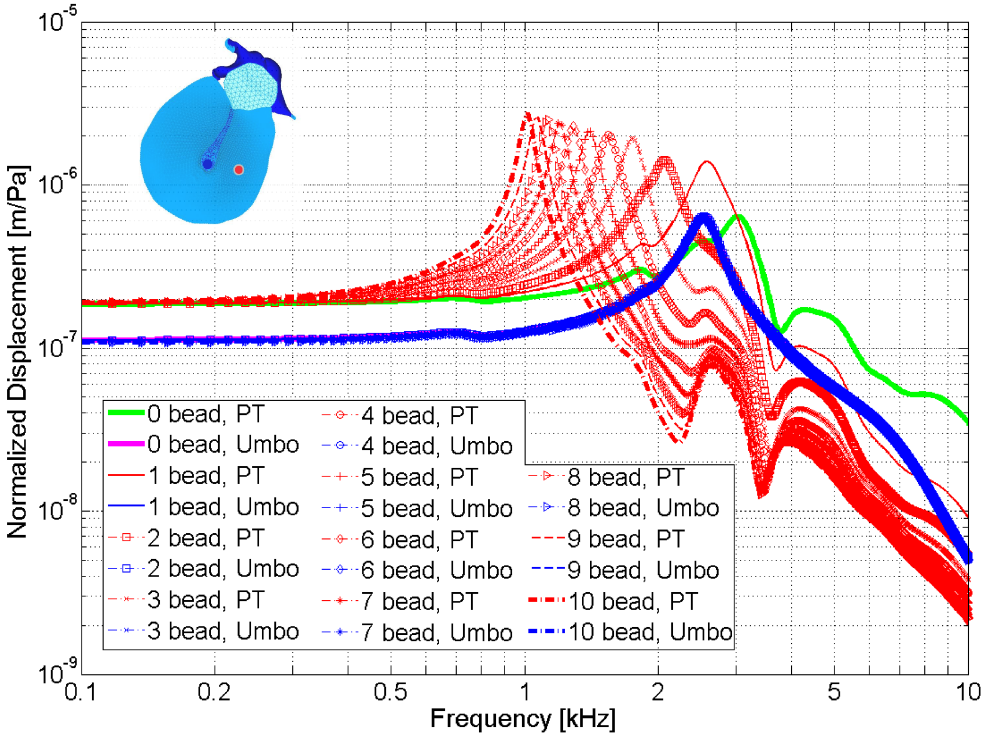

Figure 6.7: Simulated normalized displacements at the umbo (magenta and blue curves) and the centre of the posterior PT (green and red curves), with zero to ten micro-beads placed on the PT. The umbo (blue dot) and PT (red dot) locations are indicated in the TM figure.

Figure 6.8 illustrates the effects of adding mass in more detail. The responses of the PT are shown when a small mass is placed on it; the mass is varied from 0 to 1 μg, simulating the gradual changes in PT responses from no bead to one bead. The 3 kHz resonance peak (with zero bead mass) shifts leftwards with gradually increasing peak values, while other features (the small peak at 1.8 kHz, the dip at 3.6 kHz and the broad peak at 4 to 5 kHz) do not shift at all. The magnitudes at higher frequencies decrease as the bead mass increases. The fact that even an extremely small bead of 0.1 μg mass can lead to a noticeable change in the PT response further confirms the sensitivity of the PT to anything on its surface. In conclusion, the use of micro-beads imposes some effects on the PT responses, but these effects are relatively local and do not influence the behaviour of the umbo and the ossicular chain.

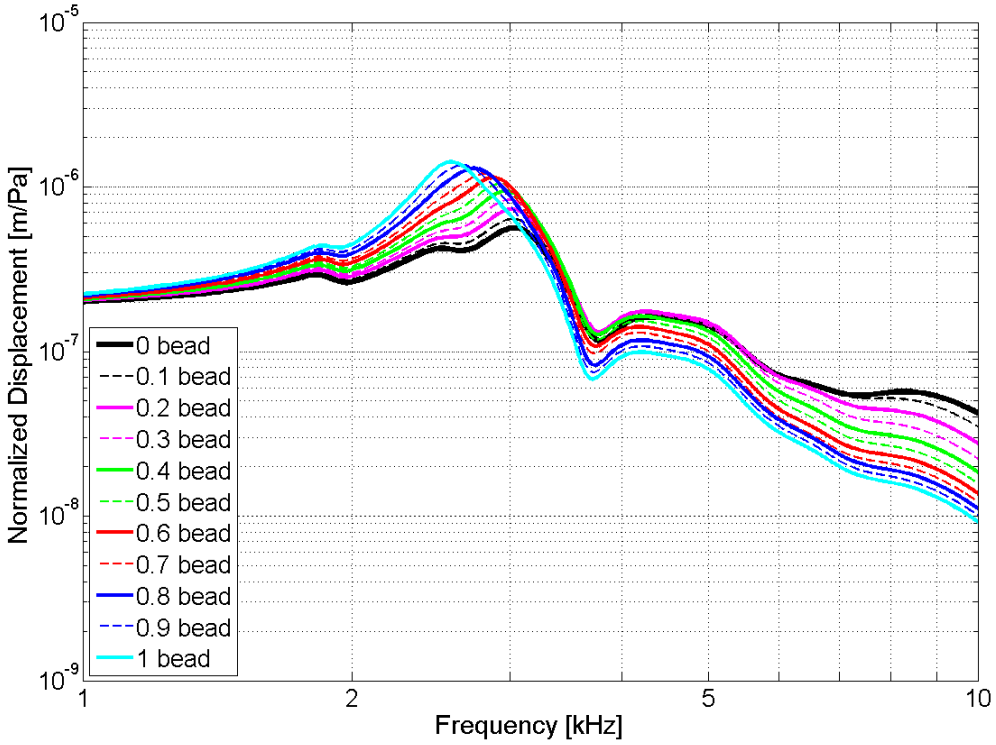

Figure 6.8: Simulated normalized displacements at the centre of the posterior PT, with fractional micro-beads placed on it.

Chapter 7
Conclusion

This thesis contributes to a better understanding of middle-ear mechanics by presenting *in vivo* measurements at multiple points over a widely exposed TM. TM vibration patterns have been measured in nine gerbils over a frequency range of 0.1 to 10 kHz. Inter-specimen variability and intra-specimen temporal effects have been studied. Our results are in general agreement with measurements at the umbo from two previous *in vivo* gerbil studies (Rosowski et al., 1997; Rosowski & Lee, 2002) and with measurements over a more restricted part of the TM from previous studies from our lab (Nambiar, 2009; Maftoon et al., 2011). Furthermore, the effects of different measurement angles and of micro-beads have been evaluated using a finite-element model.

The central contributions of this work are the development of a technique for wide exposure of the gerbil TM, and the TM vibration measurements that the wide exposure makes possible. Those results are summarized in Section 7.1, and other results are summarized in Sections 7.2 to 7.7. Potential future developments are proposed in Section 7.8.

7.1 *In vivo* measurements in a widely exposed tympanic membrane

The wide exposure of the TM has allowed us to obtain measurements at or near the local displacement maxima which are located roughly at the centres of the anterior, posterior and inferior regions of the PT, somewhat closer to the manubrium than to the annulus. Among those response maxima, the largest displacement magnitudes were found in the posterior PT. At high frequencies (> 2 kHz), the PT vibrations break into sectional modes and vary dramatically with frequency, indicating the location- and frequency-dependent behaviour of the PT at high frequencies.

The greater response in the posterior PT may be related to the fact that the PT is slightly thinner in this region than in other regions (Kuypers et al., 2005; Funnell & Decraemer, 2008), though the response also depends on other factors such as curvature and material properties.

In general, the PT appears to undergo in-and-out motions in phase with the manubrium at low frequencies, with some wave-like motions superimposed at high frequencies. How such TM surface waves contribute to high-frequency hearing remains unclear. It has been speculated that wave propagation from the periphery to the centre results in a middle-ear transmission delay (Puria & Allen, 1998; de La Rochefoucauld & Olson, 2010). Presumably the fine resonance structures of the high-frequency PT response reflect the interactions of multiple damped vibrational modes which are closely related to the boundary conditions and the inhomogeneous structural properties of the TM, such as the thickness, stiffness and density of the circular and radial fibres of the TM.

7.2 Flat vs. retracted pars flaccida

In this study, the PF's were flat in two gerbils, and were retracted (bulging inward) in the other gerbils when the measurements were made. Most of the retracted PF's were observed to be initially flat, before the surgery. Therefore, a possible explanation of the PF retraction might be a change in the middle-ear gas composition and the accumulation of negative middle-ear pressure during the surgical preparation before venting of the cavity, which eventually brought the PF in contact with the malleus head. Such contact might also persist after venting the cavity due to the surface tension of the middle-ear mucosal lining. Contact with the malleus as a result of negative middle-ear pressure accumulation was also reported by Rosowski and Lee (2002) while varying the pressure gradient across the TM.

In the cases with retracted PF's, the effects of the PF resonance (around 600 Hz) were absent in both PF and umbo responses, resulting in relatively flat displacement curves at low frequencies. Moreover, the decrease in PF displacement magnitudes at low frequencies corresponded to a slight increase in the umbo response, consistent with the suggestion of an acoustic shunting function of the PF at low frequencies by Rosowski and Lee (2002). At higher frequencies (above 800 Hz), the manubrial and PT responses were unaffected by the PF state. Our observations regarding the retracted PF agree with the findings reported in some previous studies (Rosowski et al., 1997; Teoh et al., 1997; Rosowski & Lee, 2002) in which the PF was experimentally stiffened. It therefore appears that a retracted PF results in effects similar to those of a stiffened PF.

7.3 Umbo and manubrium response

Consistent with earlier findings, the shapes of our umbo and manubrial response curves are roughly flat below 600 Hz and drop with a slope of about 12 dB/octave above 2 to 3 kHz, confirming that the middle-ear is stiffness-dominated at low frequencies and becomes more affected by mass at high frequencies. The overall increase of 2 to 4 dB in our response magnitudes compared with the results from other studies might be attributed to the different measurement angle in this study because the laser beam was almost perpendicular to the annulus plane, due to our wide exposure of the TM.

7.4 Role of middle-ear cavity

TM responses measured in both closed and open MEC configurations help to better understand the role of the MEC. Results obtained in the open MEC configuration will be particularly useful for future validation of our finite-element model, which does not contain a MEC; in other words, the model has an infinitely large effective MEC volume. As has been observed before, an opening in the MEC increased the magnitude of the TM responses at low frequencies, and introduced an anti-resonance at about 2 kHz. Such an opening increases the effective volume of the MEC and reduces the corresponding loading of the TM. The effects of changing the size of the MEC opening were investigated. The opening size had little effect on the TM response at low frequencies, but larger openings shifted the 2-kHz anti-resonance to higher frequencies. This is consistent with an interaction between the middle-ear air space and the acoustic effects of the opening.

7.5 Temporal effects

In most of our experiments, the temporal effects for measurements up to five hours were minimal with approximately ±1 dB variations. These long-term temporal effects are comparable to the short-term temporal effects reported in the earlier *post mortem* study in our lab by Nambiar (2009), demonstrating the improved consistency of *in vivo* measurements. However, slight frequency shifts and reduced displacement magnitudes were observed in the PT response, especially at high frequencies where the fine resonance structures were complex. Moreover, some of these high-frequency resonance peaks appeared to shift by different amounts, which might be attributed to spatially different drying effects resulting from the inhomogeneous material properties of the PT. Nevertheless, local variations of the PT response are spatially averaged at the manubrium and therefore do not affect the global response of the middle ear very much. In conclusion, *in vivo* measurements provide a good representation of the middle-ear response with fewer complications due to temporal effects, as the middle-ear components are well preserved. However, additional hydration of the membrane might help to further improve the quality of PT measurements.

7.6 Measurements in open and closed sound fields

The TM vibrations in response to open- and closed-sound-field stimulation have been compared. Open-sound-field experiments allowed better access to the measurement points that were close to the annulus, but some contamination of the low-frequency signals was observed. Our results suggest that the main source of this signal contamination was greater bulla vibrations in the open sound field. These vibrations affected measurements below 300 Hz and at about 550 Hz. Apart from these frequencies, the TM responses appeared the same in both types of sound field.

Closed-sound-field experiments not only provided clearer input signals through confining the sound field to a small volume lateral to the TM, but also protected the TM from dust and unanticipated bleeding of the neighbouring soft tissues. However, the measurement view was obstructed by the coupler. Furthermore, it was almost impossible to access the TM during measurements since the coupler was tightly glued onto the bulla with dental cement.

The optimal experimental set-up may be to use a closed sound field with an improved coupler which would allow both a complete view of the TM and easy access to the TM.

7.7 Effects of micro-beads

The effects of placing a micro-bead on the TM, either at the center of the PT or at the umbo, have been evaluated using a finite-element model developed in our lab. When increasing the mass of the simulated micro-bead at the umbo, no change was observed in either umbo or PT responses, implying that placing multiple micro-beads along the manubrium would not affect the TM response.

On the other hand, placing a simulated micro-bead at the center of the PT introduced a resonance peak at around 2.5 kHz to the response at that location. Increasing the bead mass shifted this peak towards low frequencies and for a certain mass superimposed the peak on the original response, while the response at frequencies above this peak gradually decreased. Regardless of such dramatic changes observed in the PT response, the umbo response remained unaffected, indicating that the micro-bead effects in this case were relatively local and would not affect the behavior of the umbo, nor that of the ossicular chain as a whole.

These simulated results suggest that the use of micro-beads can affect PT vibration measurements. Besides using other alternatives such as silver powder or paint to enhance the signal reflectivity of the TM, one possible strategy might be to include the micro-beads in our numerical model when validating the model with our experimental results.

7.8 Future directions

Since the techniques for both *in vivo* measurements and wide exposure of the TM have been developed, a direct extension to this study would be to include **more measurement points on the PT and the PF** so as to provide a more complete characterization of the TM vibrations. Specifically, more and closer measurement points on the PT are required to reconstruct the pattern of the TM surface wave and to estimate the wave speed; these measurements along with numerical simulations of the surface wave would help to address the issues discussed in Section 7.1.1. Another important extension of this work would be to **incorporate pressure gradients** across the TM, which would provide valuable insights for interpreting tympanometry measurements and for characterizing the viscoelasticity of the TM.

As the high-frequency PT response varied significantly with time, more experiments are needed to evaluate the temporal effects in order to draw more reliable conclusions about the high-frequency PT response. Furthermore, the experimental procedures to widely expose the TM require a considerable amount of time during which the TM might have become dehydrated. It is therefore important to evaluate the temporal effects of the experimental preparation by somehow **measuring the initial response (prior to surgery) as a reference**.

This study brings up an interesting issue: the **retracted PF**. A more comprehensive review of middle-ear pressure regulation and gas exchange under long-term anesthesia might be helpful to understand the cause of this phenomenon. Developing experimental techniques to prevent PF retractions or to restore a flat PF would also be important for future *in vivo* measurements.

Further investigations of TM vibrations with various **sizes of the MEC opening**, including complete removal of the bulla, would address questions regarding the acoustic effects of the MEC air space when it is opened experimentally for various purposes.

Moreover, a better understanding of the MEC air space might also clarify the **effects of MEC volume change**. As a small portion of the bulla was removed in order to widely expose the TM in this study, it would be important to determine whether such a small volume reduction in the MEC will affect the TM responses.

As the evidence for manubrial bending presented in this study is inconclusive, it would be interesting to further study this issue, and also the question of shifts in the ossicular rotational axis, by performing **three-dimensional measurements on the manubrium vibrations** in gerbils. It would also be interesting to extend the three-dimensional measurements over the TM and the ossicles, which would help to broaden our knowledge of the sound transmission from the TM to the ossicles, as well as the nature of the apparent middle-ear delay that has been observed by some researchers.

It is generally assumed that the **effects of the deep anaesthesia** used in these kinds of experiments are small because (1) the sound-pressure levels are too low to stimulate the reflexes of the middle-ear muscles; and (2) the magnitudes of otoacoustic emissions from the cochlea are very small. It is also possible, however, that anaesthesia could affect any resting tension that might be exerted on the middle ear either by the smooth-muscle fibres found in the fibrocartilaginous ring surrounding the TM, or by the tensor tympani and stapedius muscles. Investigation of this possibility would require sensitive measurements of middle-ear function that could be carried out without anaesthesia.

Last but not least, in order to enhance the efficiency and quality of measurements in such studies, further improvements in some of our experimental methods and equipment would be desirable:

- A **newly designed coupler** which would provide a better view and could also be easily removed and replaced during measurements. This coupler would need to have a larger opening to allow an unobstructed view of the exposed TM. A thin metal plate with a large enough hole for the view of the TM could be glued to the

bulla, providing a well-defined surface to which the coupler could be screwed. Threads would be machined around the hole of this plate and at the bottom of the coupler so as to ensure tight coupling without using dental cement. With this coupler, the TM could be easily accessed during measurements for various purposes.

- A better **alternative to the micro-beads**. Whether a thin layer of silver powder or a special paint as used by some other groups, it must be verified and confirmed that it not only enhances the signal reflectivity but also preserves the natural behaviour of the TM.

- A method to **keep the PT better hydrated** throughout the experiment with a widely exposed TM. Possible re-moistening techniques include the spraying of saline solution over the surface of the TM and the use of an ultrasound humidifier placed close to the specimen. The effectiveness and drawbacks of these methods must be evaluated thoroughly.

- A **computer-controlled positioning system with fixed clamps for specimens**. Such a system might incorporate high-precision linear translation stages and goniometers, allowing five or six degrees of freedom in adjusting the specimen position. It would be extremely helpful for determining the exact locations of the measurement points, which are essential for a more systematic study of the PT vibration patterns. Furthermore, it would allow more measurements to be done faster as it would replace the manual adjustments of the laser beam that are required in our current positioning system.

References

Akache F (2005): *An experimental study of middle-ear vibration in rats.* Master's thesis, McGill University, Montréal.

Akache F, Funnell WRJ, & Daniel SJ (2007): An experimental study of tympanic membrane and manubrium vibrations in rats. *Audiology & Neuro-Otology* 12: 49–58.

Arechvo I, Lasurashvili N, Bornitz M, Kevanishvili Z, & Zahnert T (2009): Laser Doppler vibrometry of the middle ear in humans: derivation dependence, variability, and bilateral differences. *Medicina (Kaunas, Lithuania)* 45(11): 878–886.

ASHA (1994): Joint Committee on Infant Hearing (JCIH). *Position Statement* 36(12): 38–41.

Beer HJ, Bornitz M, Hardtke H, Schmidt R, Hofmann G, Vogel U, Zahnert T & Hüttenbrink KB (1999): Modelling of components of the human middle ear and simulation of their dynamic behaviour. *Audiology & Neuro-Otology* 4: 156–162.

Békésy G v (1949): The Structure of the Middle Ear and the Hearing of One's Own Voice by Bone Conduction. *The Journal of the Acoustical Society of America* 21: 217–232.

Békésy G v (1960): *Experiments in Hearing.* McGraw Hill, New York, 745 pp.

Bigelow DC, Swanson P B & Saunders JC (1996): The effect of tympanic membrane perforation size on umbo velocity in the rat. *The Laryngoscope* 106(1): 71–76.

Bigelow DC, Kay D & Saunders JC (1998): Effect of healed tympanic membrane perforations on umbo velocity in the rat. *The Annals of Otology, Rhinology, and Laryngology* 107: 928–934.

Bornitz M, Zahnert T, Hardtke H & Hüttenbrink K (1999): Identification of parameters for the middle ear model. *Audiology & Neuro-Otology* 4: 163–169.

Buunen TJF & Vlaming MSMG (1981): Laser–Doppler velocity meter applied to tympanic membrane vibrations in cat. *The Journal of the Acoustical Society of America* 69(3): 744–750.

Bylander AK, Ivarsson I, Tjernstrom O & Andreasson I (1985): Middle ear pressure variations during 24 hours in children. *The Annals of Otology, Rhinology, and Laryngology* 94: 33–35.

Cohen YE, Doan DE, Rubin DM & Saunders JC (1993): Middle-ear development. V: Development of umbo sensitivity in the gerbil. *American Journal of Otolaryngology* 14(3): 191–198.

Dahmann H (1930): Zur Physiologie des Hörens- experimentelle Untersuchungen über die mechanik der Gehörknöchelchenkette, sowie über deren Verhalten auf Ton und Luftdruck. *Z Hals Nasen Ohrenheilkd* 27: 329–367.

Decraemer WF, de La Rochefoucauld O, Dong W, Khanna SM, Dirckx JJJ & Olson ES (2007): Scala vestibuli pressure and three-dimensional stapes velocity measured in direct succession in gerbil. *The Journal of the Acoustical Society of America* 121: 2774–2791.

Decraemer WF, de La Rochefoucauld O & Olson ES (2011): Measurement of the Three-Dimensional Vibration Motion of the Ossicular Chain in the Living Gerbil. (CA Shera & ES Olson, Eds.) *AIP Conference Proceedings* 1403(1), 528–533.

Decraemer WF & Khanna SM (1994): Modelling the malleus vibration as a rigid body motion with one rotational and one translational degree of freedom. *Hearing Research* 72: 1–18.

Decraemer WF & Khanna SM (1996): Malleus vibrations in the cat ear are three dimensional. *Diversity in Auditory Mechanics*. Berkeley, California, 158–164.

Decraemer WF & Khanna SM (1997): Vibrations on the malleus measured through the ear canal. *Middle ear mechanics in research and otosurgery.* Dresden, 32–39.

Decraemer WF, Khanna SM & Funnell WRJ (1991): Malleus vibration mode changes with frequency. *Hearing Research* 54(2): 305–318.

Decraemer WF, Khanna SM & Funnell WRJ (1994a): Bending of the manubrium in cat under normal sound stimulation. *SPIE* 2329: 74–84.

Decraemer WF, Khanna SM & Funnell WRJ (1994b): A method for determining three-dimensional vibration in the ear. *Hearing Research* 77: 19–37.

Decraemer WF, Khanna SM, Rosowski JJ & Merchant SN (2001): Complete 3-dimensional motion of the ossicular chain in a human temporal bone. *Presented at the ARO Midwinter Mtg*.

de La Rochefoucauld O, Decraemer WF, Khanna SM & Olson ES (2008): Simultaneous Measurements of Ossicular Velocity and Intracochlear Pressure Leading to the Cochlear Input Impedance in Gerbil. *Journal of the Association for Research in Otolaryngology* 9: 161–177.

de La Rochefoucauld O & Olson ES (2007): Exploring sound transmission through the middle ear by tracing middle ear delay. *Presented at the ARO Midwinter Mtg*. Denver, Colorado, USA.

de La Rochefoucauld O & Olson ES (2010): A sum of simple and complex motions on the eardrum and manubrium in gerbil. *Hearing Research* 263: 9–15.

Didyk LA, Dirckx JJJ, Bogdanov VB, Lysenko VA & Gorgo YP (2007): The mechanical reaction of the pars flaccida of the eardrum to rapid air pressure oscillations modeling different levels of atmospheric disturbances. *Hearing Research* 223: 20–28.

Dirckx JJJ & Decraemer WF (1991): Human tympanic membrane deformation under static pressure. *Hearing Research* 51(1): 93–105.

Dirckx JJJ & Decraemer WF (2001): Effect of middle ear components on eardrum quasi-static deformation. *Hearing Research* 157: 124–137.

Dirckx JJJ, Decraemer WF, von Unge M & Larsson C (1997): Measurement and modeling of boundary shape and surface deformation of the Mongolian gerbil pars flaccida. *Hearing Research* 111: 153–164.

Dirckx JJJ, Decraemer WF, von Unge M & Larsson C (1998): Volume displacement of the gerbil eardrum pars flaccida as a function of middle ear pressure. *Hearing Research* 118: 35–46.

Doan DE, Igic PG & Saunders JC (1996): Middle-ear development VII: umbo velocity in the neonatal rat. *The Journal of the Acoustical Society of America* 99(3): 1566–1572.

Doyle WJ, Rosowski JJ & Merchant SN (2000): Middle ear pressure regulation. *The Function and Mechanics of Normal, Diseased and Reconstructed Middle Ears.* Kugler, The Hague, 3–21.

Doyle WJ, Seroky JT & Alper CM (1995): Gas exchange across the middle ear mucosa in monkeys. Estimation of exchange rate. *Archives of Otolaryngology — Head & Neck Surgery* 121(8): 887–892.

Elkhouri N (2006): *Finite-element modelling of the gerbil middle ear.* Master's thesis, McGill University, Montréal.

Elkhouri N, Liu H & Funnell WRJ (2006): Low-frequency finite-element modeling of the gerbil middle ear. *JARO* 7(4): 399–411.

Ellaham N (2007): *An experimental study of middle-ear vibrations in gerbils*. Master's thesis, McGill University, Montréal.

Elner A (1976): Normal gas exchange in the human middle ear. *The Annals of Otology, Rhinology, and Laryngology* 85: 161–164.

Felding JU, Rasmussen JB & Lildholdt T (1987): Gas composition of the normal and the ventilated middle ear cavity. *Scandinavian Journal of Clinical and Laboratory Investigation* 186, 31–41.

Finck A & Sofonglu M (1966): Auditory sensitivity of the mongolian gerbil (Meriones unguiculatus). *Journal of Auditory Research* 6(3): 313–319.

Flisberg K & Zsigmond M (1965): The size of the mastoid air cell system. Planimetry — Direct volume determination. *Acta Oto-Laryngologica* 60: 23–29.

Funnell WRJ (1972): *The acoustical impedance of the guinea-pig middle ear and the effects of the middle-ear muscles*. Master's thesis, McGill University, Montréal.

Funnell WRJ (1996): Low-frequency coupling between eardrum and manubrium in a finite-element model. *The Journal of the Acoustical Society of America* 99(5): 3036–3043.

Funnell WRJ & Decraemer WF (2008): Anatomical and mechanical properties of the tympanic membrane. *Chronic otitis media: Pathogenesis-oriented therapeutic management.* Kugler, The Hague, 51–84.

Funnell WRJ, Decraemer WF & Khanna SM (1987): On the damped frequency response of a finite-element model of the cat eardrum. *The Journal of the Acoustical Society of America* 81(6): 1851–1859.

Funnell WRJ, Decraemer WF, von Unge M & Dirckx JJJ (1999): Finite-element modelling of the gerbil eardrum and middle ear. *Presented at the 22rd Midwinter Res Mtg*. Assoc Res Otolaryngol, St Petersburg Beach.

Funnell WRJ, Decraemer WF, von Unge, M & Dirckx JJJ (2000): Finite-element modelling of the gerbil eardrum and middle ear. *Presented at the 23rd Midwinter Res Mtg*. Assoc Res Otolaryngol, St Petersburg Beach.

Funnell WRJ, Heng Siah T, McKee MD, Daniel SJ & Decraemer WF (2005): On the coupling between the incus and the stapes in the cat. *JARO* 6(1): 9–18.

Funnell WRJ, Khanna SM & Decraemer WF (1992): On the degree of rigidity of the manubrium in a finite-element model of the cat eardrum. *The Journal of the Acoustical Society of America* 91(4): 2082–2090.

Funnell WRJ & Laszlo CA (1978): Modeling of the cat eardrum as a thin shell using the finite-element method. *The Journal of the Acoustical Society of America* 63(5): 1461–1467.

Funnell WRJ & Laszlo CA (1982): A critical review of experimental observations on ear-drum structure and function. *ORL* 44(4): 181–205.

Gaihede M, Dirckx JJJ, Jacobsen H, Aernouts J, Søvsø M & Tveterås K (2010): Middle ear pressure regulation — complementary active actions of the mastoid and the Eustachian tube. *Otology & Neuro-Otology* 31(4): 603–611.

Gariepy B (2011): *Finite-element modelling of the newborn ear canal and middle ear*. Master's thesis, McGill University, Montréal.

Gea SLR, Decraemer WF, Funnell WRJ, Dirckx JJJ & Maier H (2010): Tympanic membrane boundary deformations derived from static displacements observed with computerized tomography in human and gerbil. *JARO* 11(1): 1–17.

Gentil F, Parente M, Martins P, Garbe C, Jorge RN, Ferreira A & Tavares JMRS (2011): The influence of the mechanical behaviour of the middle ear ligaments: a finite element analysis. *Proceedings of the Institution of Mechanical Engineers. Part H, Journal of Engineering in Medicine* 225(1): 68–76.

Goode RL, Ball G, Nishihara S & Nakamura K (1996): Laser Doppler vibrometer (LDV)–a new clinical tool for the otologist. *The American Journal of Otology* 17(6): 813–822.

Graham MD, Reams C & Perkins R (1978): Human tympanic membrane malleus attachment. Preliminary study. *The Annals of Otology, Rhinology, and Laryngology* 87: 426–431.

Gray H (1918): *Anatomy of the Human Body*. Lea & Febiger.

Gundersen T & Høgmoen K (1976): Holographic vibration analysis of the ossicular chain. *Acta Oto-Laryngologica* 82: 16–25.

Gyo K, Aritomo H & Goode RL (1987): Measurement of the ossicular vibration ratio in human temporal bones by use of a video measuring system. *Acta Oto-Laryngologica* 103: 87–95.

Hariharan P (2006): *Basics of Interferometry, Second Edition* (2nd ed). Academic Press.

Helmholtz H (1869): *Die Mechanik der Gehörknöchelchen und des Trommelfells, Pflügers Archiv Physiol* (1st ed). Bonn. [English translations — (1) Bucks AH & Smith N (1873): The Mechanism of the Ossicles of the Ear and Membrana Tympani (Woods, New York), 69 pp. (2) Hilton J (1874): The Mechanism of the Ossicles and the Membrana Tympani (New Sydenham Society, London), 62: 97–155.]

Henry KR, McGinn, MD & Chole RA (1980): Age-related auditory loss in the Mongolian gerbil. *Archives of Oto-Rhino-Laryngology* 228: 233–238.

Huber AM, Schwab C, Linder T, Stoeckli SJ, Ferrazzini M, Dillier N & Fisch U (2001): Evaluation of eardrum laser doppler interferometry as a diagnostic tool. *The Laryngoscope* 111(3): 501–507.

Khanna SM & Tonndorf J (1972): Tympanic membrane vibrations in cats studied by time-averaged holography. *The Journal of the Acoustical Society of America* 51: 1904–1920.

Koike T, Wada H & Kobayashi T (2002): Modeling of the human middle ear using the finite-element method. *The Journal of the Acoustical Society of America* 111(3): 1306–1317.

Kuypers LC (2005). *Determination of the thickness of the tympanic membrane by confocal laser scanning microscopy.* Doctoral thesis, University of Antwerp, Antwerp, Belgium.

Kuypers LC, Decraemer WF & Dirckx JJJ (2006): Thickness distribution of fresh and preserved human eardrums measured with confocal microscopy. *Otology & Neuro-Otology* 27(2): 256–264.

Kuypers LC, Dirckx JJJ, Decraemer WF & Timmermans JP (2005): Thickness of the gerbil tympanic membrane measured with confocal microscopy. *Hearing Research* 209: 42–52.

Lay DM (1972): The anatomy, physiology, functional significance and evolution of specialized hearing organs of gerbilline rodents. *Journal of Morphology* 138: 41–120.

Maftoon N, Nambiar S, Funnell WRJ, Decraemer WF & Daniel SJ (2011): Experimental and modelling study of gerbil tympanic-membrane vibrations. *Presented at the 34th Midwinter Res Mtg*. Assoc Res Otolaryngol, Baltimore.

Marazita ML, Ploughman LM, Rawlings B, Remington E, Arnos KS & Nance WE (1993): Genetic epidemiological studies of early-onset deafness in the U.S. school-age population. *American Journal of Medical Genetics* 46(5): 486–491.

Moore KL (1992): *Clinically Oriented Anatomy* (3rd ed). Williams & Wilkins.

Nakajima HH, Ravicz ME, Rosowski JJ, Peake WT & Merchant SN (2005): Experimental and clinical studies of malleus fixation. *The Laryngoscope* 115(1): 147–154.

Nambiar S (2009): *An experimental study of middle-ear vibrations in gerbils*. Master's thesis, McGill University, Montréal.

NIDCD (1993): Early Identification of Hearing Impairment in Infants and Young Children. *National Institutes of Health Consensus Statement* 11(1): 1–24.

Overstreet EH & Ruggero MA (2002): Development of wide-band middle ear transmission in the Mongolian gerbil. *The Journal of the Acoustical Society of America* 111: 261–270.

Prendergast PJ, Ferris P, Rice HJ & Blayney AW (1999): Vibro-acoustic modelling of the outer and middle ear using the finite-element method. *Audiology & Neuro-Otology* 4: 185–191.

Puria S & Allen JB (1998): Measurements and model of the cat middle ear: Evidence of tympanic membrane acoustic delay. *The Journal of the Acoustical Society of America* 104(6): 3463–3481.

Qi L, Funnell WRJ & Daniel SJ (2008): A nonlinear finite-element model of the newborn middle ear. *The Journal of the Acoustical Society of America* 124(1): 337–347.

Ravicz ME, Cooper NP & Rosowski JJ (2008): Gerbil middle-ear sound transmission from 100 Hz to 60 kHz. *The Journal of the Acoustical Society of America* 124(1): 363–380.

Ravicz ME & Rosowski JJ (1997): Sound-power collection by the auditory periphery of the Mongolian gerbil Meriones unguiculatus: III. Effect of variations in middle-ear volume. *The Journal of the Acoustical Society of America* 101: 2135–2147.

Ravicz ME, Rosowski JJ & Voigt HF (1992): Sound-power collection by the auditory periphery of the Mongolian gerbil Meriones unguiculatus. I: Middle-ear input impedance. *The Journal of the Acoustical Society of America* 92(1): 157–177.

Ravicz ME, Rosowski JJ & Voigt HF (1996): Sound-power collection by the auditory periphery of the mongolian gerbil Meriones unguiculatus. II. External-ear radiation impedance and power collection. *The Journal of the Acoustical Society of America* 99(5): 3044–3063.

Romer AS & Parsons TS (1977): *The Vertebrate Body.* Holt-Saunders International, Philadelphia, 481–482.

Rosen J & Gothard LQ (2009): *Encyclopedia of Physical Science (Vol 1)*. Infobase Publishing, New York.

Rosowski JJ, Cheng JT, Ravicz ME, Hulli N, Hernandez-Montes M, Harrington E & Furlong C (2009): Computer-assisted time-averaged holograms of the motion of the surface of the mammalian tympanic membrane with sound stimuli of 0.4-25 kHz. *Hearing Research* 253: 83–96.

Rosowski JJ & Lee CY (2002): The effect of immobilizing the gerbil's pars flaccida on the middle-ear's response to static pressure. *Hearing Research* 174: 183–195.

Rosowski JJ, Mehta RP & Merchant SN (2003): Diagnostic utility of laser-Doppler vibrometry in conductive hearing loss with normal tympanic membrane. *Otology & Neuro-Otology* 24(2): 165–175.

Rosowski JJ, Nakajima HH & Merchant SN (2008): Clinical Utility of Laser-Doppler Vibrometer Measurements in Live Normal and Pathologic Human Ears. *Ear and hearing* 29(1): 3–19.

Rosowski JJ, Ravicz ME, Teoh SW & Flandermeyer DT (1999): Measurements of middle-ear function in the Mongolian gerbil, a specialized mammalian ear. *Audiology & Neuro-Otology* 4: 129–136.

Rosowski JJ, Teoh SW & Flandermeyer DT (1997). The effect of pars flaccida on the sensitivity to sound. *International Symposium on Diversity in Auditory Mechanics*. Singapore, World Scientific, 129–135.

Ryan A (1976): Hearing sensitivity of the mongolian gerbil, Meriones unguiculatis. *The Journal of the Acoustical Society of America* 59: 1222–1226.

Sadé J & Ar A (1997): Middle ear and auditory tube: middle ear clearance, gas exchange, and pressure regulation. *Otolaryngology — Head and Neck Surgery* 116(4): 499–524.

Sadé J, Meyer FA, King M & Silberberg A (1975): Clearance of middle ear effusions by the mucociliary system. *Acta Oto-Laryngologica* 79: 277–282.

Schön F & Müller J (1999): Measurements of ossicular vibrations in the middle ear. *Audiology & Neuro-Otology* 4: 142–149.

Shannon CE (1984): Communication in the presence of noise. *Proceedings of the IEEE* 72(9): 1192–1201.

Stanfield CL & Germann WJ (2007): *Principles of Human Physiology* (3rd ed). Benjamin Cummings.

Sun Q, Gan RZ, Chang KH & Dormer KJ (2002): Computer-integrated finite element modeling of human middle ear. *Biomechanics and Modeling in Mechanobiology* 1(2): 109–122.

Teoh SW, Flandermeyer DT & Rosowski JJ (1997): Effects of pars flaccida on sound conduction in ears of Mongolian gerbil: acoustic and anatomical measurements. *Hearing Research* 106: 39–65.

Tonndorf J & Khanna SM (1972): Tympanic-membrane vibrations in human cadaver ears studied by time-averaged holography. *The Journal of the Acoustical Society of America* 52(4): 1221–1233.

Tos M, Stangerup SE, Holm-Jensen S & Sørensen CH (1984): Spontaneous course of secretory otitis and changes of the eardrum. *Archives of Otolaryngology* 110(5): 281–289.

Tuck-Lee JP, Pinsky PM, Steele CR & Puria S (2008): Finite element modeling of acousto-mechanical coupling in the cat middle ear. *The Journal of the Acoustical Society of America* 124(1): 348–362.

von Unge M, Decraemer WF, Bagger-Sjöbäck D & Dirckx JJJ (1993): Displacement of the gerbil tympanic membrane under static pressure variations measured with a real-time differential moire interferometer. *Hearing Research* 70(2): 229–242.

Uno Y (2000): The attachment structure of the guinea pig tympanic membrane. *Auris, Nasus, Larynx* 27(1): 45–50.

Volandri G, Di Puccio F, Forte P & Carmignani C (2011): Biomechanics of the tympanic membrane. *Journal of Biomechanics* 44(7): 1219–1236.

Wada H, Metoki T & Kobayashi T (1992): Analysis of dynamic behavior of human middle ear using a finite-element method. *The Journal of the Acoustical Society of America* 92: 3157–3168.

Webster DB (1962): A function of the enlarged middle-ear cavities of the kangaroo rat, dipodomys. *Physiological Zoology* 35(3): 248–255.

Webster DB & Webster M (1972): Kangaroo rat auditory thresholds before and after middle ear reduction. *Brain, Behavior and Evolution* 5: 41–53.

Wever EG & Lawrence M (1954): *Physiological acoustics*. Princeton University Press, Princeton, NJ.

Whittemore KR, Merchant SN, Poon BB & Rosowski JJ (2004): A normative study of tympanic membrane motion in humans using a laser Doppler vibrometer (LDV). *Hearing Research* 187: 85–104.

Willi UB (2003): *Middle ear mechanics: the dynamic behavior of the incudo-malleolar joint and its role during the transmission of sound*. Doctoral thesis, Universität Zürich.

Yang X & Henson OW Jr (2002): Smooth muscle in the annulus fibrosus of the tympanic membrane: physiological effects on sound transmission in the gerbil. *Hearing Research* 164(1-2): 105–114.

audilab.bme.mcgill.ca: *Structure and function of the middle ear.*
Funnell WRJ (n.d.). Retrieved Dec 13, 2011, from
http://audilab.bme.mcgill.ca/AudiLab/teach/me_saf/me_saf.html

audilab.bme.mcgill.ca: *Finite-element method.*
Funnell WRJ (n.d.). Retrieved Aug 4, 2011, from
http://audilab.bme.mcgill.ca/AudiLab/teach/fem/fem.html

audilab.bme.mcgill.ca: *3D Ear - An ear anatomy tutorial.*
Funnell WRJ, Daniel SJ & Nicholson D (n.d.). Retrieved Dec 13, 2011, from
http://audilab.bmed.mcgill.ca/~daren/3Dear/index.html

etymotic.com: *ER-2 Technical Specifications.*
Etymotic Research, Inc. (n.d.). Retrieved Aug 4, 2011, from http://www.etymotic.com/pro/er2-ts.aspx

etymotic.com: *ER-7C Series B Microphone System Technical Specifications.*
Etymotic Research, Inc.(n.d.). Retrieved Aug 4, 2011, from http://www.etymotic.com/pro/er7c-ts.aspx

clinicaladvisor.com: *The Clinical Advisor — Chronic dysfunction of the eustachian tube.*
Lisano Valentino R (2009). Retrieved from http://www.clinicaladvisor.com/chronic-dysfunction-of-the-eustachian-tube/article/131610/

polytec.com: *Basic Principles of Vibrometry.*
Polytec (n.d.). Retrieved Aug 4, 2011, from http://www.polytec.com/us/solutions/vibration-measurement/basic-principles-of-vibrometry/

who.int: *Worldwide hearing care for developing countries.*
World Health Organization (2011). Retrieved Dec 8, 2011, from http://www.who.int/pbd/deafness/activities/WWHearing/en/index.html

wikibook.org: *Human Physiology (Wikibook)*
Young K, nursing students PCSG & PCDS (2010, Nov 12).
Retrieved Dec 13, 2011, from http://en.wikibooks.org/wiki/Human_Physiology